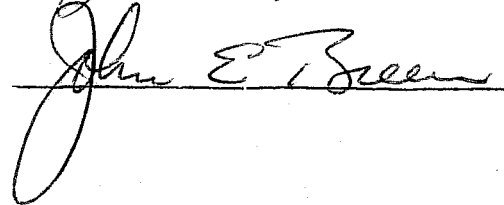A COMPARATIVE STUDY OF BIAXIALLY LOADED REINFORCED
CONCRETE BEAM-COLUMN JOINTS

APPROVED:

To my parents
Eldin and Garnet Longwell

A COMPARATIVE STUDY OF BIAXIALLY LOADED REINFORCED
CONCRETE BEAM-COLUMN JOINTS

by

JOE ELDON LONGWELL, B.S.C.E.

THESIS

Presented to the Faculty of the Graduate School of

The University of Texas at Austin

in Partial Fulfillment

of the Requirements

for the Degree of

MASTER OF SCIENCE IN ENGINEERING

THE UNIVERSITY OF TEXAS AT AUSTIN

May 1980

ACKNOWLEDGMENTS

TABLE OF CONTENTS

LIST OF TABLES

LIST OF FIGURES

C H A P T E R   1

INTRODUCTION

1.1 Background

Recent earthquakes have stimulated an interest in the behavior of reinforced concrete structures subjected to seismic loadings. Of particular interest is the behavior of beam-column joints which must resist very high shear when lateral deformations are imposed on a moment-resisting frame (see Fig. 1.1). The strength and stiffness of the joints undergoing inelastic deformations will have a large influence on the overall frame performance.

Figure 1.2 shows the forces on a typical interior joint. The tensile forces produced by the longitudinal beam reinforcement plus the compressive forces on the opposite face of the joint must be resisted by either the concrete or the reinforcement in the joint. A better understanding of the mechanism of shear transfer across the joint is the key to improving the design of beam-column joints. In addition, the bond and anchorage behavior of the reinforcement, loss of cross-sectional area due to local spalling, and cracking of the joint region have an important influence on joint behavior.

Investigations in the past generally have been limited to beam-column joints of planar frames; however, researchers have recognized that two-way frames with lateral loads applied simultaneously in orthogonal directions may produce a more severe condition at the joint than has been observed in studies of planar joints.[1,2,3,4] Hinging of orthogonal beams at the joint boundary will increase the resultant shearing forces on the joint and will

1
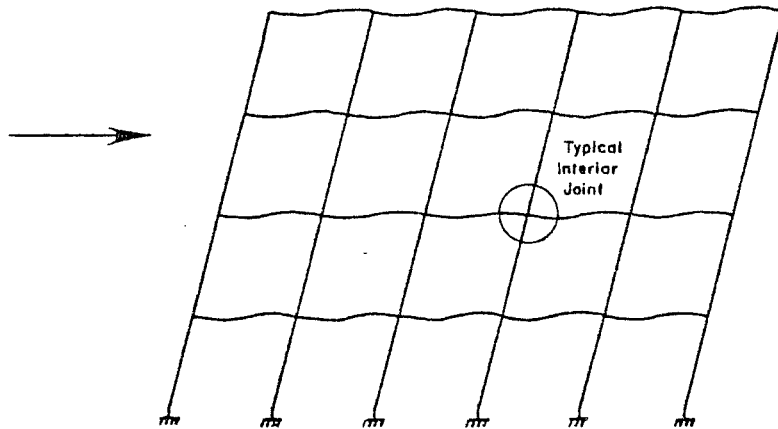
Fig. 1.1 Building frame subjected to lateral force[6]
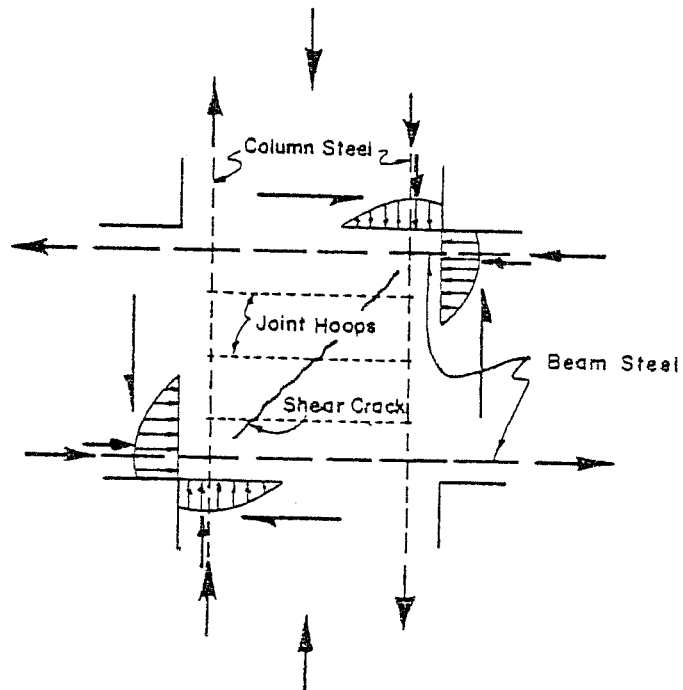
Fig. 1.2 Equivalent member forces on an interior joint[6]

alter the cracking behavior of the joint region. Also,
bidirectional loadings can produce higher moments on the columns
than could occur under unidirectional loadings. Greater column
moments combined with the decreased flexural strength of diagonally
loaded rectangular columns is a potential problem that should be
considered. Figure 1.3 shows the forces which occur on three
faces at an interior joint when subjected to skewed lateral loads.

The design procedure for beam-column joints which is
currently used in the United States was developed by the ACI-ASCE
Committee 352. Beam-column joints with beams framing into the
column from two principal directions are designed to resist joint
shear in each direction independently and without regard to the
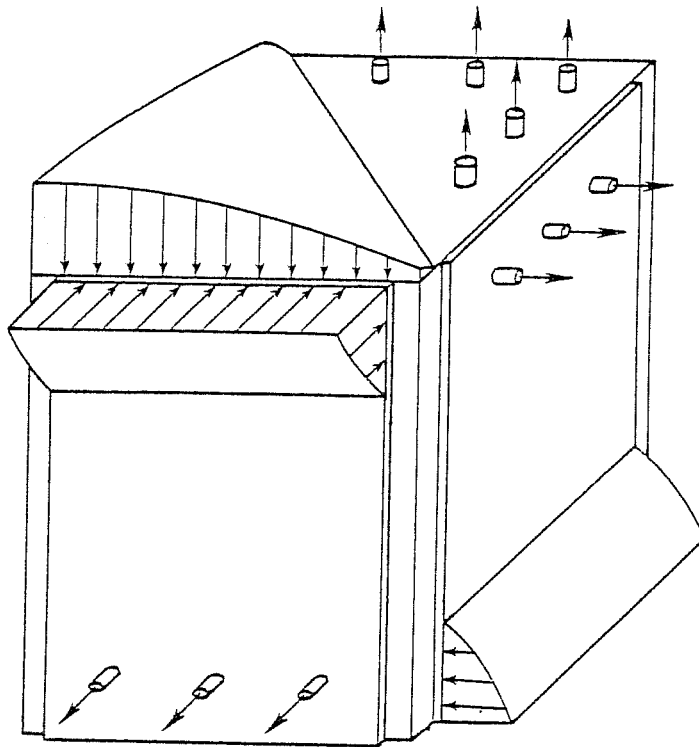
Fig. 1.3 Forces on joint subjected to bidirectional loads

influence of bidirectional loads. This shortcoming did not go
unrecognized, and in the Committee 352 report, "the influence of
biaxial forces on shear strength" was recommended as an area of
needed research.[5] A magnification of unidirectional design loads
to account for the possibility of simultaneous loadings in both
directions is an approach which may be suitable for design of beam-
column joints. Selection of the proper magnification factor,
however, is a problem which can only be resolved through experimenta-
tion. These needs led to the current investigation of the behavior
of interior beam-column joints subjected to bidirectional load
reversals.

1.2 Test Program

The fifth and sixth tests of a seven-test program are the
subject of this study. To give the reader an overall view of the
test program, a brief description of all of the specimens and their
loadings is given. Each of the seven specimens had the same
geometry as shown in Fig. 1.4. The reinforcement sizes and ratios
and the type of loading for each specimen are given in Table 1.1.
The specimens were named according to the test sequence, the type of
loading, and the reinforcement details. For example, specimen
5-BS-A was tested fifth in the series, was loaded in both directions
simultaneously (Biaxial Simultaneous), and had "A" reinforcement
details. The "A" designates one of the four different reinforce-
ment details (A, B, C, D) that were used (see Table 1.1). Other
loading patterns which were used are Uniaxial (U), Biaxial
Alternate (BA), and Monotonic Biaxial Simultaneous (MBS).

The reinforcement details of the first three specimens,
1-U-C, 2-BS-C, and 3-BA-C, were identical, but the load histories
were different for each specimen. Specimen 1-U-C was loaded
uniaxially and was the control specimen for the following two
biaxial tests. Racking deformations were applied only to the
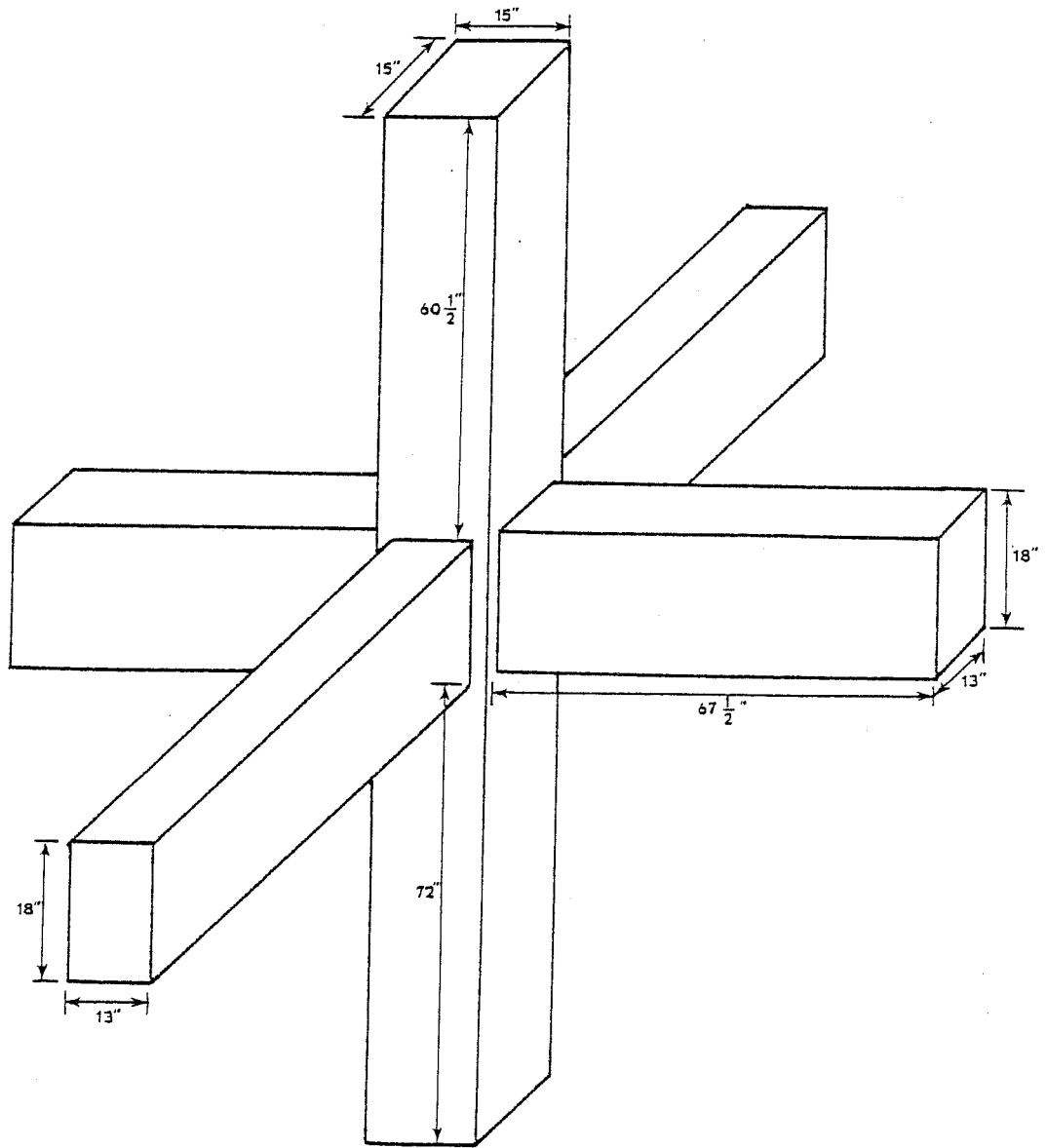
Fig. 1.4 Specimen geometry

TABLE 1.1 SUMMARY OF SPECIMEN REINFORCEMENT

Specimen	Column Reinforcement		Beam Reinforcement				Joint Reinforcement	Loading
			Top		Bottom			
	Bars	Percent	Bars	Percent	Bars	Percent		
1-U-C	12 #9	5.33	3 #10	1.89	3 #8	1.17	2 #4 ties	Uniaxial
2-BS-C	12 #9	5.33	3 #10	1.89	3 #8	1.17	2 #4 ties	Biaxial Simultaneous
3-BA-C	12 #9	5.33	3 #10	1.89	3 #8	1.17	2 #4 ties	Biaxial Alternate
4-BS-B	12 #9	5.33	2 #10	1.25	2 #8	0.78	2 #4 ties	Biaxial Simultaneous
5-BS-A	12 #9	5.33	3 #8	1.17	3 #6	0.64	2 #4 ties	Biaxial Simultaneous
6-MBS-A	12 #9	5.33	3 #8	1.17	3 #6	0.64	2 #4 ties	Monotonic Biaxial Simultaneous
7-BS-D	12 #9	5.33	3 #8	1.17	3 #6	0.64	10 #4 ties	Biaxial Simultaneous

North-South beams of specimen 1-U-C. Specimen 2-BS-C was loaded simultaneously in both the East-West (E-W) and North-South (N-S) directions simulating the racking loads which would occur if the lateral forces were skewed at a 45° angle with respect to the axes of the structure. Specimen 3-BA-C was also loaded biaxially, but deformations were applied alternately to the N-S and E-W beams. For example, the N-S beams were cycled once while the E-W beams were held at the dead load deflection, and then the E-W beams were cycled once while the N-S beams were held at the dead load deflection. Failure occurred in the joint of both specimens 1-U-C and 3-BA-C, but specimen 2-BS-C, which was simultaneously loaded in both directions had a column failure. Since column failure of the specimens was undesirable, a reevaluation of the design of the specimens for the remainder of the test program was necessary.

The percentage of beam-longitudinal reinforcement was reduced in the remaining four specimens to increase the strength of the column relative to the strength of the beams. The beam reinforcement of specimen 4-BS-B was reduced by 1/3 to two #10's top and two #8's bottom. The bar diameters were kept the same as the previous specimens, so that a comparison of specimens 4-BS-A and 2-BS-C, which had similar bond behavior but different beam reinforcement ratios, could be made. The beam reinforcement of specimens 5-BS-A, 6-MBS-A, and 7-BS-D consisted of three #8's top and three #6's bottom. In those specimens, the beam reinforcement ratios were similar to the reinforcement ratios of specimen 4-BS-B, but the bar diameters were smaller. The effect of the bond characteristics of the smaller bars was an interesting aspect of these tests. Each of the last four specimens was loaded simultaneously in both directions and all the specimens were cyclically loaded except for specimen 6-MBS-A which was loaded monotonically. Future tests will explore the behavior of beam-column joints with slabs.

1.3 Scope and Objective

This study of reinforced concrete beam-column joints will be based on the test results of specimens 5-BS-A and 6-MBS-A. Both specimens had the same steel reinforcement details and were loaded in both principal directions simultaneously. The difference in the two tests was the applied load history. Specimen 6-MBS-A was loaded monotonically and specimen 5-BS-A was loaded cyclically. The primary objective is to compare the results of the two tests and to evaluate the performance of beam-column joints under the effects of racking moments applied to the joint in both directions. In addition, the measured joint shear strength of the specimens was compared with the calculated shear strengths obtained with design approaches based on previous studies of planar joints subjected to unidirectional loads.

CHAPTER 2

SPECIMEN DESIGN

2.1 General

The beam-column joint specimens were specifically designed
so that the joint core strength would be the controlling factor in
specimen behavior. Also, the specimens were designed to have
proportions typical of reinforced concrete framed structures. The
column extended to mid-story height above and below the joint,
based on the assumption that the mid-story height is a point of
contraflexure in the column. The column and beam cross-sections
were chosen to be 15 in. x 15 in. and 13 in. x 18 in., respectively,
which were similar to the dimensions used by Meinheit and Jirsa in
a previous study of planar joints at The University of Texas at
Austin.[6]

2.2 Design Calculations

The design of the specimens was based on the following
calculations. Assume:

$$f'_c = 4000 \text{ psi}$$

$$f_y = 60000 \text{ psi}$$

15 in. x 15 in. square column

13 in. wide x 18 in. deep beams

Design:

(1) <u>Joint core shear</u>: Given a 15 in. x 15 in. column and 18 in.
   deep beams, the joint core shear strength formula developed
   by Meinheit and Jirsa was used to compute a joint core shear
   strength.

$$v_u = 5.1 \ \beta \zeta \ (f'_c)^{\frac{2}{3}}$$

where v_u = ultimate joint shear stress, psi

   f'_c = concrete compressive strength, psi

   β = 1 + 0.25w_L/h_c (influence of lateral beams)

   w_L = width of the lateral beam perpendicular to the
      applied joint shear, in.

   h_c = width of the column into which the lateral
      beam frames, in.

   ζ = 1 + 6ρ_s ≤ 1.6 (influence of joint hoop
      reinforcement)

   ρ_s = the volumetric percentage of transverse hoop
      reinforcement

   $$= \frac{A_h (2b^* + 2h^*)}{s_h b^* h^*}$$

   A_h = area of the joint hoop bar (one bar area) in²

   b^* = joint core dimension to outside of hoop, in.

   h^* = joint core dimension to outside of hoop, in.

   s_h = spacing of joint hoops, in.

   Assuming #4 ties at 5 in. through joint core,

   $$\rho_s = \frac{0.20 \left[2(12) + 2(12) \right]}{5(12)(12)}$$

$$= 0.0133$$

$$\zeta = 1 + 6(0.0133) = 1.08$$

$$\beta = 1 + 0.25(13/15) = 1.22$$

therefore,

$$v_u = 5.1(1.22)(1.08)(4000)^{2/3}$$

$$= 1690 \text{ psi}$$

$$V_u = \text{ultimate joint shear}$$

$$= v_u bd$$

$$= 1.69(15)(12.5) = 317 \text{ kips}$$

(2) Beam flexural reinforcement necessary to generate the above joint shear strength, V_u: using the relationship,

$$V_u = A_s^+ f_y + A_s^- f_y - V_{col}$$

where A_s^+ and A_s^- are the areas of positive and negative flexural reinforcement in the beams. Assuming $V_{col} \approx 40$ kips (see Fig. 2.1) and $A_s^+ \approx \frac{1}{2}A_s^-$, the areas of flexural reinforcement required can be determined as

$$317^k = A_s^-(60) + \frac{1}{2}A_s^-(60) - 40^k$$

$$A_s^- = 3.97 \text{ in.}^2 \Rightarrow \text{use three \#10's top,}$$

$$A_s^- = 3.81 \text{ in.}^2, \quad \rho = 0.0189$$

$$A_s^+ = 1.98 \text{ in.}^2 \Rightarrow \text{use three \#8's bottom,}$$

$$A_s^+ = 2.37 \text{ in.}^2, \quad \rho = 0.0117$$

(3) Determine the maximum expected loads which will be applied to the specimen assuming the full yield moment of the beams is developed (refer to Fig. 2.1):
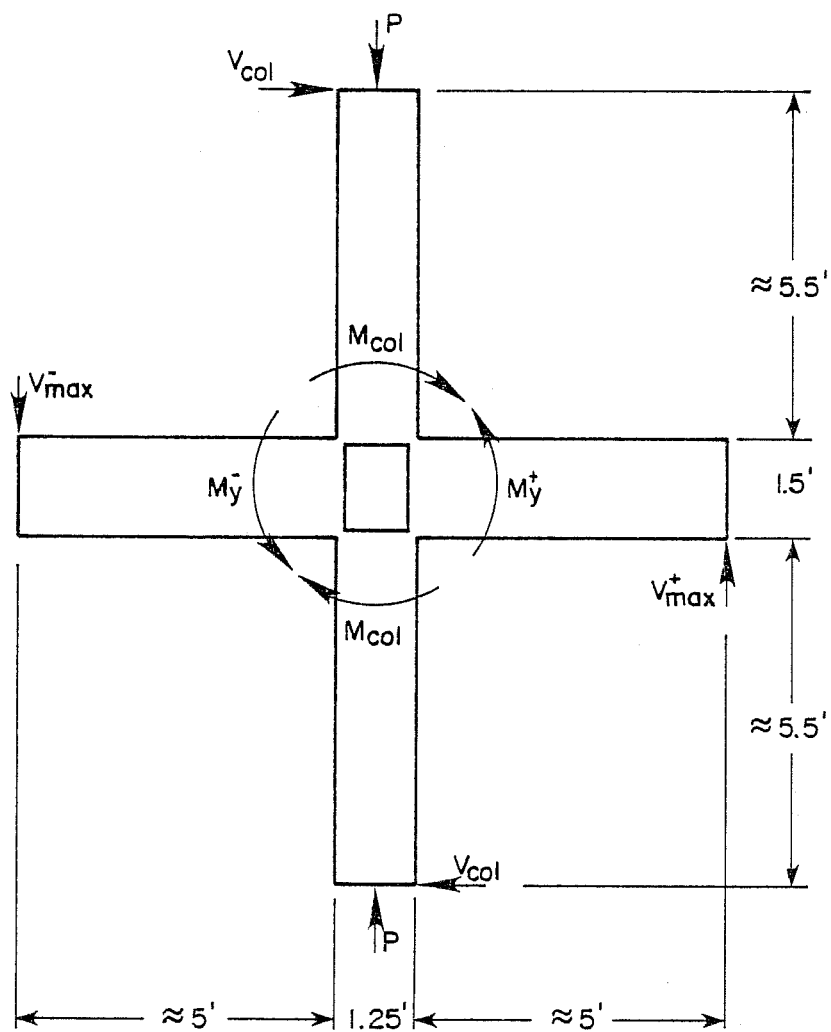
Fig. 2.1 Forces acting on specimen

$$M_y^- = A_s\, f_y(d - \frac{a}{2})$$

$$= 3(1.27)(60)(0.95)(15.5)$$

$$= 3370 \text{ in.-kips}$$

$$V_{max}^- = \frac{3370}{5(12)} = 56 \text{ kips}$$

$$M_y^+ = A_s\, f_y(d - \frac{a}{2})$$

$$= 3(0.79)(60)(0.95)(15.5)$$

$$= 2090 \text{ in.-kips}$$

$$V_{max}^+ = \frac{2090}{5(12)} = 35 \text{ kips}$$

$$M_{col} = \frac{M_y^- + M_y^+}{2}$$

(Assuming equal distribution of total beam moment to column above and below.)

$$= \frac{3370 + 2090}{2}$$

$$= 2730 \text{ in.-kips}$$

(4) Determine longitudinal column reinforcement required to resist column moment developed. Consider the column as a simple flexural member with one layer of reinforcement:

$$(A_s)_{required} = \frac{M_{col}}{f_y(d - \frac{a}{2})} = \frac{2730}{60(0.95)(12.5)}$$

$$= 3.83 \text{ in}^2$$

Therefore, use four #9's; A_s = 4.00 in^2 The above calculations indicate the need for twelve #9 longitudinal reinforcing bars in the column giving an effective four bars per face for flexure.

$$\rho_{col} = \frac{12(1.00)}{15(15)} = 0.0533$$

(5) Check shear capacity of column above and below the joint: assume $V_{col\ max}$ = 50^k due to possible unequal distribution of column shears, P = 0, and V_c = 0 (shear carried by concrete).

$$V_s = \frac{V_{col\ max}}{\varphi} = \frac{50}{0.85}$$

$$= 59 \text{ kips}$$

Assume #4 ties; A_s = 0.20 in.^{2}

$$s = \frac{A_v f_y d}{V_s} = \frac{0.40\ (60)\ 12.5}{59}$$

$$= 5.1 \text{ in.}$$

To be conservative, use #4 ties at 4 in.

(6) Check shear capacity of beams: assume V_{max} = 60^k and #3 stirrups; A_s = 0.11 in.^{2}

$$V_n = \frac{V_{max}}{\varphi} = \frac{60}{0.85}$$

$$= 70.6 \text{ kips}$$

$$V_c = 2\sqrt{f'_c}\ bd = 2\sqrt{4000}\ (13)(15.5)$$

$$= 25,500 \text{ lbs.}$$

$$V_s = V_n - V_c = 70.6 - 25.5$$

$$= 45.1 \text{ kips}$$

$$s = \frac{A_v f_y d}{V_s} = \frac{0.22\ (60)\ (15.5)}{45.1}$$

$$= 4.5 \text{ in.}$$

Use #3 stirrups at 4 in.

After testing the first three specimens, it was apparent that biaxial loadings on the column together with a deterioration of the bond of the column reinforcement produced greater distress in the column than had been anticipated. Therefore, the amount of beam longitudinal reinforcement was reduced in subsequent specimens to increase the relative strength of the column. The design of specimens 5-BS-A and 6-MBS-A was the same as the first three except that the beam reinforcement consisted of three #8's top and three #6's bottom.

2.3 Specimen Details

The details of both specimens 5-BS-A and 6-MBS-A were identical. The beams were 13 in. x 18 in. with 1½ in. cover and had #3 stirrups at a 4 in. spacing (see Fig. 2.2). Top and bottom longitudinal reinforcement consisted of three #8 bars and three #6 bars, respectively and was continuous through the joint. Crossing of the beams at the joint required the placement of the E-W longitudinal reinforcement below the N-S longitudinal reinforcement as shown in Fig. 2.3. This slightly increased the positive moment capacity and decreased the negative moment capacity of the E-W beams compared to the N-S beams. Moment-curvature diagrams for both positive and negative bending of the beams are shown in Fig. 2.4.

The column had a 15 in. x 15 in. square cross section with twelve equally spaced #9 bars as shown in Fig. 2.5. Transverse reinforcement consisted of #4 ties at a 4 in. spacing with 1½ in. cover. At the joint, the tie spacing was increased to 5 in., with two ties within the joint core. Figure 2.6 is an interaction diagram for the column cross section and has curves for both uniaxial and 45° biaxial loading. In either case, the moment capacity shown is the component for each principal direction. The diagram shows that the balanced condition occurs at 300 kips which

16
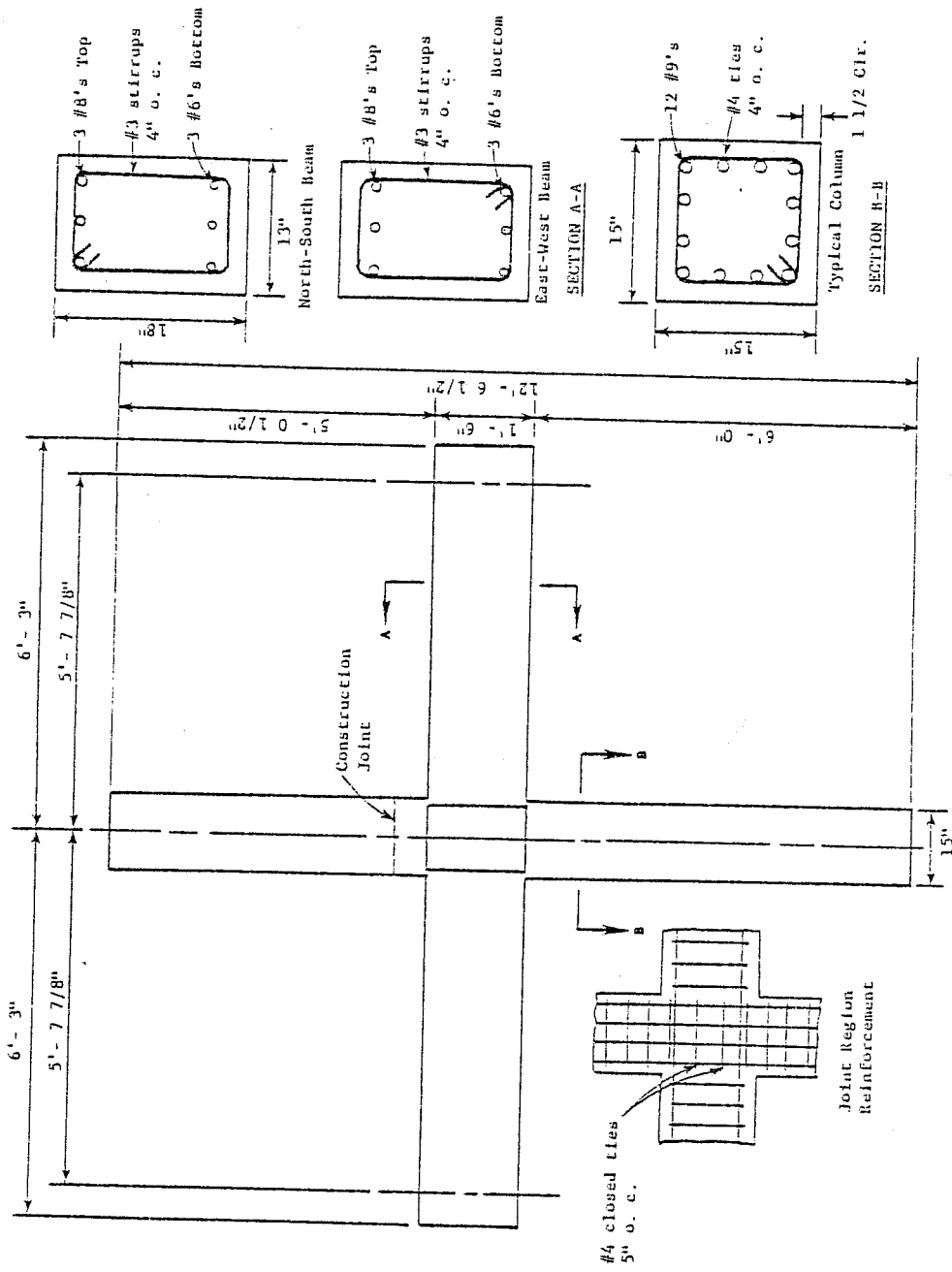
Fig. 2.2   Specimen details
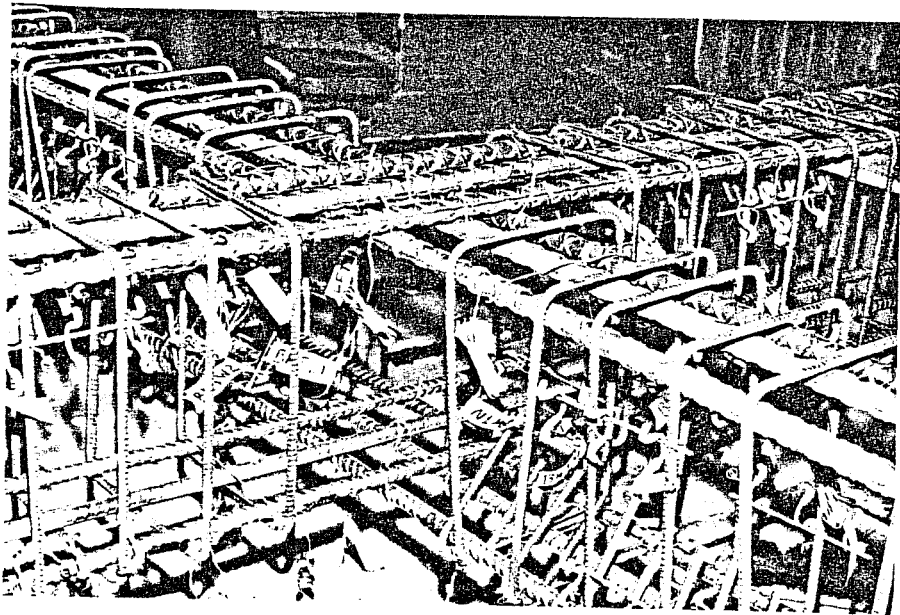
Fig. 2.3 Beam cage
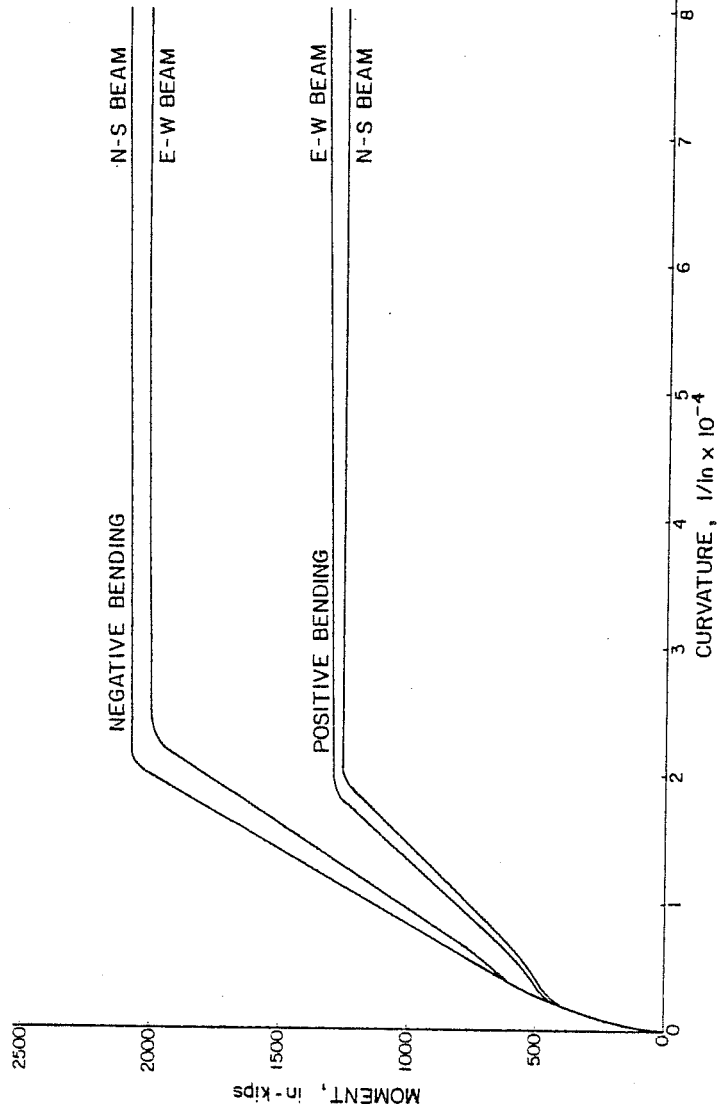
Fig. 2.4 Moment-curvature diagram for beams
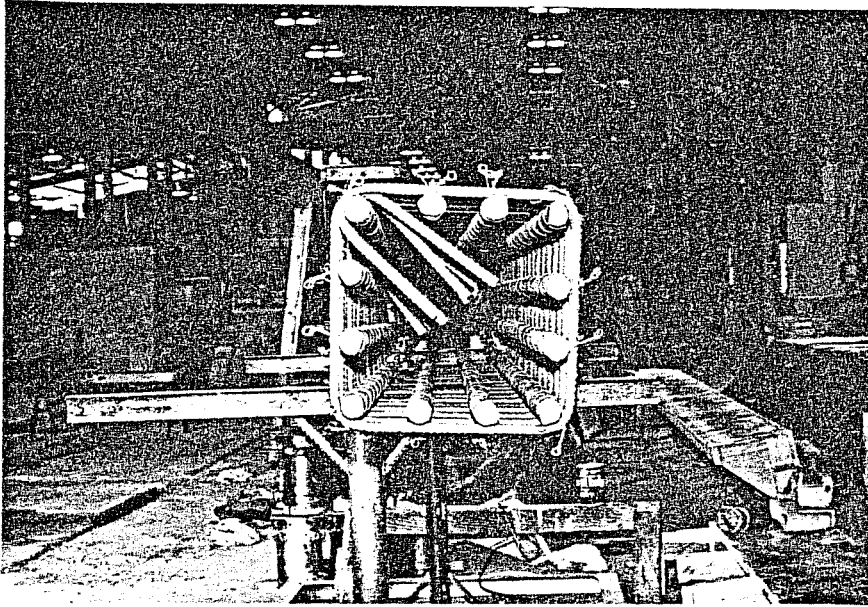
Fig. 2.5 Column cross section
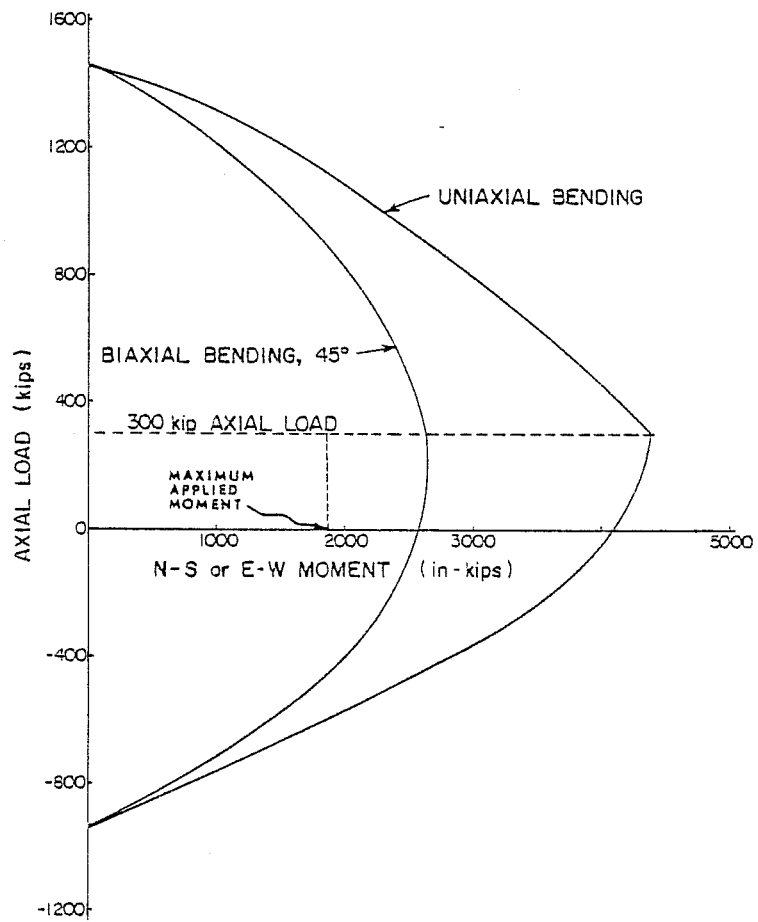
Fig. 2.6 Column interaction diagram

is the axial load that was applied to the specimens. Figure 2.7
shows combinations of the N-S and E-W components of moment capacity
at a 300-kip axial load. The resultant moment capacity of the
column loaded on a 45° angle is approximately 90 percent of the
"uniaxial" strength.
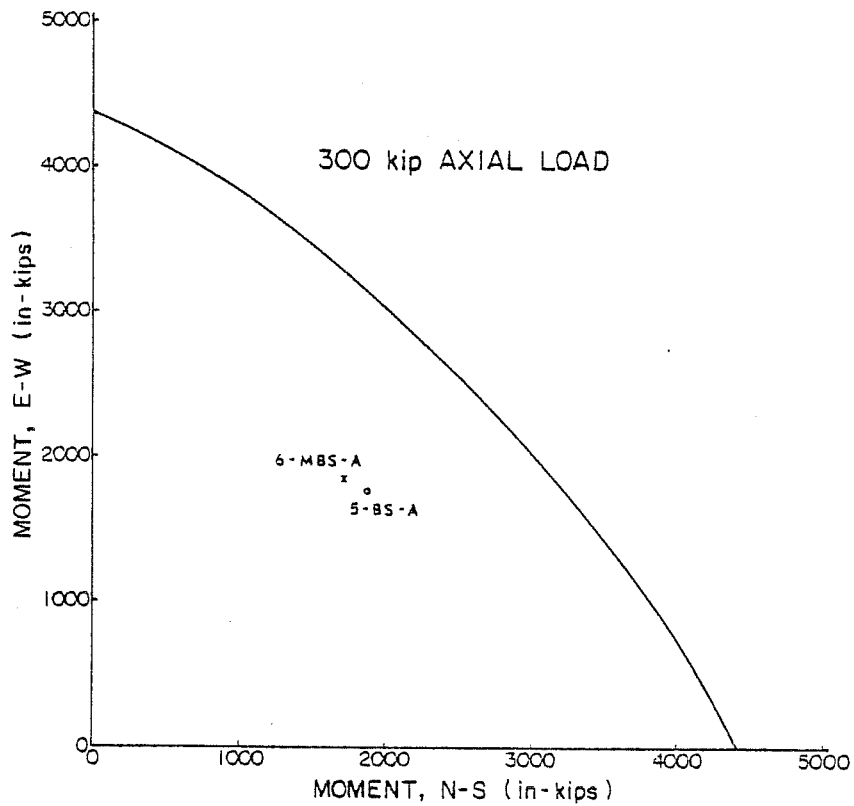
Fig. 2.7   Interaction of N-S and E-W moment
           capacities of column

CHAPTER 3

EXPERIMENTAL STUDY

3.1 Specimen Fabrication

Fabrication of each specimen consisted of tieing the beam and column cages, placing the cages in the forms, securing the instrumentation reference inserts, placing the concrete, and curing the specimen.

First, the column bars and the lower column hoops were tied together to form the column cage which was placed in the form with four 1 in. diameter column base anchor bolts in position (see Fig. 3.1). Next, the lower column forms were lightly oiled and bolted in place securing the column cage in its final position. The beam cages and the two joint core ties were simultaneously lowered over the column bars as shown in Fig. 3.2. With the beam cages resting on the surface of the platform (see Figs. 3.3 and 3.4) the rest of the forms were bolted in place.

In order to provide fixed references from which to measure joint shear strain, joint rotation, beam rotation, and bar slip, steel inserts were secured at various locations in the joint region (see Fig. 3.5). All the inserts were insulated from the cover concrete by pieces of foam rubber taped to the inserts. This method was adopted to prevent erroneous measurements due to spalling of the cover concrete.

Each specimen was cast in two stages. The first cast included the lower column, the beams, and the joint region. After casting, the specimen was covered with a plastic sheet and cured for several days before the forms were removed. The specimen was
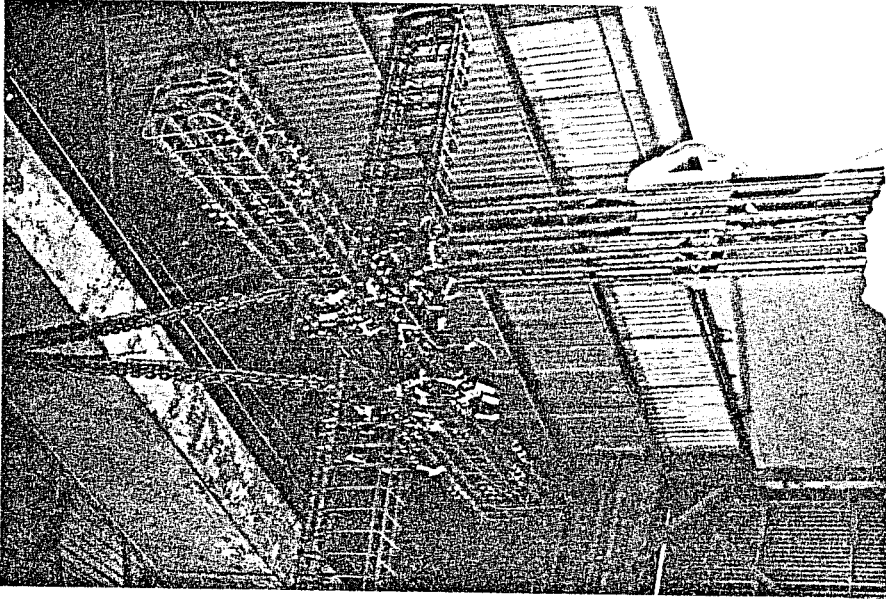
Fig. 3.2 Placement of beam cages
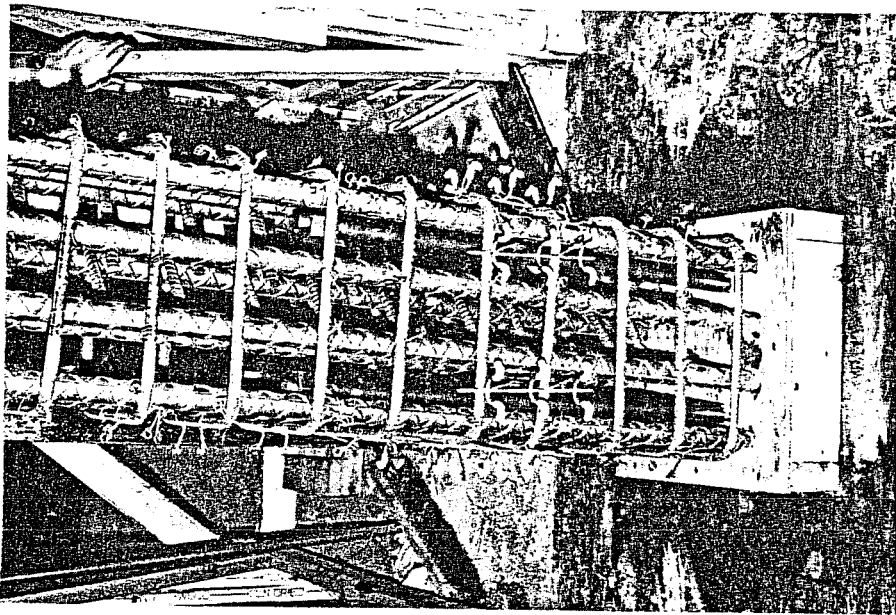
Fig. 3.1 Lower column cage
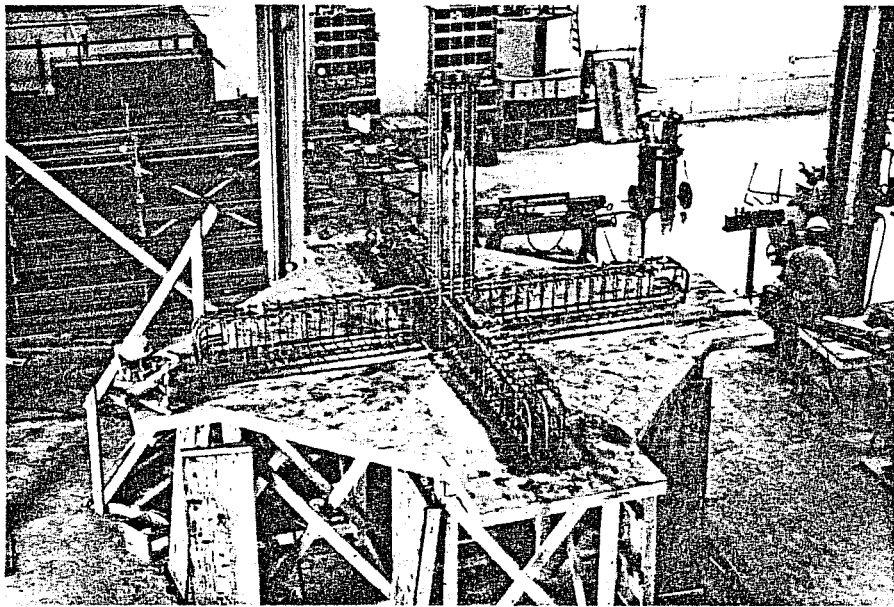
Fig. 3.3 Final position of beam and column cages
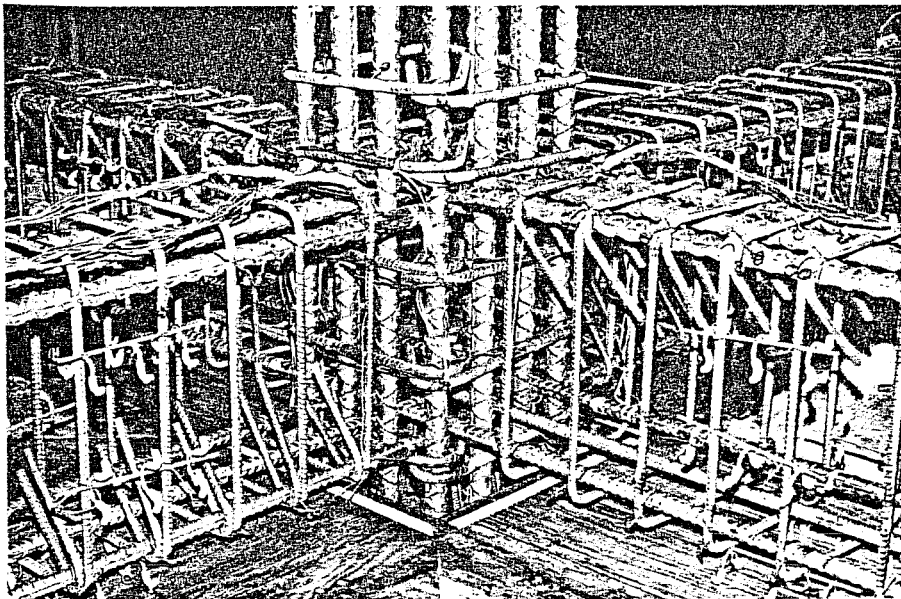
Fig. 3.4 Joint region reinforcement
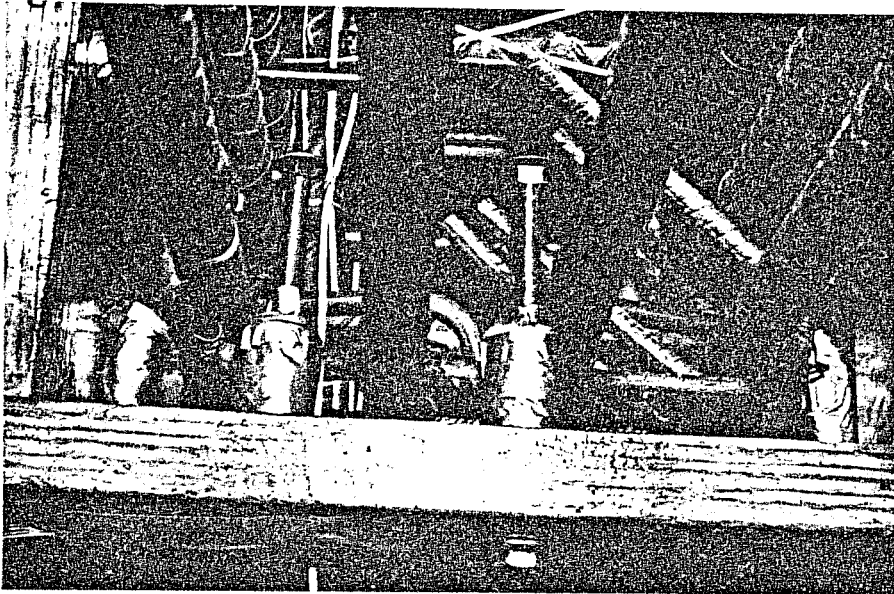
Fig. 3.5   Instrumentation reference inserts
          mounted to formwork

then moved to a rack where the upper column hoops were positioned
and tied (see Fig. 3.6). The upper column anchor bolts were also
positioned and tied before the upper column forms were bolted in
place (see Fig. 3.7). The specimen was then ready for casting of the
upper column. After casting, the specimen was again covered with a
plastic sheet and cured for several days before removing the forms.
The concrete mix proportions given in Table 3.1 were used for
all specimens.

3.2 Material Properties

Concrete cylinders (6 in. x 12 in.) were cast with each
batch of concrete and were cured in the same manner as the specimen.
Average cylinder strengths for the specimens are given in Table 3.2.
Since the concrete strengths of the joint region (first cast) were
fairly close for the two specimens, comparisons of the tests were
possible without normalizing concrete strength.

Steel reinforcement for the two specimens consisted of #3
beam stirrups, #4 column ties, #6 bottom beam bars, #8 top beam bars,
and #9 column bars. The same lot of steel for each bar diameter
was used for both the monotonically and cyclically loaded specimens.
Several coupon tests were conducted for each bar diameter using a
600-kip Universal Testing Machine. Stress and strain measurements
were taken electronically and plotted with an x-y recorder as shown
in Fig. 3.8. The steel reinforcement properties are summarized
in Table 3.3.

3.3 Testing Apparatus

The testing apparatus shown in Fig. 3.9 consisted of an upper
and lower loading head, two column shear struts, and a reaction wall.
Both the upper and lower loading heads were grouted and bolted to
the column. The lower loading head was bolted to the floor as well,
while the top loading head was pin connected to two shear struts.
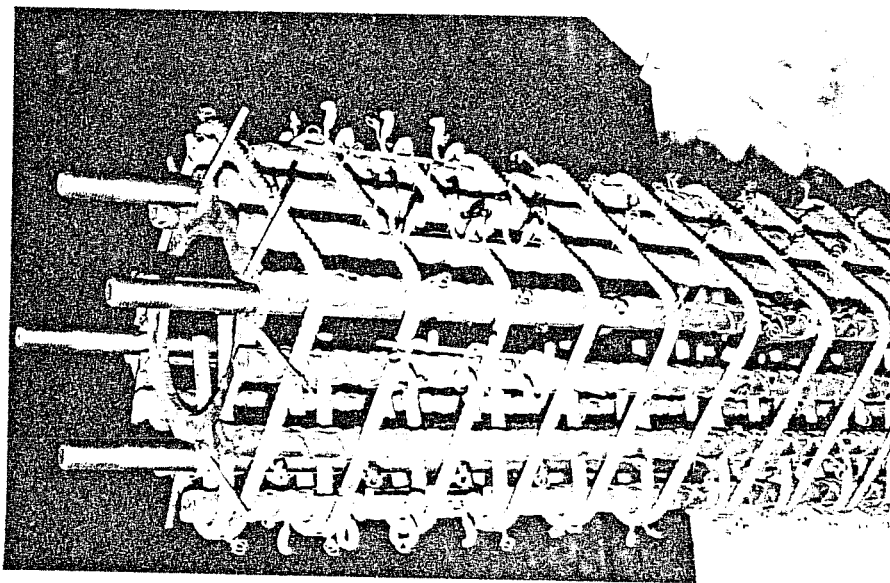
Fig. 3.7 Upper column cage
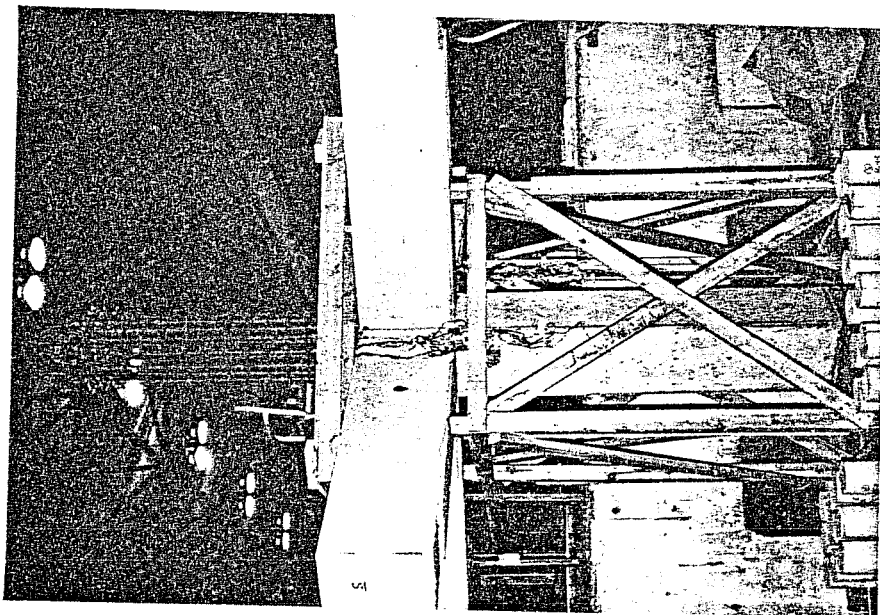
Fig. 3.6 Upper column preparation

TABLE 3.1   CONCRETE BATCH PROPORTIONS

Cement	470 lbs./cu. yd.
Sand	1530 lbs./cu. yd.
Gravel (max. size 5/8")	1830 lbs./cu. yd.
Water*	20 gal./cu. yd.
Admixture: Airsene L (water reducing retardant)	30 oz./cu. yd.

*Additional water was added to achieve a slump of 8"

TABLE 3.2   CONCRETE STRENGTH

Specimen	Cast	Strength (ksi)	Age at Testing (days)
6-MBS-A	First	4.29	42
	Second	4.74	25
5-BS-A	First	4.41	51
	Second	4.20	28

29

Fig. 3.8 Stress versus strain curves for steel reinforcement

TABLE 3.3   STEEL REINFORCEMENT PROPERTIES

Bar Size	Yield Strength (ksi)	Ultimate Strength (ksi)	Strain at Strain Hardening	Ultimate Strain
#3	59.0	87.0	--	--
#4	63.8	97.7	0.016	≈0.13
#6	63.1	97.6	0.015	≈0.14
#8	61.9	102.7	0.008	≈0.11
#9	78.5	115.8	0.010	≈0.11
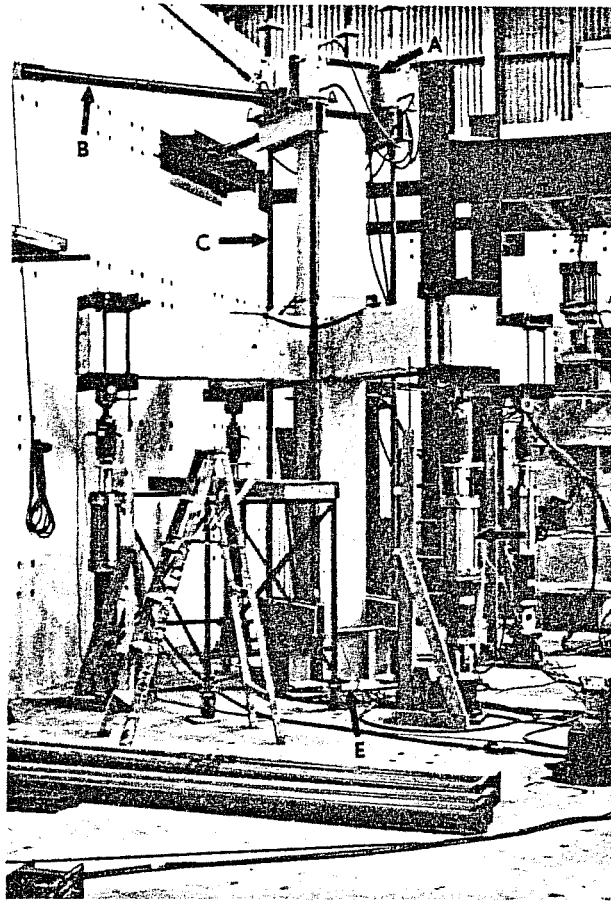
A   upper loading head
B   shear strut
C   axial rod
D   beam ram
E   lower loading head

Fig. 3.9   Testing apparatus

The other ends of the shear struts were pin connected to the reaction wall.

Four axial rod assemblies were used to apply the axial load to the column. Each rod was positioned with the upper and lower loading heads between two bearing plates of the axial rod assembly. Four hydraulic rams at the top of the axial rod assemblies were connected with hydraulic hoses to a manifold which maintained equal pressure in the four rams. A floor pump provided hydraulic pressure to the manifold where it was distributed to the rams. As the rams extended, tensile stresses in the rods and compressive stresses in the column were produced.

Beam loads were applied with double-rodded hydraulic rams. Two independent hydraulic systems which are illustrated in Fig. 3.10 were used for loading the N-S and the E-W beam systems. To simulate dead load, both beams were displaced downward by an equal amount. Oil was pumped through the right pump manifold and into the top of the two rams, forcing the beams down. Simultaneously, oil was forced from the bottom of the rams and back to the pump through the left manifold. This is a closed hydraulic system, and ideally, the amount of oil in the system remains constant.

In addition to applying dead load, the hydraulic system was used to apply the racking load to the specimens. After the dead load was applied, the south (east) beam was displaced upward. Hydraulic oil was pumped through the right manifold to the bottom of the south (east) beam ram forcing the beam up. At the same time, oil was forced out of the top of the south (east) beam ram and into the top of the north (west) beam ram forcing the north (west) beam down by an equal amount. Oil then returned to the pump from the bottom of the north (west) beam ram. To reverse the load, pressure was released with value 2, and then oil was pumped in the opposite direction.

33

(a) Application of dead load   (b) Application of racking load
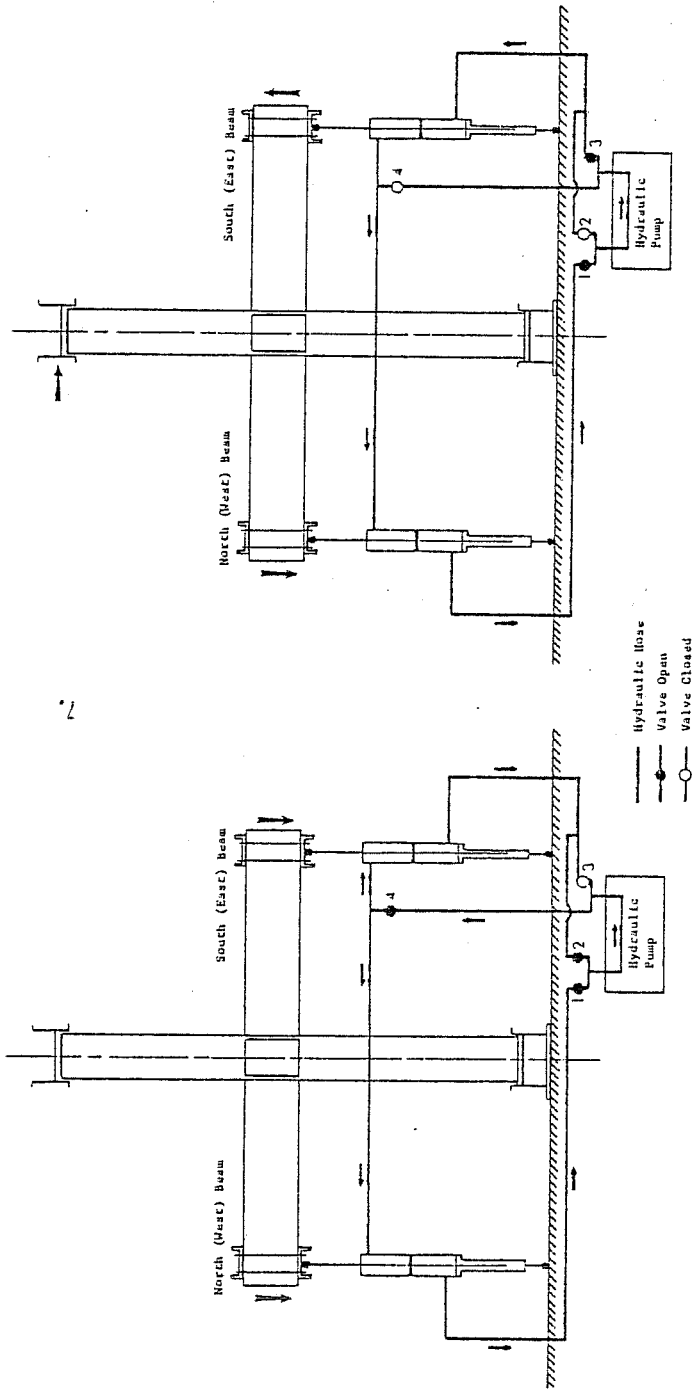
Fig. 3.10 Beam hydraulic loading system

3.4 Specimen Instrumentation

3.4.1 Joint Shear Strain. Joint shear strain was measured
with the device shown in Figs. 3.11(a) and (b). A potentiometer
was mounted on a sliding arm of the triangle formed by the
extensions of the rods connected to three pins embedded in the
joint core. The potentiometer was used to measure the change in
length of the side of the triangle as changes in joint shear
strain occurred. Having this measurement, the law of cosines was
used to calculate joint shear strain (see Fig. 3.12).

3.4.2 Joint Rotation. Joint rotation was measured using
two potentiometers mounted to a stationary frame independent of
the specimen (see Fig. 3.13). Two plates were connected to bolts
embedded in the column above and below the joint providing a
reference from which to measure joint rotation. Figure 3.14 is an
exaggerated illustration of the deformation of the specimen which
shows the joint rotation geometry. The calculation of the joint
rotation which follows refers to this figure.

JR = joint rotation, rad.

h_j = height of joint, in.

x = difference in potentiometer readings, in.

a = distance of potentiometer above and below beam, in.

L_c = distance from joint to point of inflection, in.

θ_f = elastic flexural rotation of column, rad. (see Fig. 4.20)

$x_1 = a(JR + \theta_1 - \theta_f)$

$x_2 = a(JR + \theta_2 - \theta_f)$
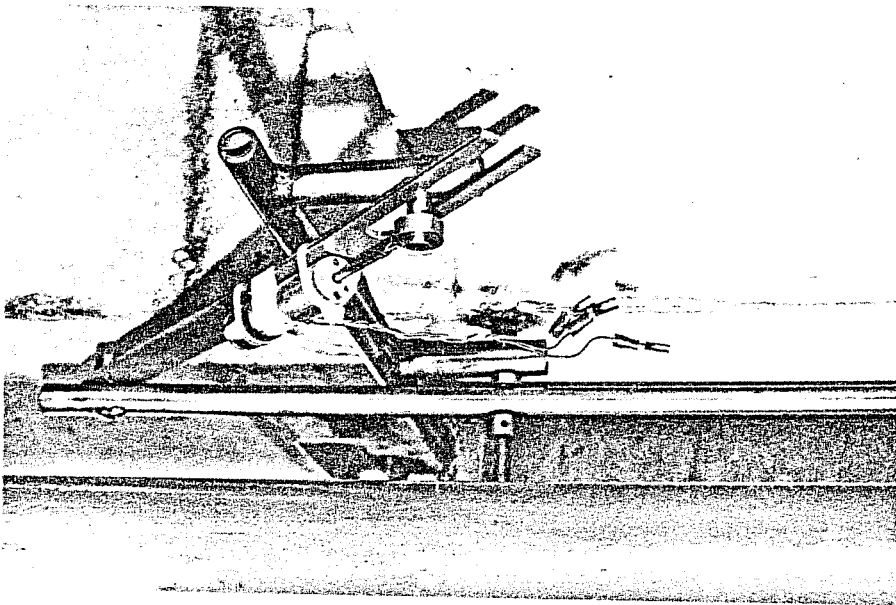
(b)
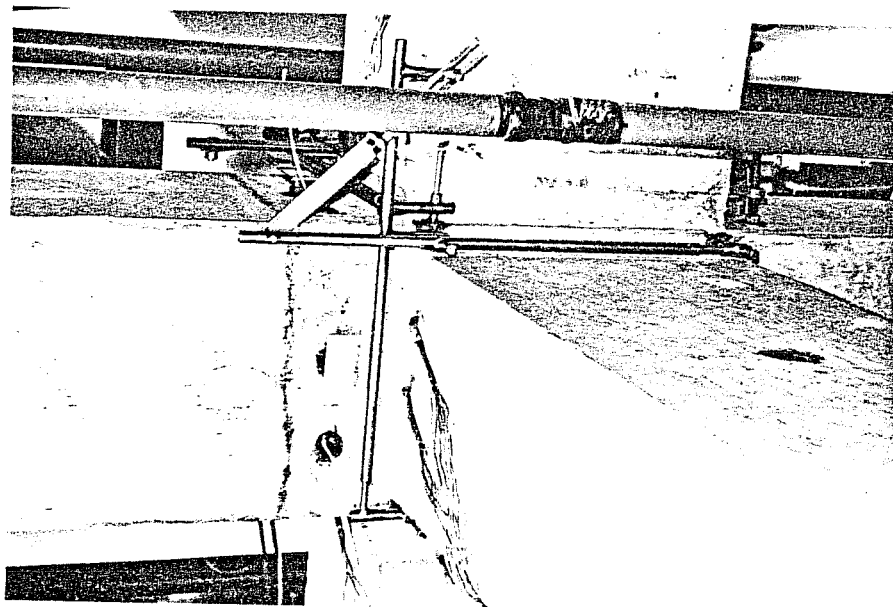
(a)

Fig. 3.11   Shear strain instrumentation
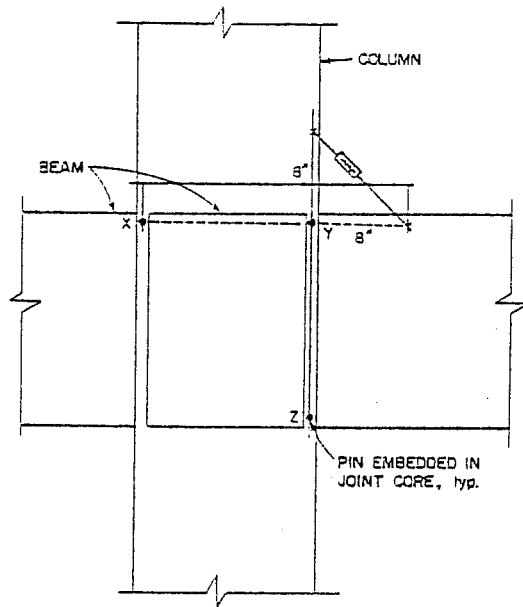
(a) Schematic of joint shear
    strain instrumentation
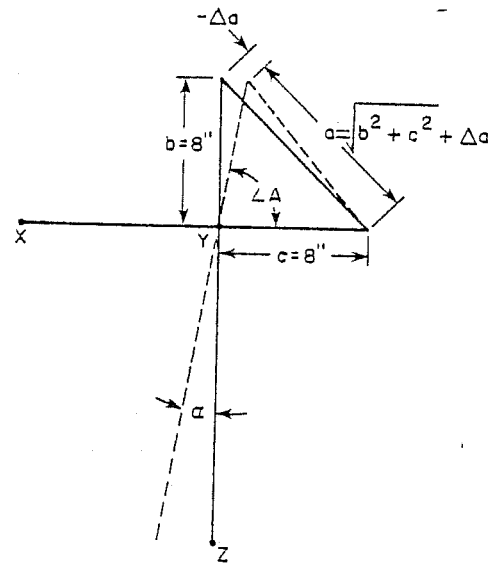
(b) Joint shear strain
    geometry

α = joint shear strain, radians

Δ_a = potentiometer measurement, in.

Law of cosines:

$$a^2 = b^2 + c^2 - 2bc \cos\angle A$$

$$\angle A = \cos^{-1}\left(\frac{b^2 + c^2 - a^2}{2bc}\right)$$

$$= \cos^{-1}\left(\frac{b^2 + c^2 - (\sqrt{b^2 + c^2} + \Delta a)^2}{2bc}\right)$$

$$= \cos^{-1}\left(\frac{128 - (11.31 + \Delta a)^2}{128}\right)$$

$$\alpha = \pi/2 - \angle A$$

Fig. 3.12 Joint shear strain calculation
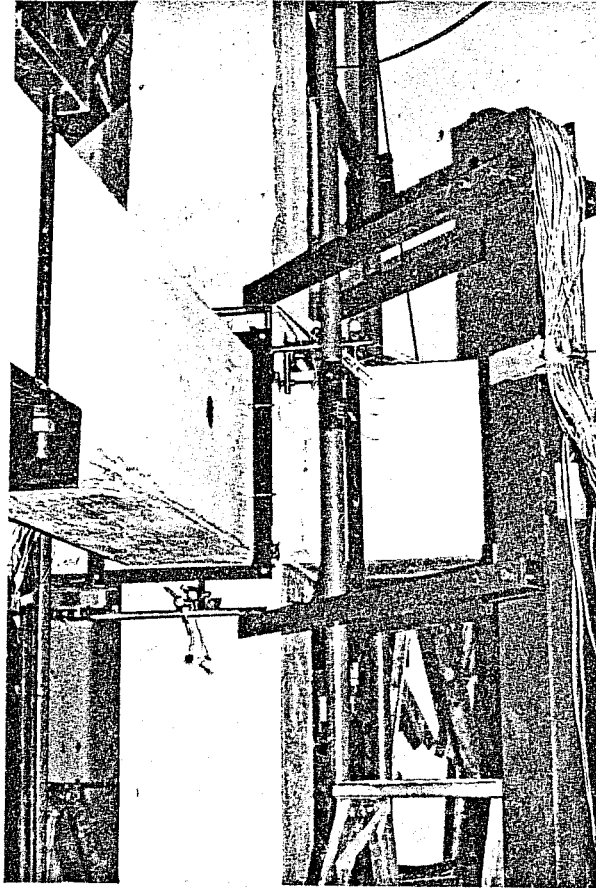
Fig. 3.13 Joint rotation instrumentation
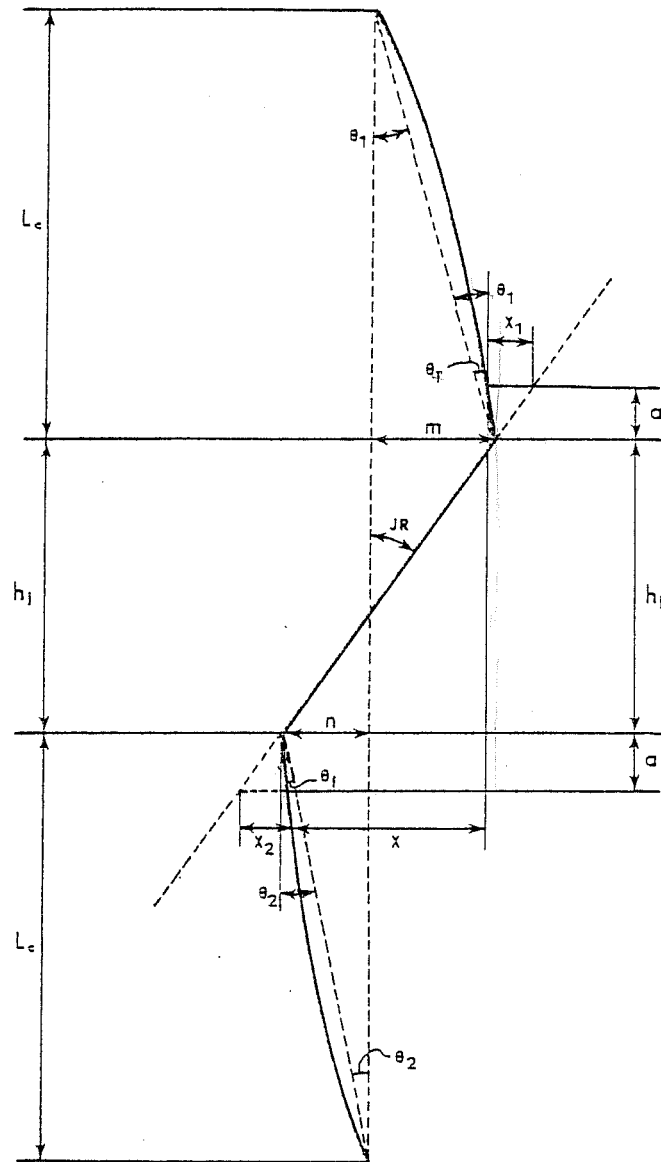
Fig. 3.14 Joint rotation geometry

By geometry,

$$m + n = JR(h_j)$$

$$\theta_1 L_c + \theta_2 L_c = JR(h_j)$$

$$\theta_1 + \theta_2 = \frac{h_j}{L_c} JR$$

$$JR = \frac{x + x_1 + x_2}{h_j + 2a}$$

$$= \frac{x}{h_j + 2a} + \frac{2JR(a) + a(\theta_1 + \theta_2) - 2\theta_f(a)}{h_j + 2a}$$

$$= \frac{x}{h_j + 2a} + \frac{JR(a)}{h_j + 2a}\left(2 + \frac{h_j}{L_c}\right) - \frac{2\theta_f(a)}{(h_j + 2a)}$$

For this geometry, a = 4 in. h_j = 18 in., L_c = 63 in.

$$JR = 0.0593x + 0.475\theta_f$$

3.4.3 <u>Beam Rotation</u>. Rotations of the south and east beams were measured with potentiometers in a similar manner as joint rotation, except that the potentiometers were mounted on a bracket which was attached to the beam (see Fig. 3.15). The bracket was attached to the beam at 7 in. from the face of the column, so that the measurement included both elastic and inelastic beam rotation concentrated within the 7 in. length. Figure 3.16 shows the deformation geometry for the calculation of beam rotation which follows.

BR = beam rotation, radians

y = difference in potentiometer readings

b = distance of potentiometers above and below beam

Fig. 3.15 Beam rotation instrumentation
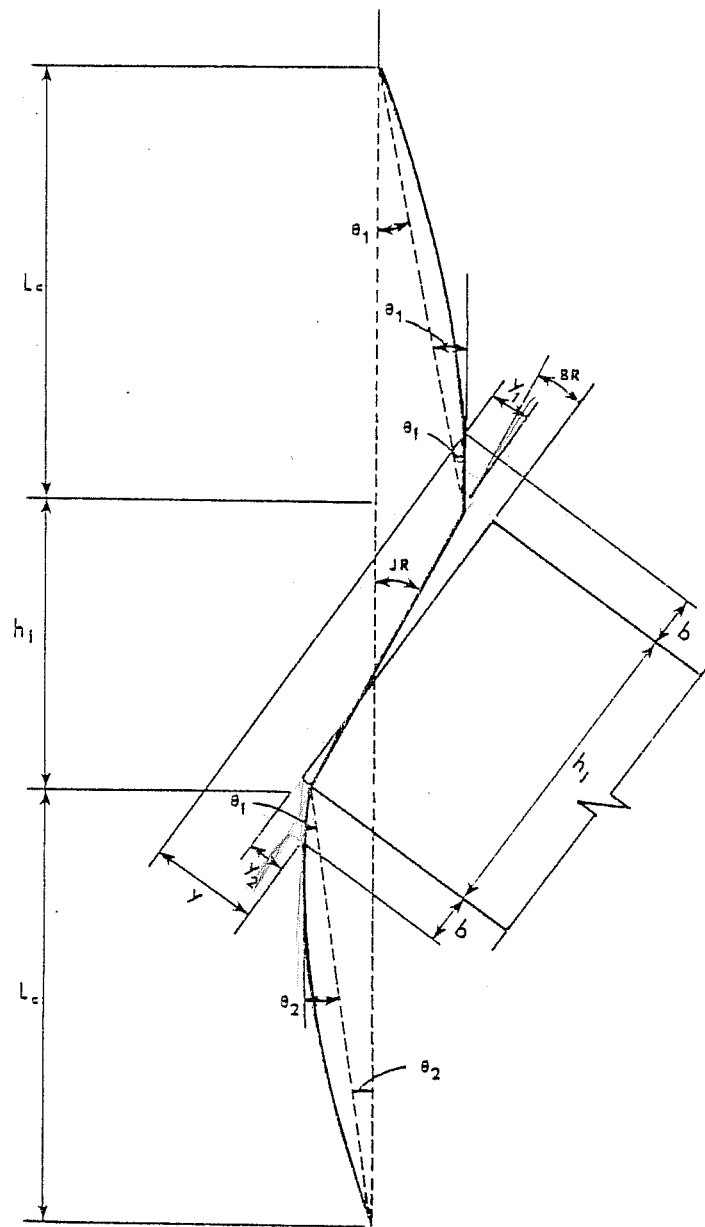
Fig. 3.16 Beam rotation geometry

$$y_1 = b(JR + \theta_1 - \theta_f)$$

$$y_2 = b(JR + \theta_2 - \theta_f)$$

$$BR = \frac{y - (y_1 + y_2)}{h_j + 2b}$$

$$= \frac{y}{h_j + 2b} - \frac{2JR(b) + b(\theta_1 + \theta_2) - 2\theta_f(b)}{h_j + 2b}$$

From joint rotation calculation, recall that:

$$\theta_1 + \theta_2 = \frac{h_j}{L_c} JR$$

$$BR = \frac{y}{h_j + 2b} - b\left(\frac{2JR + \dfrac{h_j}{L_c}(JR) - 2\theta_f}{h_j + 2b}\right)$$

For this geometry, $b = 3\frac{1}{2}$ in., $h_j = 18$ in., $L_c = 63$ in.

$$BR = 0.040y - 0.320JR + 0.280\theta_f$$

3.4.4 <u>Beam Deflection</u>. Beam deflections were measured
with twelve-inch potentiometers mounted to the beam rams as shown
in Fig. 3.17. The slide rod of the potentiometer was connected
to the piston of the ram so that when the ram extended, the rod
extended the same amount.

3.4.5 <u>Loads</u>. Beam loads, axial column load, and column
shear were all measured electronically with load cells. Beam loads
were measured with load cells connected between the beam rams and
the beam ends. To measure column axial load, four strain gages
were mounted on two of the axial rods and connected to form a
Wheatstone bridge. The rods were then calibrated prior to testing
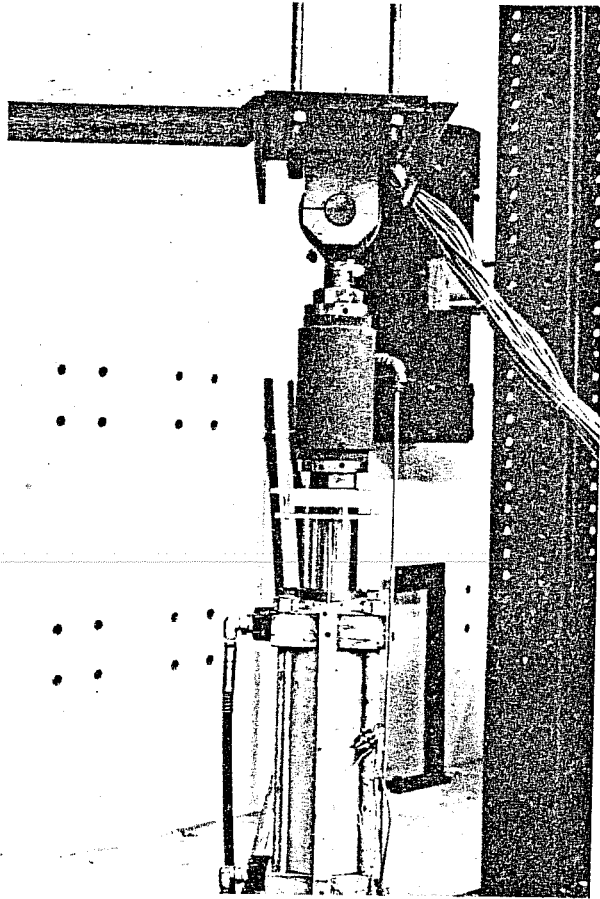
Fig. 3.17 Beam deflection instrumentation

of the specimens. Column shear was measured in the same manner with
full bridge circuitry mounted on each of the two shear struts
connecting the upper loading head and the reaction wall.

3.4.6 <u>Reinforcing Bars</u>. Electrical resistance strain gages
were mounted on beam, column, and joint hoop reinforcement. Strain
gages for the beam and column bars were located at the beam-
column boundaries (see Fig. 3.18). In addition, selected bars had
strain gages at 8 in. and 16 in. from the critical section, and
joint hoops had gages on each of the four sides of the hoop. Paper
gages with 0.64 in. gage length were used throughout. Figure 3.19
shows several bars with mounted gages and waterproof protection.

In addition to strain, slip of the longitudinal beam
reinforcement was measured at the joint boundaries. This was done
with a piece of piano wire attached to the bar at the critical
section and extended through the joint and out the face of the
column as illustrated in Fig. 3.20. The slipwire was attached to
the reinforcing bar by inserting the wire with a 90° bend into
a hole drilled in the bar and using a plastic tie to secure the
connection (see Fig. 3.21). In addition, plastic tubing was used
to provide a passage for the slip wire. As shown in Fig. 3.22,
a potentiometer was mounted on a bolt connected to a reference
insert embedded in the column. Both the slipwire and the plunger
of the potentiometer were spring loaded to provide continuous
contact as movement of the slipwire occurred.

Column and joint rotations introduced an error in the slip
measurements which required a correction. Correction of individual
bar slips depended on both instrument location and on the division
of column rotation above and below the joint. It was assumed that
the column rotation was split evenly. Figure 3.23 shows the
geometry of the joint region with regard to bar slip and the
correction is calculated as follows:

#8 Top Beam Bars

#6 Bottom Beam Bars

#9 Column Bars

* Critical Section

#4 Joint Core Ties
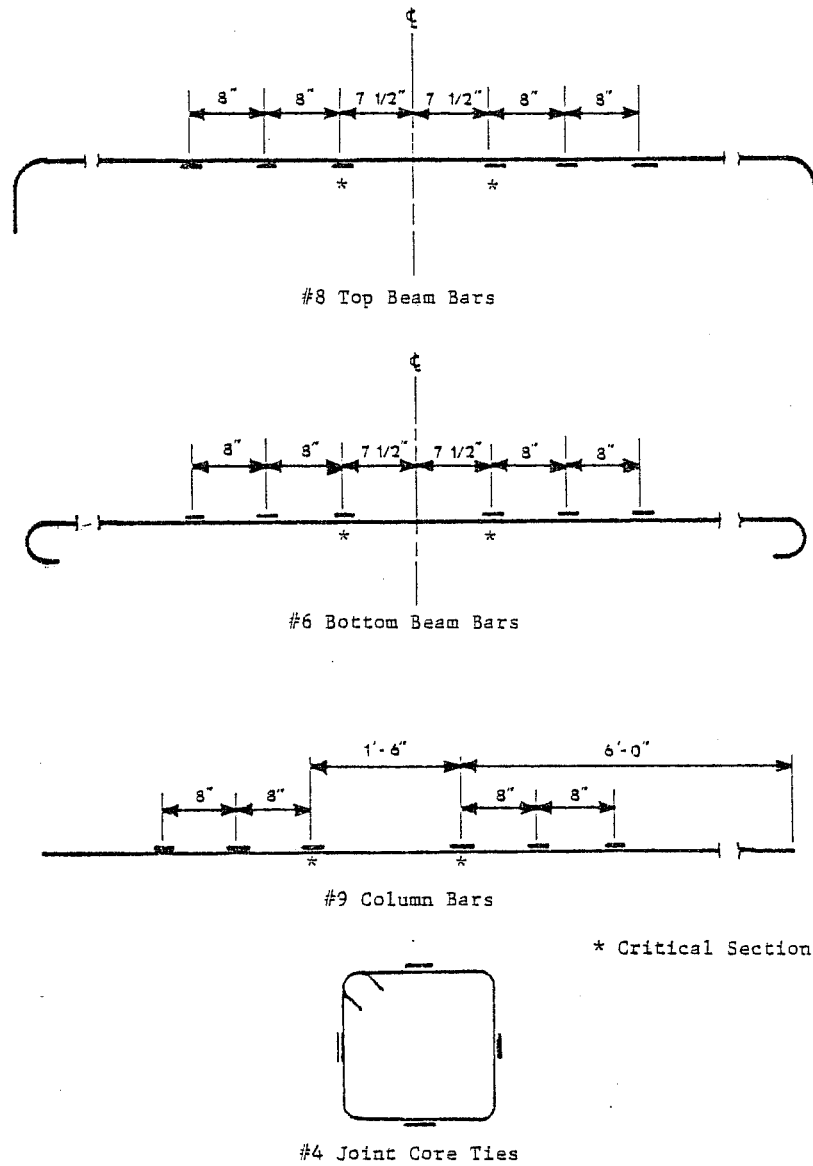
Fig. 3.18 Strain gage locations
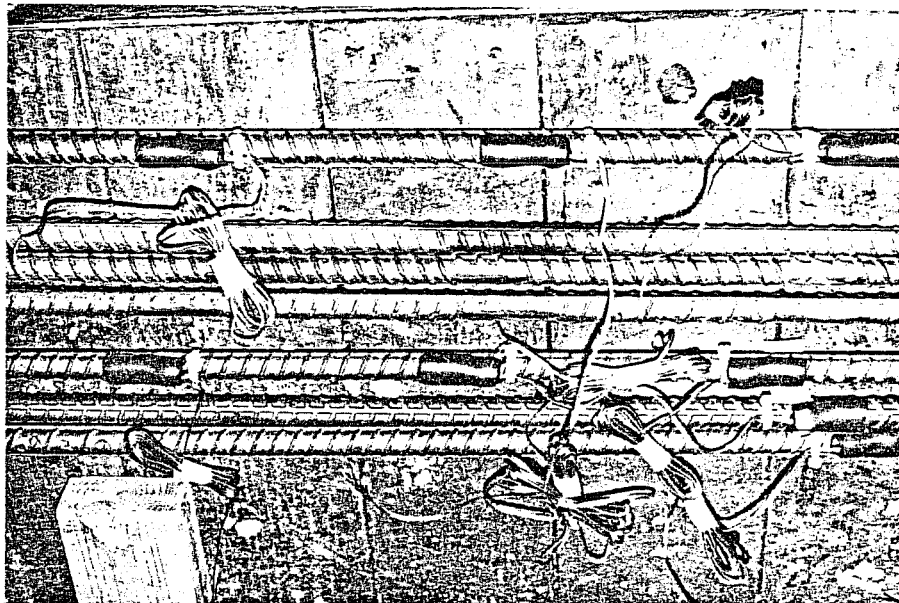
Fig. 3.19 Mounted strain gages
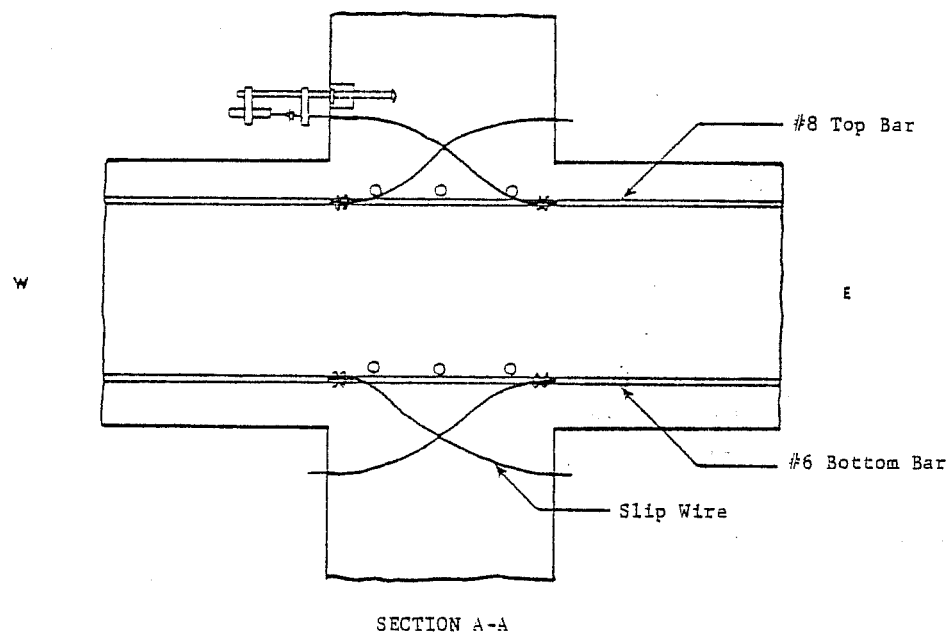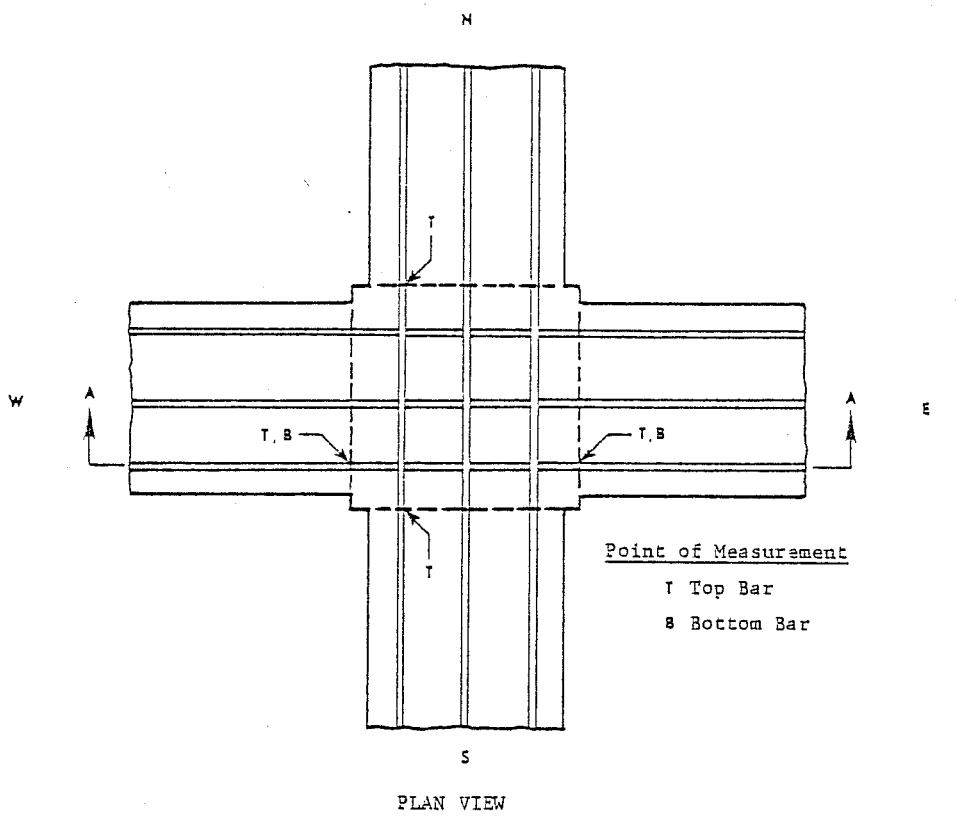
Fig. 3.20 Bar slip instrumentation

48
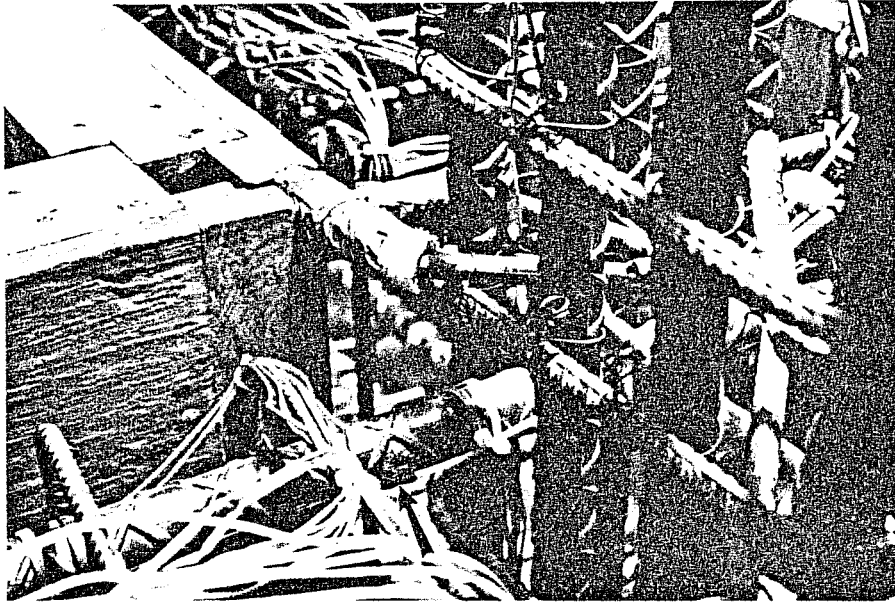
Fig. 3.21 Slip wire connection (see arrow)
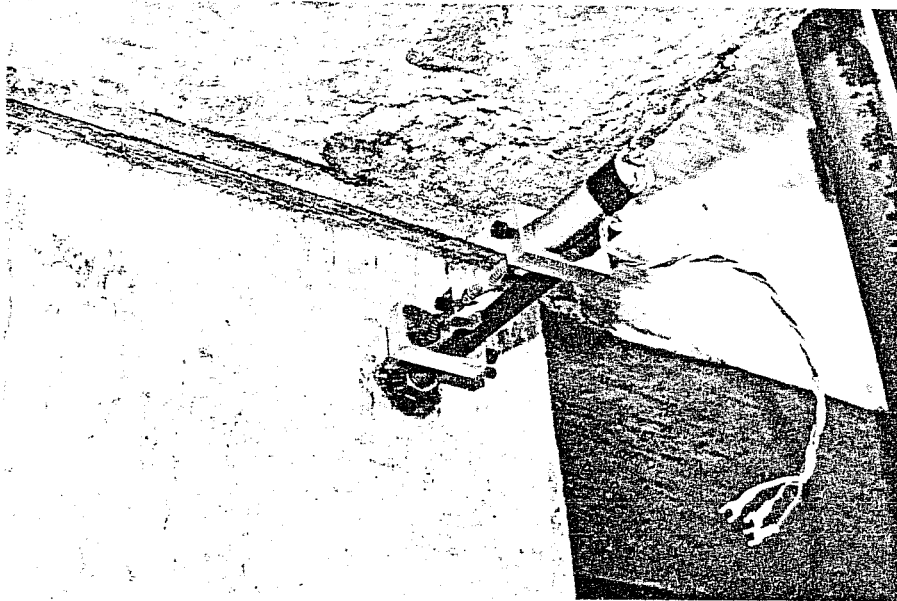
Fig. 3.22 Bar slip measuring device
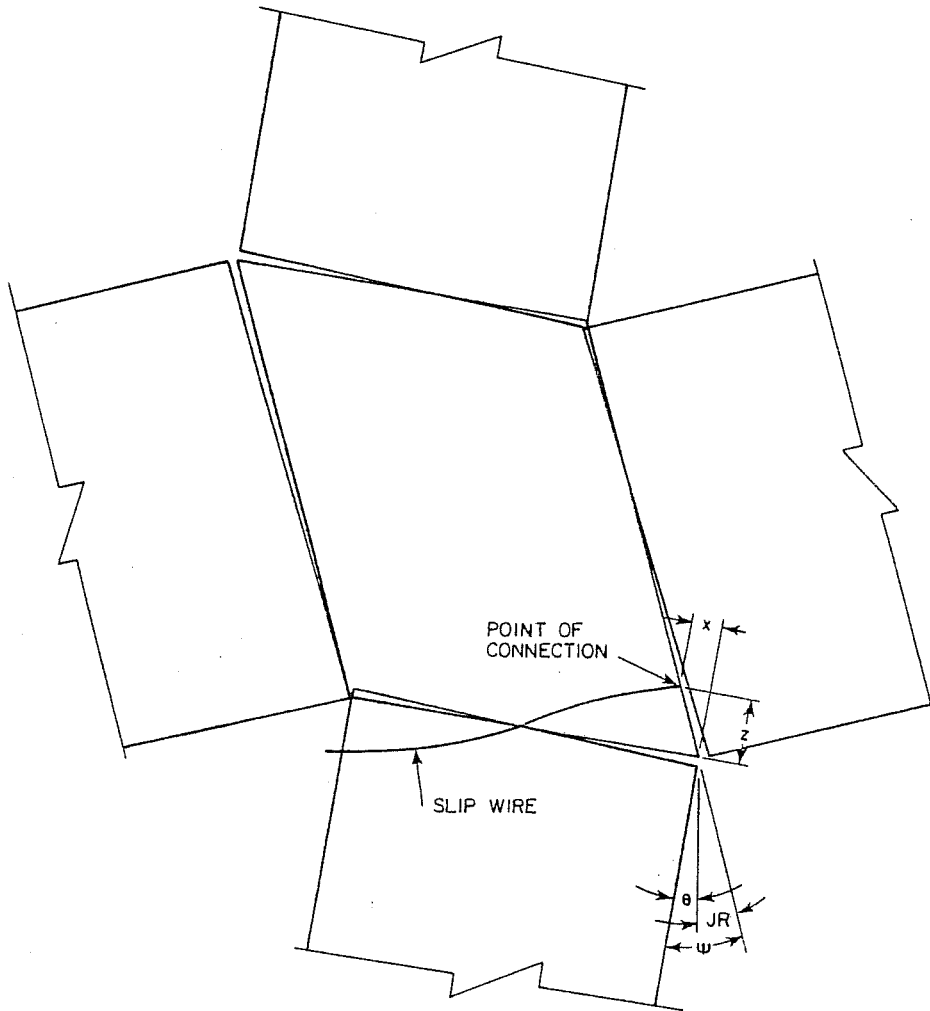
Fig. 3.23 Bar slip geometry

SL_c = corrected bar slip

SL = measured bar slip

z = distance from face of joint to $\mathcal{C}$ of bar

x = amount of correction

θ_1 = column rotation above (see Fig. 3.14)

θ_2 = column rotation below (see Fig. 3.14)

θ_f = elastic column rotation (see Fig. 4.20)

JR = joint rotation

θ = total column rotation (above or below)

Assuming an even split of column rotation above and below,

$$\theta = \frac{\theta_1 + \theta_2}{2} - \theta_f$$

From joint rotation calculation, recall that:

$$\theta_1 + \theta_2 = \frac{h_j}{L_c} JR$$

$$\theta = \frac{h_j}{2L_c} JR - \theta_f$$

$$\psi = \theta + JR$$

$$= \left(1 + \frac{h_j}{2L_c}\right) JR - \theta_f$$

$$x = \psi z$$

and

$$SL_c = SL - x$$

3.5 Test Procedure

Each specimen was pretested prior to the day of the full test. The specimens were subjected to one elastic cycle during the pretest, the purpose of which was to check the operation of the hydraulic and electrical systems. The maximum beam deflection at the peak of the elastic cycle was 0.3 in.

To start the main test, a data reading was taken with the specimen under zero load. The first reading is referred to as the zero reading and is the base from which all other readings are referenced. Next, a 300-kip axial load was applied to the column and another reading was taken. Readings were also taken after the N-S and E-W beam dead load deflections were imposed. Racking loads were then applied simultaneously to the N-S and E-W beams in increments, and data readings were taken at each increment. Loading of the beams was controlled with valves on the hydraulic consoles while the level of deflection of the north and west beams was continuously monitored with x-y recorders (see Fig. 3.24). A complete description of the applied load histories is given in Chapter 4.

3.6 Data Acquisition and Reduction

Data were taken electronically with a digital data acquisition system in conjunction with a mini-computer. On line data reduction enabled teletype monitoring of selected channels as the test progressed. The test data were stored on a computer disk and were later run through a data reduction program which converted the voltage readings into engineering units. Plot files of the channels were then created, and plots of selected channels were made. A digital plotter was a valuable tool which permitted the user to make plots of desired size and scale and to put titles on the plots.
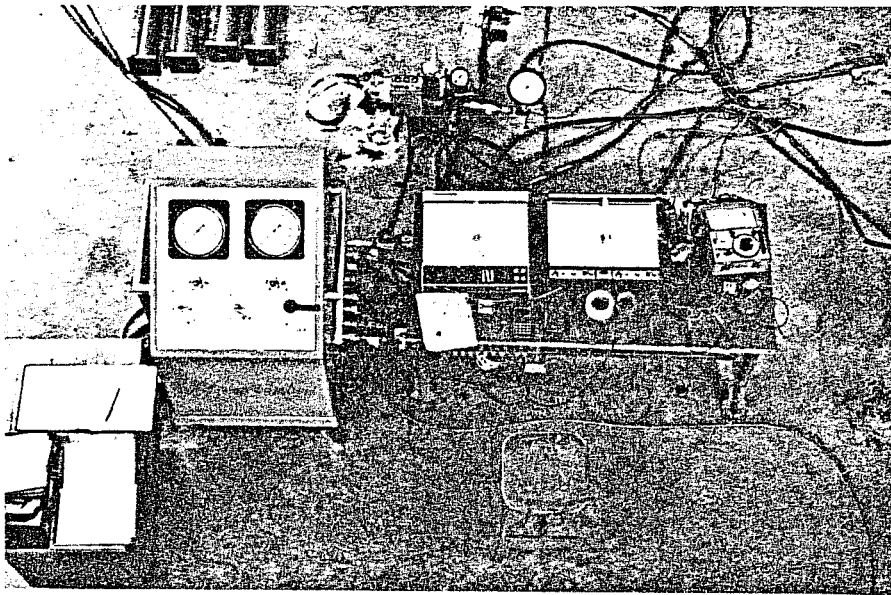
Fig. 3.24 Testing controls

C H A P T E R   4

TEST RESULTS AND BEHAVIOR

4.1 General

In this chapter, the test results of specimens 5-BS-A and
6-MBS-A are presented. Both specimens were subjected to deforma-
tion controlled racking loads at a 45° angle to the principal axes
of the subassembly. The loading pattern was chosen to simulate
seismic loadings which are produced at the beam-column joints of
reinforced concrete frames when the ground motion is skewed to the
principal axes of the structure. The difference in the two
tests was that specimen 6-MBS-A was monotonically loaded, and
specimen 5-BS-A was cyclically loaded. Comparisons of the test
results will show the effects of cycling of deformations on joint
performance.

The deformation levels which the specimens were subjected
to are denoted by multiples of Δ_i ($1\Delta_i$, $2\Delta_i$, etc.) which was
determined to be the yield deflection of the beams in specimen 1-U-C
and was established as the nominal yield deflection for all the
specimens. Specimens 5-BS-A and 6-MBS-A, however, had smaller
diameter beam reinforcement than specimen 1-U-C. Consequently,
the bond characteristics were better for specimens 5-BS-A and
6-MBS-A, and the beams reached yield at a lower deflection than
1-U-C. To maintain uniformity in the testing program, all the
specimens were subjected to the same levels of deformation. For
the two tests referred to in this chapter, the Δ_i designation
is only a reference deflection and does not correlate directly
with yield of the specimens.

4.2 Monotonic Test, 6-MBS-A

4.2.1 Description of Load History. The column of the monotonically loaded specimen was axially loaded with approximately 300 kips which was maintained throughout the test. After applying the axial load, a dead load deflection of 1/10 in. was imposed on each of the four beams. Next, the deflections producing racking were applied to the beams (see Fig. 4.1). The north and west beams were deflected downward (+), while the south and east beams were simultaneously deflected upward (-) by the same amount. The specimen was loaded in this direction until the loading ram reached maximum extension of 5 in. Although this concluded the monotonic test, the specimen was then cycled at the $3\Delta_i$ deformation level.

4.2.2 Load-Deflection Behavior. Plots of beam load versus beam end deflection in Figs. 4.2 and 4.3 show that the beam ultimate loads were very close to the calculated ultimate loads and remained essentially constant as the beams were deflected to the limit of the loading apparatus. This indicates that any strength degradation of the specimen subjected to cyclic loads is due to load reversal and cycling rather than a decrease in the capacity of the joint at high deformations. The cycles subsequent to the monotonic loading show a large reduction in strength and stiffness. Near the neutral position, deflections of the beams were accompanied by only slight changes in load. The low stiffness could be due to a combination of both beam and column bar slip and shearing of the joint region, and the loss of strength may be due to degradation of concrete strength and loss of cross-sectional area due to spalling of cover concrete.

4.2.3 Cracking Patterns. Joint shear cracks were first visible at the northeast and southwest corners of the joint at load stage 9 as shown in Fig. 4.4. At this stage, the north and south beam deflections were +0.52 and -0.43 in., respectively. In

55
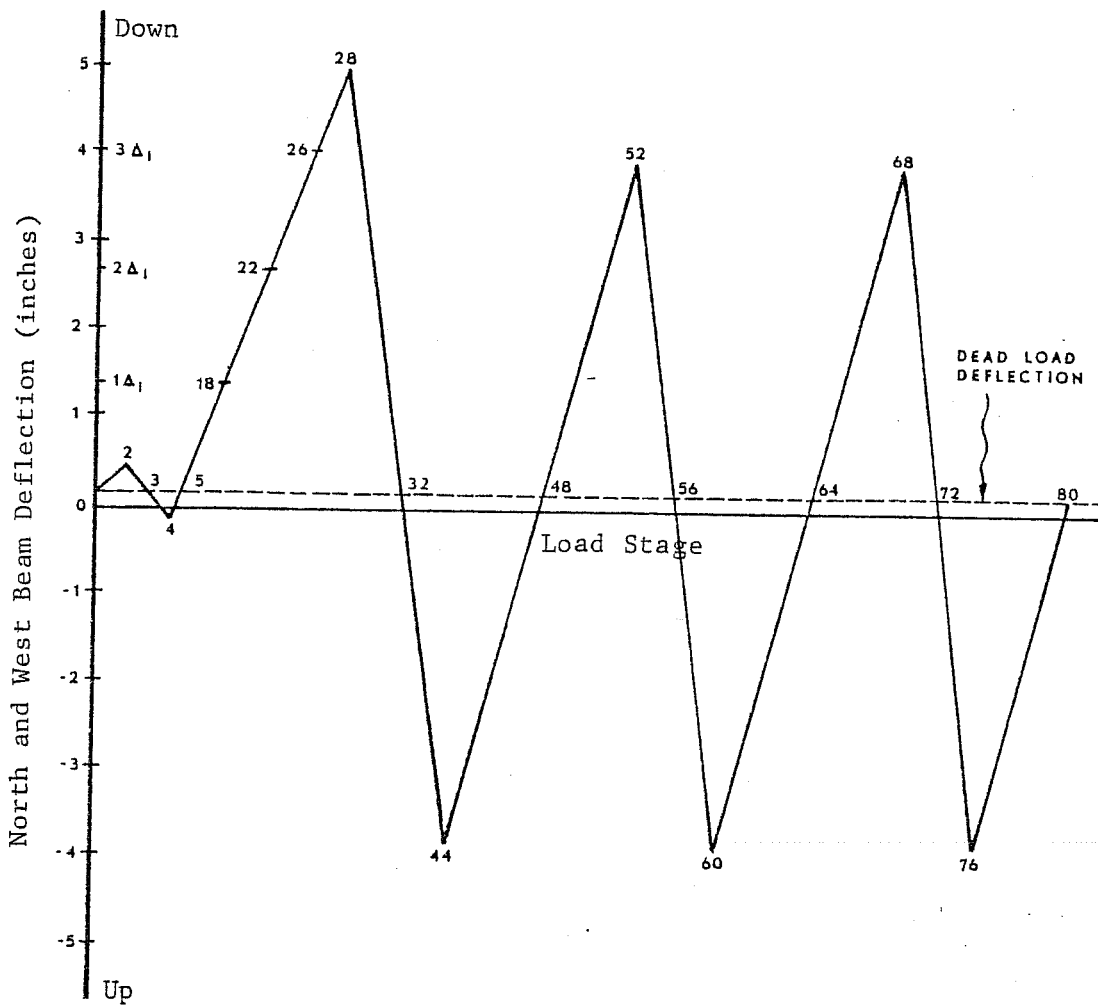
Fig. 4.1   Specimen 6-MBS-A load history
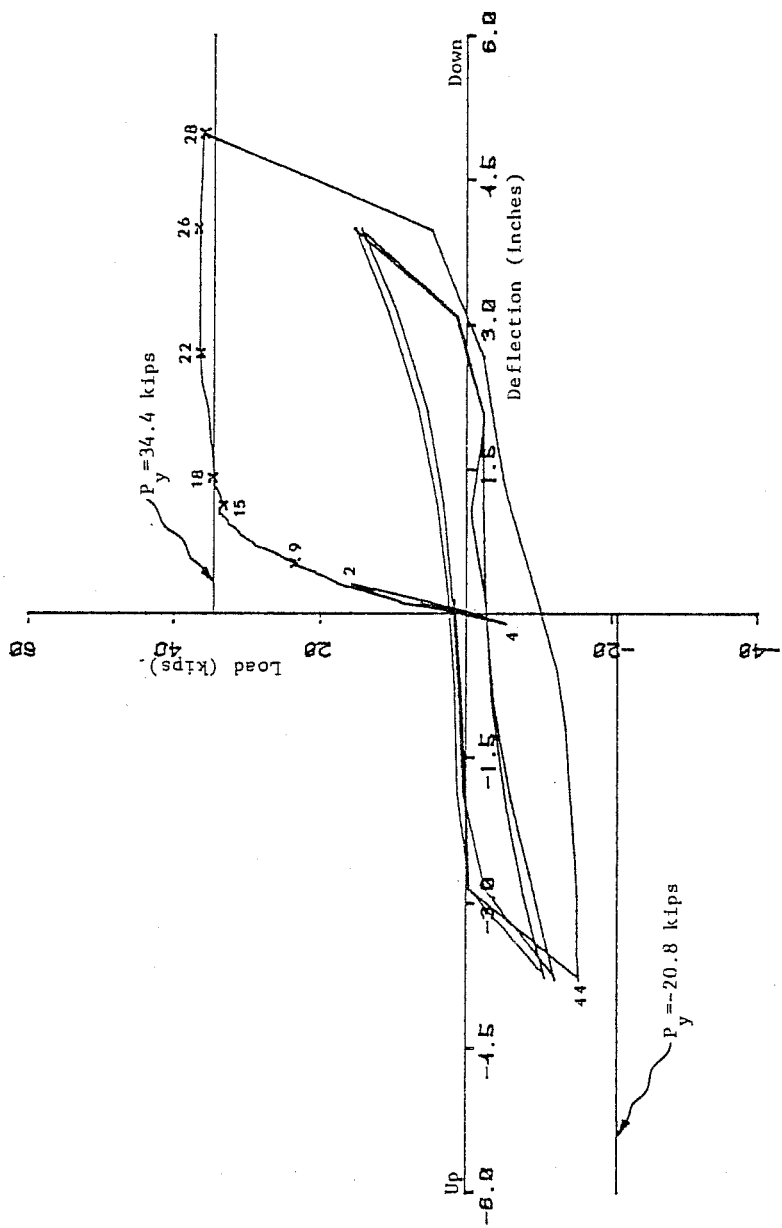
Fig. 4.2   Load deflection behavior, 6-MBS-A (north beam)
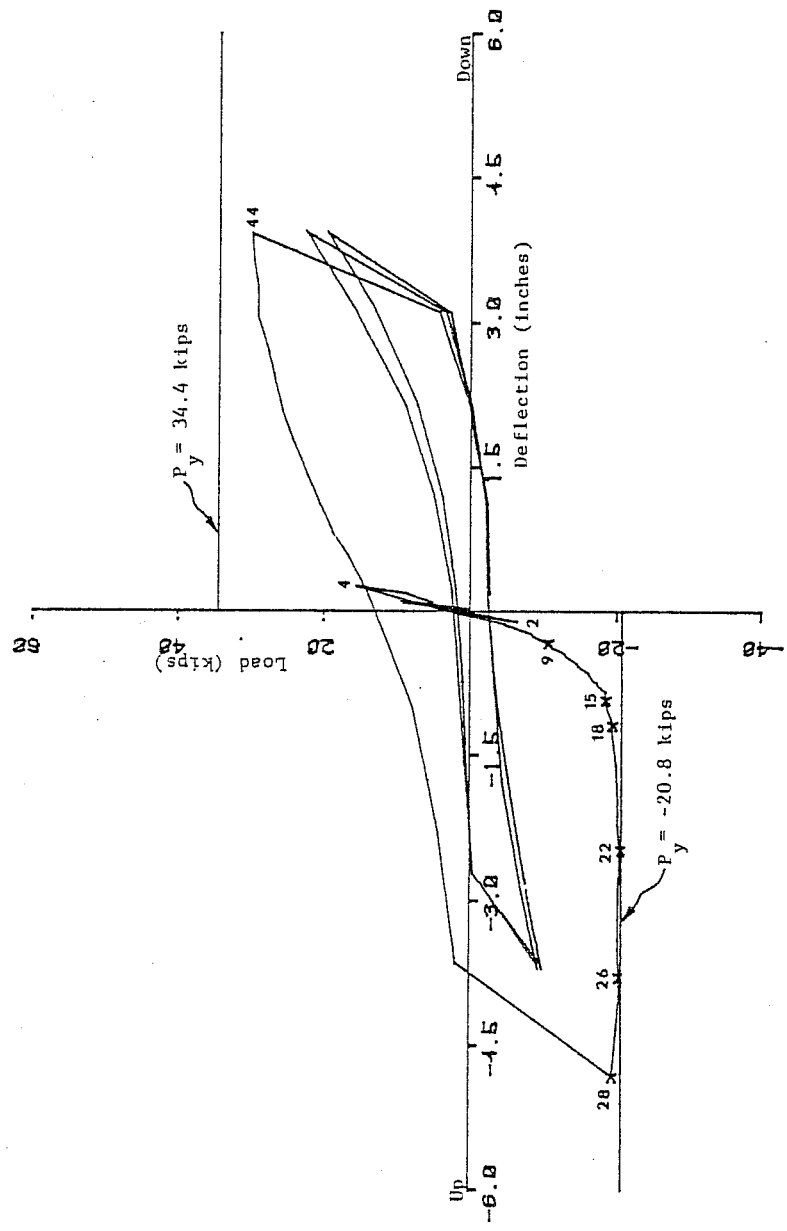
Fig. 4.3 Load deflection behavior, 6-MBS-A (south beam)
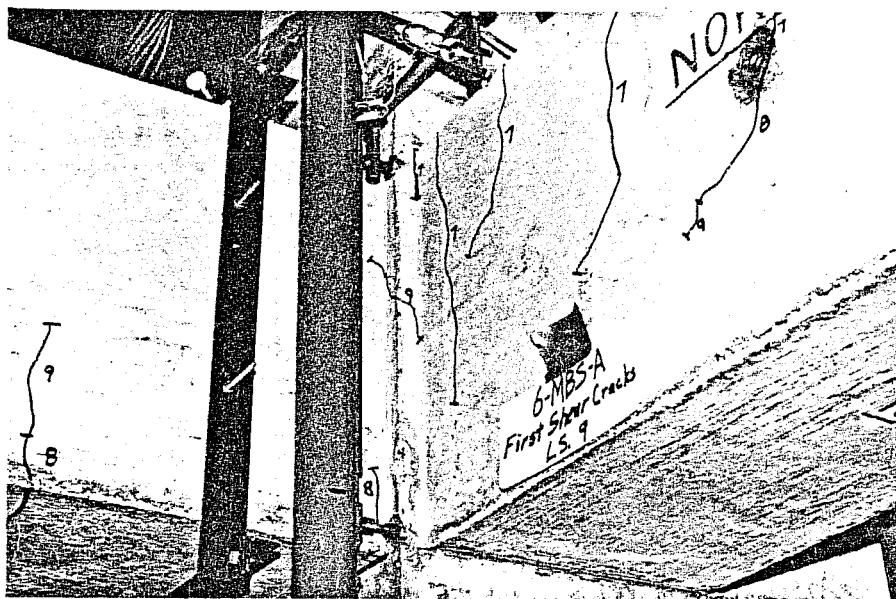
Fig. 4.4   First shear cracks, 6-MBS-A

addition to joint shear cracks, flexural and flexural-shear cracks in the beams were also visible. At load stage 15, the north and south beam deflections were 1.12 and -0.92 in., respectively, and first yielding of the beam reinforcement was evident as the beam loads increased very little as higher deformations were imposed. Figure 4.5 shows that joint shear cracking extended well into the beams at this stage. At the $1\Delta_i$ deformation, considerable cracking of the joint region had occurred and in Fig. 4.6, the diagonal shear cracks of the southwest corner of the joint are shown. Figure 4.7 shows that at $2\Delta_i$ deformation, crushing of the cover concrete had occurred in the compressive zone of the lower column. In addition, splitting cracks were observed on the top of the north and west beams. The north beam, which had an inch less top cover concrete than the west beam, had more splitting along the longitudinal beam bars (see Fig. 4.8). At peak deformation under monotonic loading, extensive joint shear cracking was visible as shown in Fig. 4.9. Joint shear cracking extended into the compression zone of the north beam fracturing the corner of the beam cross section. Also, the compression zone of the lower column showed considerable distress.

4.3 Cyclic Test, 5-BS-A

4.3.1 Description of Load History. The cyclically loaded specimen was initially subjected to a 300-kip axial load and 1/10 in. beam dead load deflections (same as the monotonic test). Then cracking loads were applied as shown in Fig. 4.10. The north and west beams were deflected downward (+) while the south and east beams were simultaneously deflected upward (-) by the same amount. The beams were loaded to a deflection of $1\Delta_i$ and then cyclic loading was applied. The same loading procedure was used for the $2\Delta_i$ and $3\Delta_i$ deformation levels with three cycles at each level.
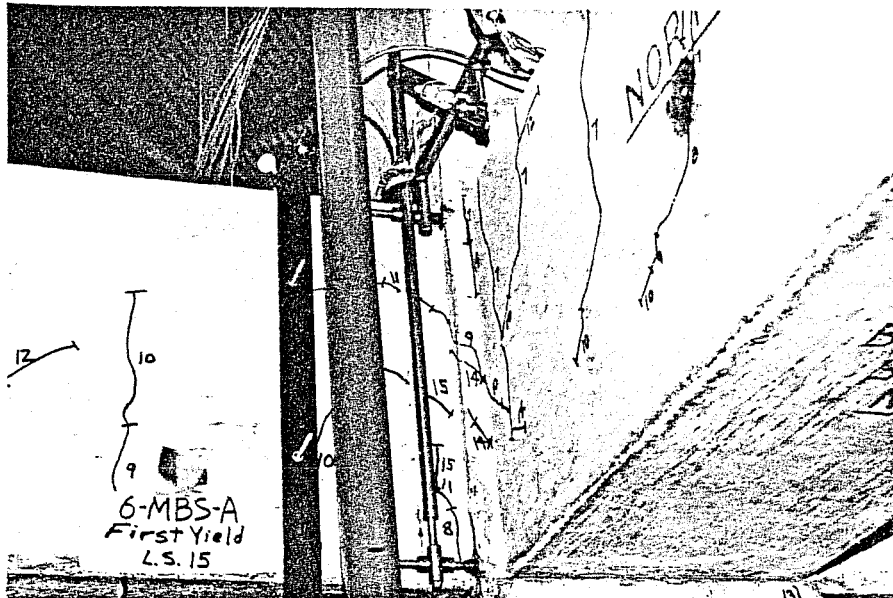
Fig. 4.5   Shear cracking at first yield, 6-MBS-A
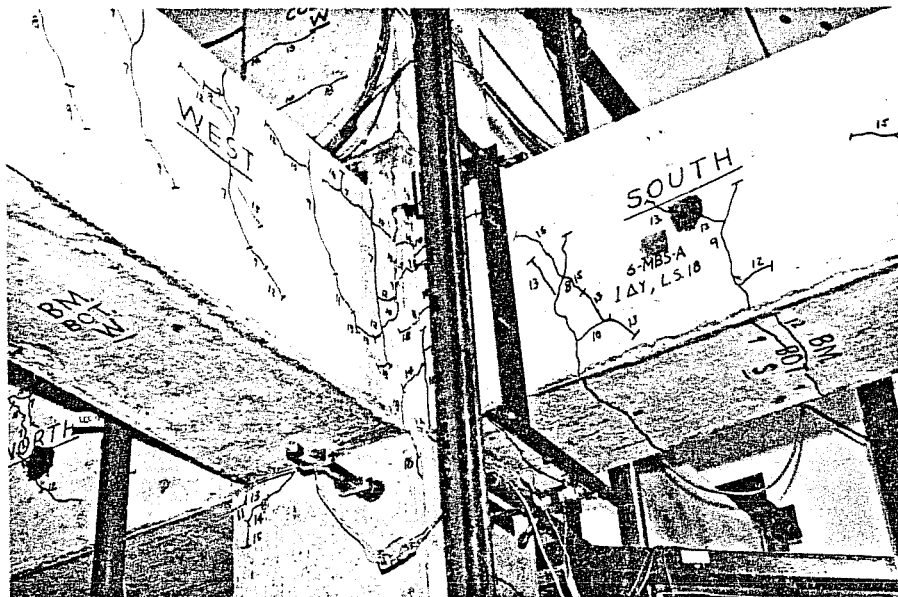
Fig. 4.6   Shear cracking at $1\Delta_i$, 6-MBS-A
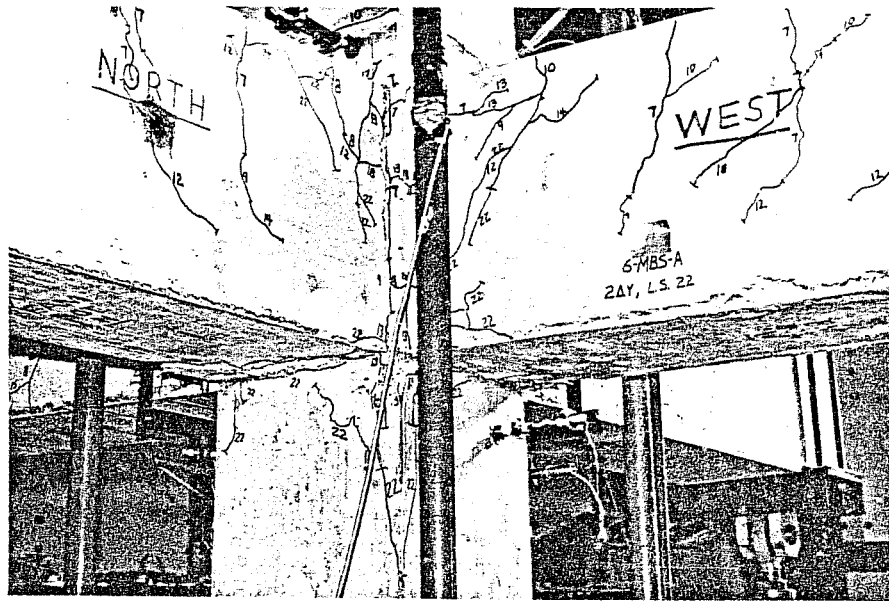
Fig. 4.7   Shear cracking at $2\Delta_i$, 6-MBS-A
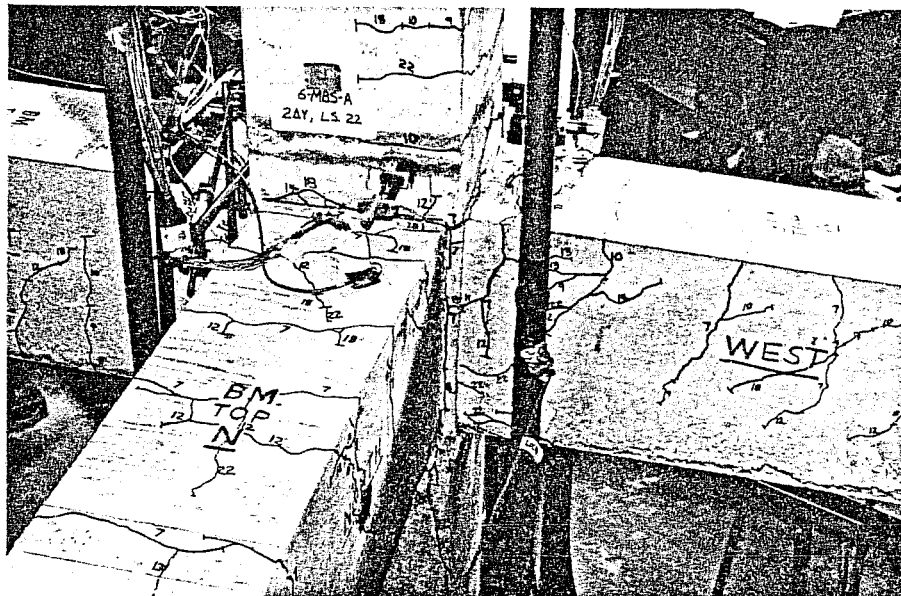
Fig. 4.8   Splitting cracks at $2\Delta_i$, 6-MBS-A
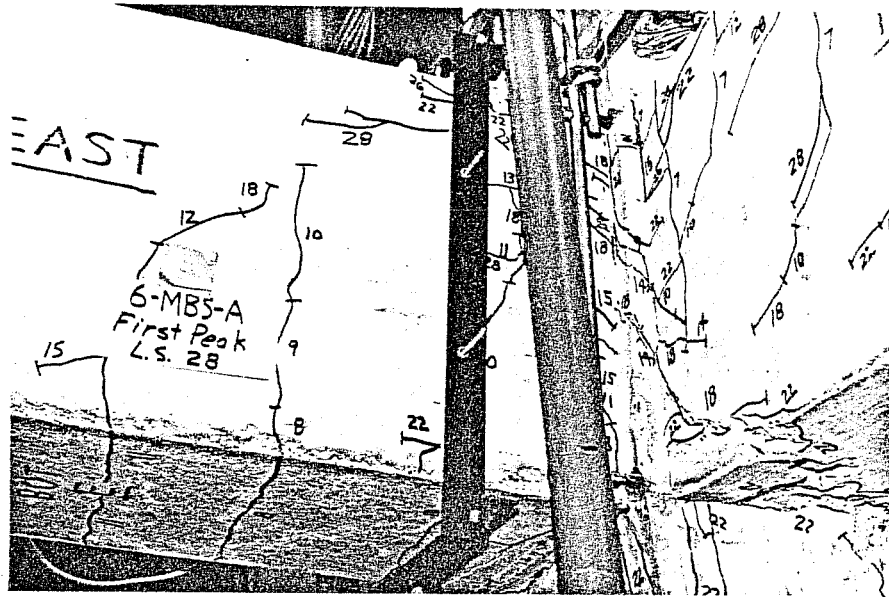
Fig. 4.9 Shear cracking at peak deformation, 6-MBS-A
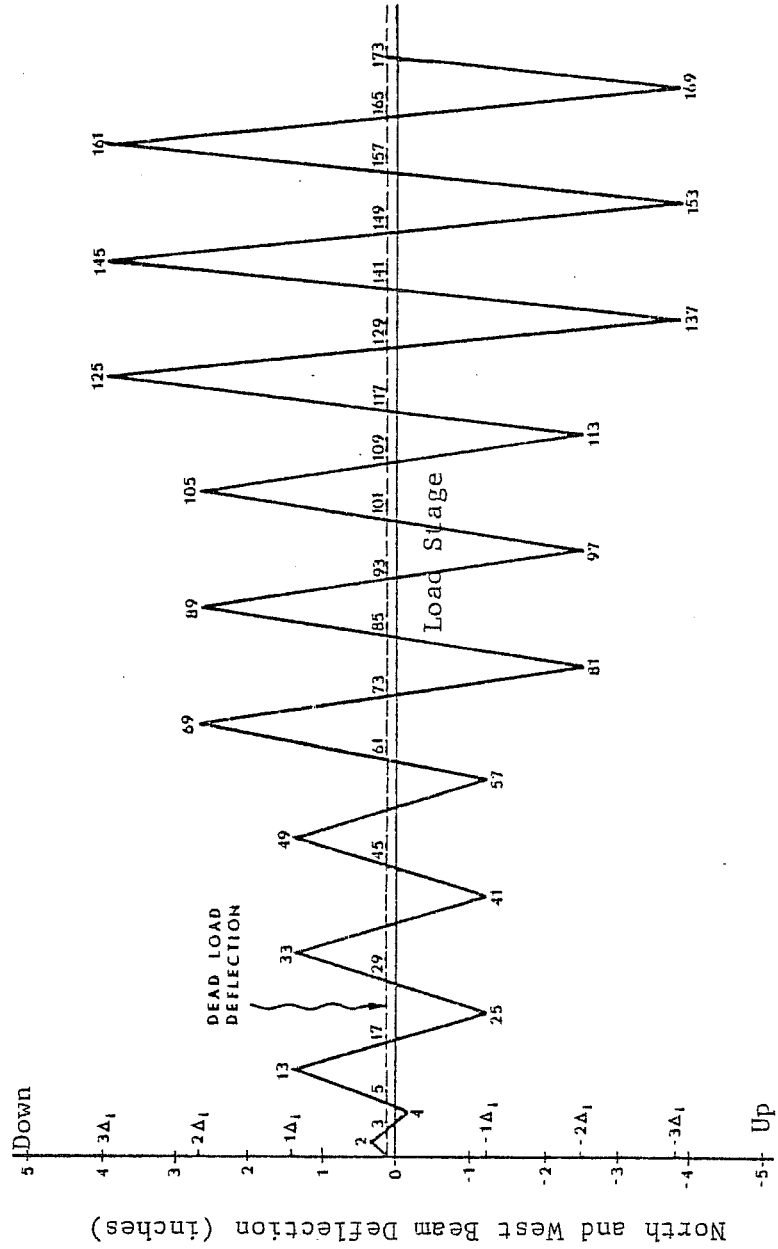
Fig. 4.10 Specimen 5-BS-A load history

4.3.2 <u>Load-Deflection Behavior</u>. The beam load versus beam end deflection plots (see Figs. 4.11 and 4.12) show that the stiffness degrades substantially during the first cycle at a deformation level. This indicates that most of the damage to the joint occurs during the initial excursion to a higher deformation. There was some further degradation of stiffness during the second and third cycles as well. Except for the initial loading at a given deformation, the load-deflection behavior was characterized by severe pinching of the hysteresis loops. This behavior indicates that joint shear distortion and/or reinforcing bar slip was a major influence on the performance of the joint.

Although there was a large degradation of stiffness after cycling at $1\Delta_i$, the beam loads reached calculated ultimate load when the beams were deformed to $2\Delta_i$. At $3\Delta_i$, however, strength degradation was evident as the beam loads were well below the calculated strengths. The initial direction of loading influenced the strength when the load was reversed. The beam loads were always less than the calculated strength at the second peak of the first cycle at any given deformation. This may be due to degradation of bond of the tensile reinforcement during the initial excursion, so that the reinforcement was not effective in compression when the load was reversed. Also, degradation of the bond through the joint will cause tensile stresses to be produced in the reinforcement in the compressive zones of the beams. The result will be higher compressive stresses in the concrete and will lead to faster deterioration of the beam (see Fig. 4.13). Similar behavior can occur in the column as well.

4.3.3 <u>Cracking Patterns</u>. The cracking patterns of the cyclically loaded specimen were similar to the monotonically loaded specimen up to the first peak at $1\Delta_i$ deformation. The load histories for the two specimens were the same at this stage. After

65
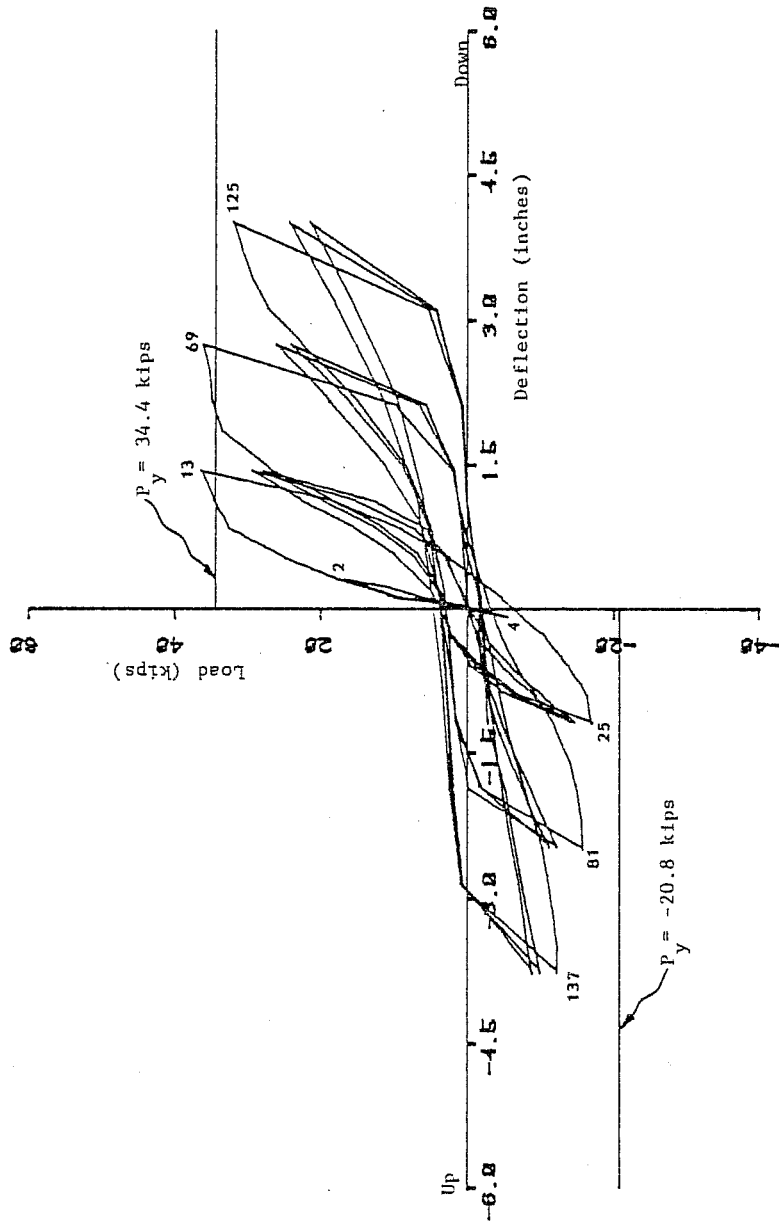
Fig. 4.11 Load deflection behavior, 5-BS-A (north beam).
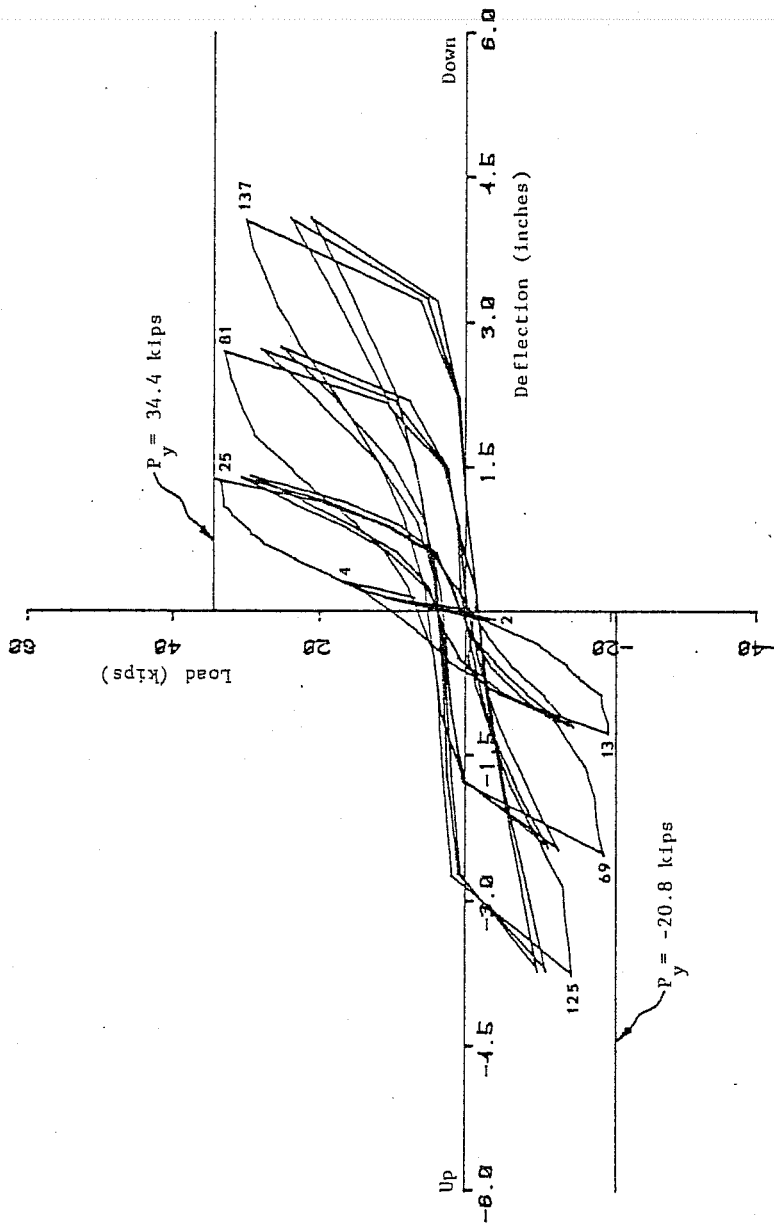
Fig. 4.12   Load deflection behavior, 5-BS-A (south beam)

East   Bond Forces   West
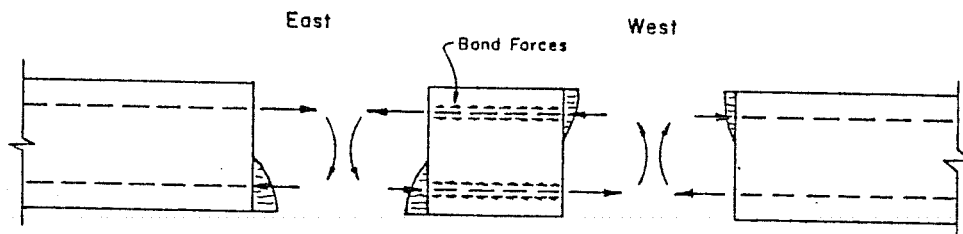
a) Force Equilibrium Required by Strain Compatibility

Shear Cracks   Loss of Bond
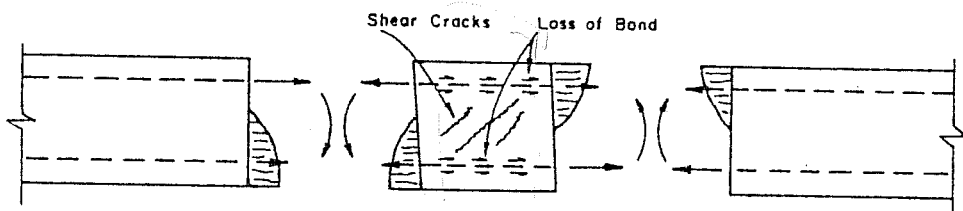
b) Force Equilibrium Because of Shear and Bond Failure

Fig. 4.13   Force equilibrium of joint failing by shear and bond[6]

reversing the load, crossing of the joint shear cracks was observed in the northeast and southwest corners of the joint. The joint shear cracks are visible where the north and east beams frame into the column as shown in Fig. 4.14. An overall view of the cracking patterns is shown in Fig. 4.15. In addition, splitting cracks were observed on top of the north and south beams. Few splitting cracks were observed on the top of the east and west beams since the top cover concrete was greater for those beams. However, splitting cracks were observed on the sides of the east and west beams. After cycling three times at $1\Delta_i$, very few new cracks appeared, but extensions of existing cracks were observed. Figure 4.16 shows a general view of the specimen after three cycles at $1\Delta_i$

68
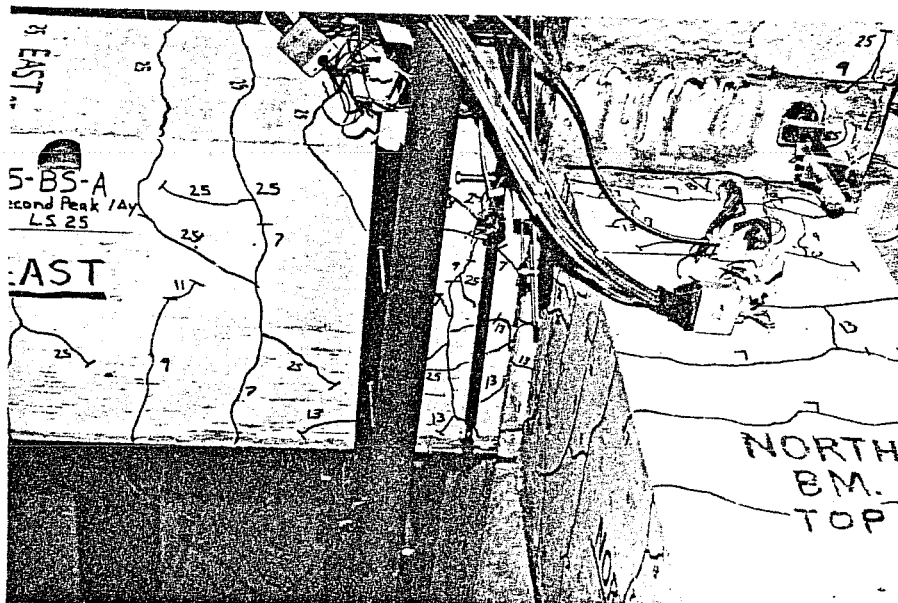
Fig. 4.14 Joint shear cracking at second peak, $1\Delta_i$, 5-BS-A
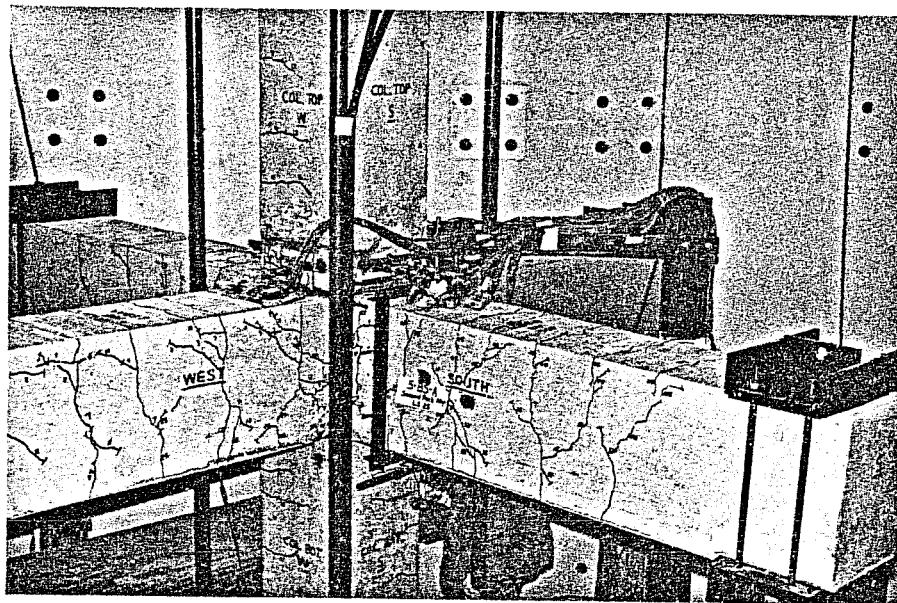
Fig. 4.15 General view at second peak, $1\Delta_i$, 5-BS-A

Fig. 4.16   General view after 3 cycles, 5-BS-A

As cycling at higher deformations continued, the concrete
cover at the column compression zones progressively deteriorated.
Figure 4.17 is a photograph of the specimen after the loose concrete
had been removed upon completion of the test. Notice that the
deterioration of the column was greater at the bottom of the joint
than at the top. Another interesting observation was that the
cracks that formed at the beam-column boundaries varied in width
from one side of the beam to the other. It was not apparent
whether the cracks were a result of column or beam rotation, but the
varying width indicated that the cracks were formed at least
partially by column rotation.

4.4 Comparison of Monotonic and Cyclic Tests

4.4.1 General. A decline in joint performance due to cycling
of deformations can be shown by comparing the plots of joint rotation
versus interstory displacement for the cyclic and monotonic tests
(see Fig. 4.18). At equivalent deflections, the cyclically loaded
specimen had higher joint rotation than the monotonically loaded
specimen. At $3\Delta_i$, the joint rotation for the cyclic test was
44 percent higher than that of the monotonic test. This indicates
that cycling caused damage to the joint which resulted in higher
joint rotation when the next deformation level was imposed.

4.4.2 Components of Beam Deflection. Several of the
mechanisms which contributed to the total deformation of the
specimens were either calculated or measured. The mechanisms were
inelastic beam rotation, inelastic column rotation, joint shear
strain, and elastic flexural deformation of both the column and beams.
To appreciate the relative influence of the component deformations,
beam-end deflection was selected as a common reference and deflec-
tions were calculated for each of the components. Figure 4.19
shows schematic representations of the various components. Notice
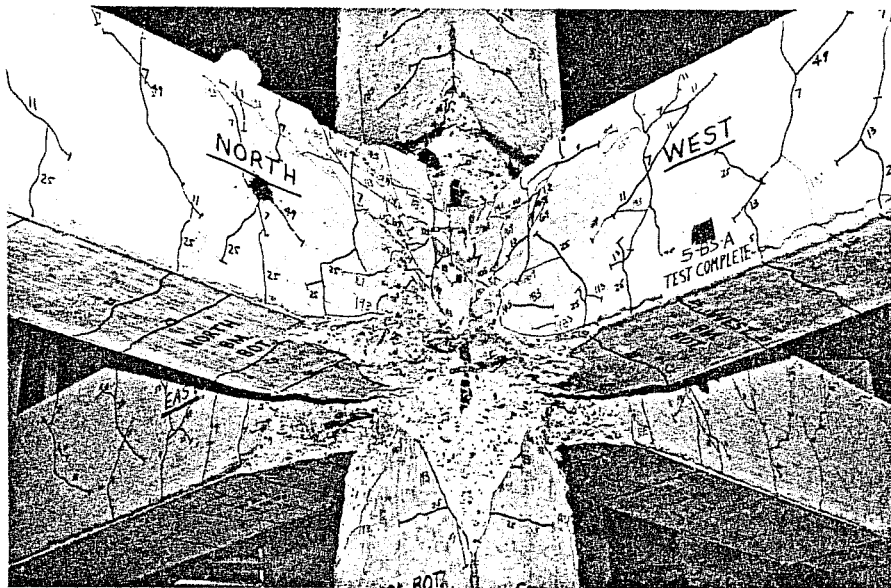
Fig. 4.17   Specimen 5-BS-A after testing
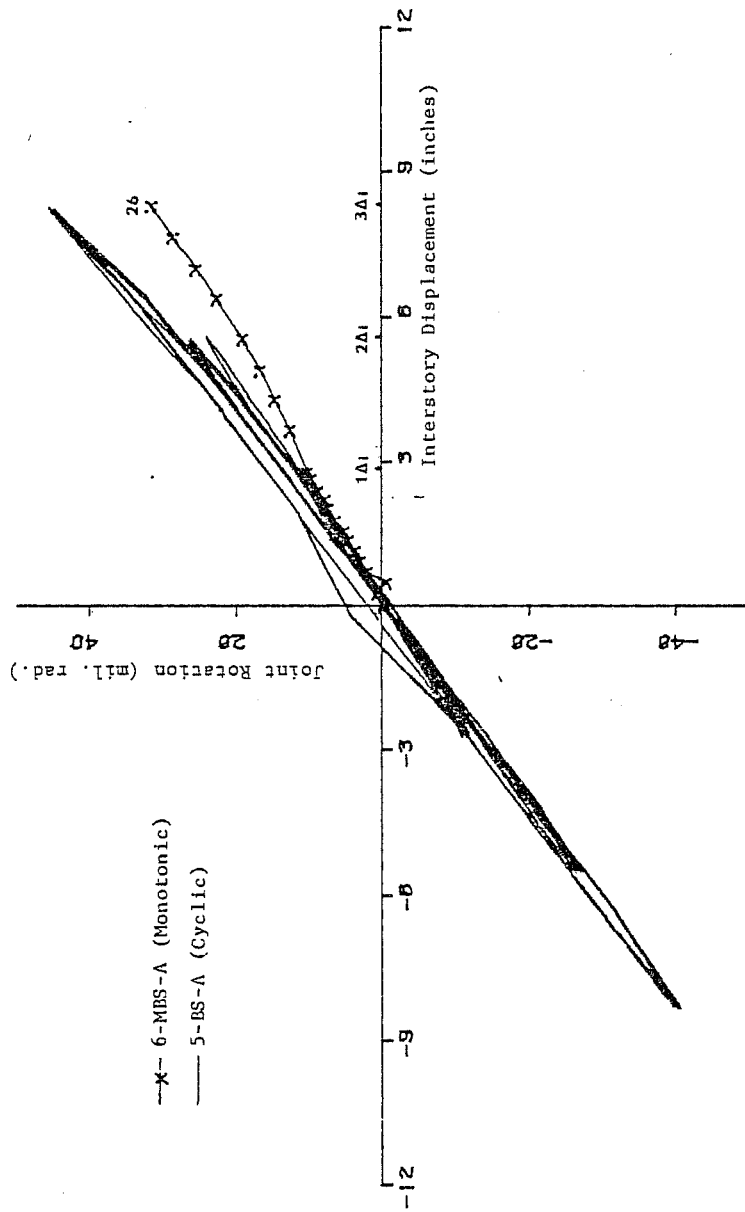
Fig. 4.18 Joint rotation versus interstory displacement (N-S direction)

73

a) Elastic Flexure

b) Beam Inelastic Rotation

c) Joint Shear Strain

d) Column Inelastic Rotation
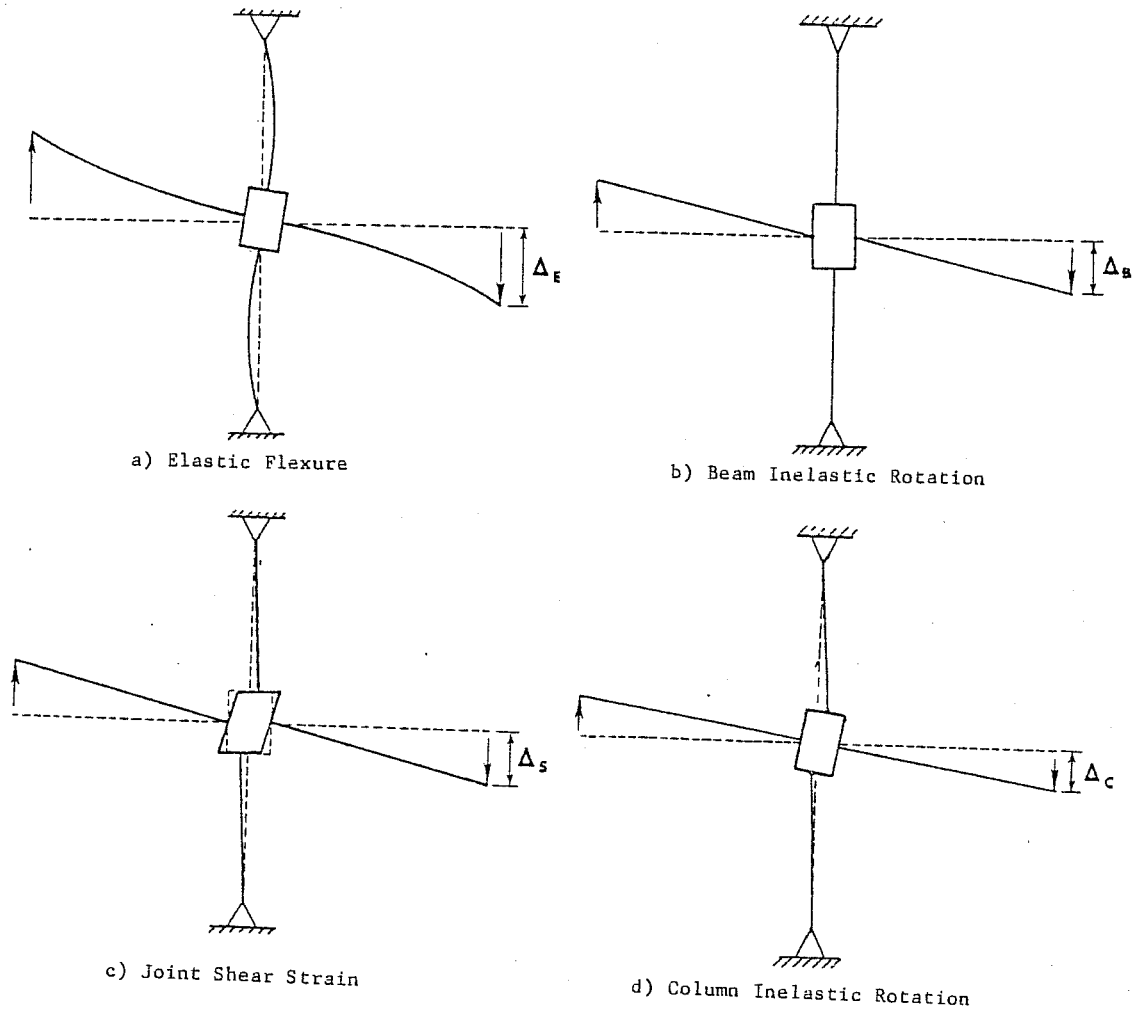
Fig. 4.19   Components of beam deflection

that all of the mechanisms except beam rotation, contribute to the rotation of the joint.

Beam deflection due to beam and column <u>elastic flexural deformation</u>, Δ_E, was calculated as shown in Fig. 4.20. The gross moment of inertia of the column was used in the calculations, and based on the results of the elastic test, the moment of inertia of the beam was determined to be approximately ¼ the gross value. Figure 4.21 shows the geometry of the specimen due to joint shear strain and the calculation of the beam deflection due to <u>joint shear strain</u>, Δ_S, is given below.

$$\Delta_S = \varphi_2 L_b - \varphi_1 W_j / 2$$

where φ_2 = component of joint rotation due to joint shear strain, rad.

Note: $\Delta_1 = \varphi_1 \ell_c = \varphi_2 h_j / 2 \Rightarrow \varphi_1 = \dfrac{\varphi_2 h_j}{2L_c}$

α = joint shear strain, rad.

$$= \varphi_1 + \varphi_2$$

$$= \frac{\varphi_2 h_j}{2L_c} + \varphi_2$$

Therefore,

$$\varphi_2 = \frac{\alpha L_c}{L_c + h_j/2}$$

From above,

$$\varphi_1 = \varphi_2 \frac{h_j}{2L_c}$$
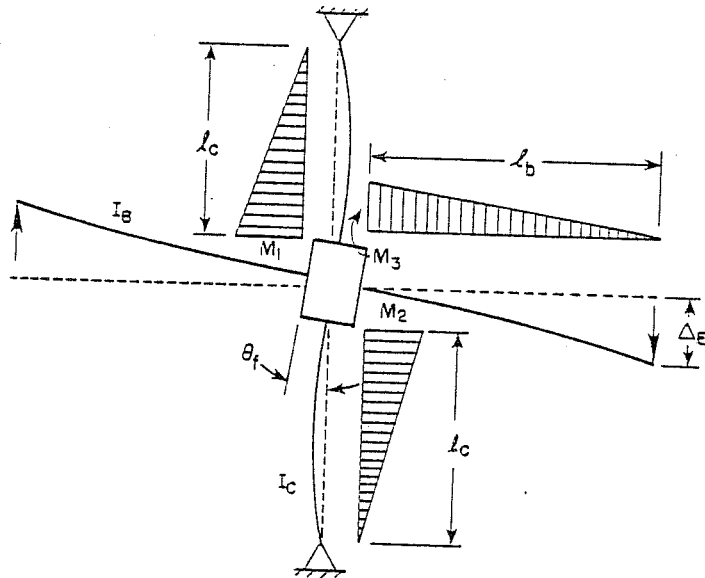
$$\theta_f = \left(\frac{M_1 + M_2}{2}\right) \frac{1}{EI_c} \; (\ell_c)(\tfrac{1}{2}) \frac{2}{3}$$

$$\Delta_E = \theta_f(\ell_b + W_j/2) + \frac{M_3}{3EI_B} \ell_b^2$$

$$E = 57000\sqrt{f'_c} \approx 3800 \text{ ksi}$$

$$I_c = \frac{bh^2}{12} = \frac{15^4}{12} = 4220 \text{ in.}^4$$

$$I_B \approx \frac{1}{4}\frac{bh^3}{12} \approx 1500 \text{ in.}^4 \text{ (based on test results)}$$

$$\ell_c = 63 \text{ in.}$$

$$\ell_b = 54 \text{ in.}$$

$$W_j = 15 \text{ in.}$$

$$\therefore \Delta_E = (1.31 \times 10^{-6})\left(\frac{M_1 + M_2}{2}\right) + (1.71 \times 10^{-4})M_3$$

Fig. 4.20   Calculation of elastic flexural deformation
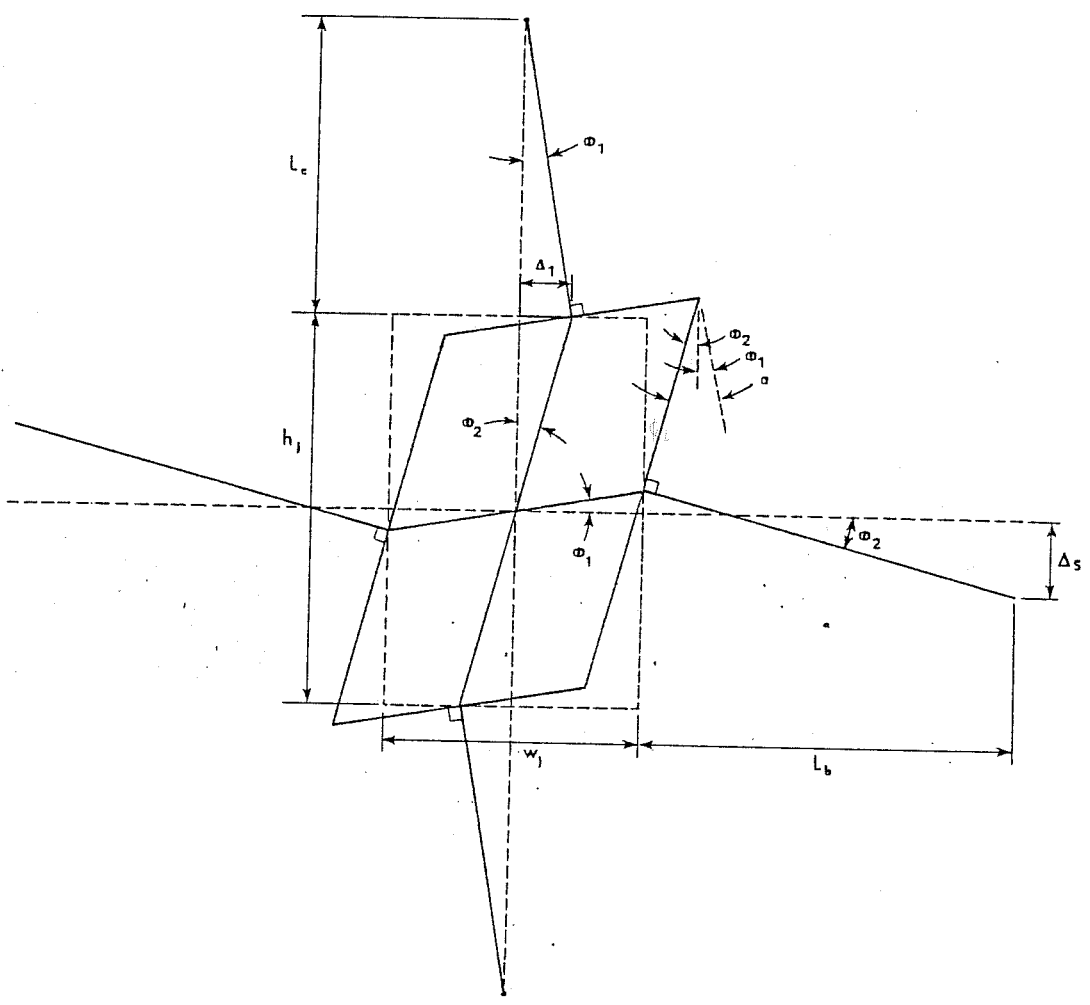
Fig. 4.21   Joint shear strain geometry

$$\varphi_1 = \left(\frac{\alpha L_c}{L_c + h_j/2}\right)\frac{h_j}{2L_c}$$

$$= \frac{\alpha h_j}{2L_c + h_j}$$

$$\Delta_S = \left(\frac{\alpha L_c}{L_c + h_j/2}\right)L_b - \left(\frac{\alpha h_j}{2L_c + h_j}\right)\frac{W_j}{2}$$

For this geometry, L_c = 63 in., L_b = 60.5 in., h_j = 18 in., W_j = 15 in.

Therefore,

$$\Delta_S = 52\ \alpha,\ \text{in.}$$

Beam deflection due to <u>beam inelastic rotation</u>, Δ_B, was simply the beam rotation multiplied by the length of the beam. This component also includes the flexural rotation of the beam between the column face and the bracket from which the beam rotation was measured. The fourth component of beam deflection was due to <u>the inelastic rotation of the column</u>, Δ_c. This component was calculated by subtracting the other components from the measured total beam deflection.

$$\Delta_c = \Delta_{total} - \Delta_E - \Delta_S - \Delta_B$$

Ratios of the components of beam deflection were calculated using the total beam deflection as the base. Comparisons of the monotonic and cyclic tests are shown in Figs. 4.22 through 4.25 which show the component ratios plotted against the total beam deflection. Figure 4.22 shows that the ratio of elastic flexural deformation decreased as the total deformation increased. At high beam deflections, the inelastic mechanisms contributed a greater percentage of the total deflection and the percentage of elastic

78
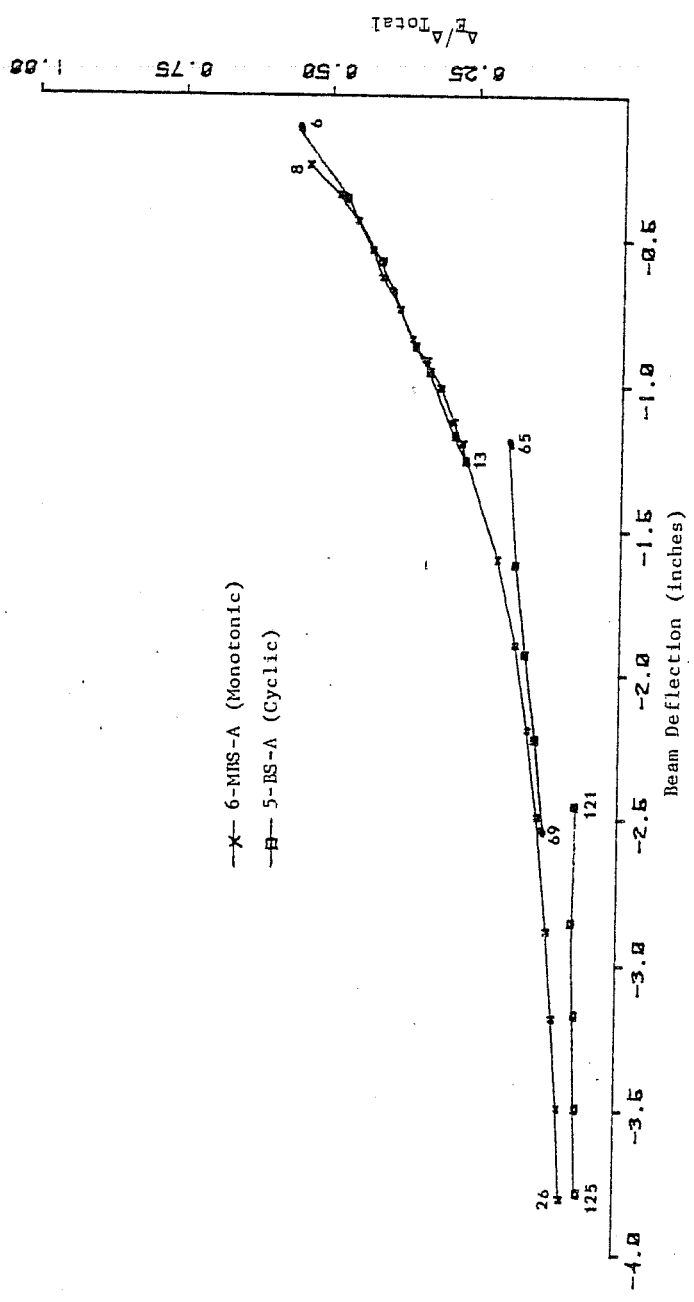
Fig. 4.22 Ratio of elastic flexural deformation
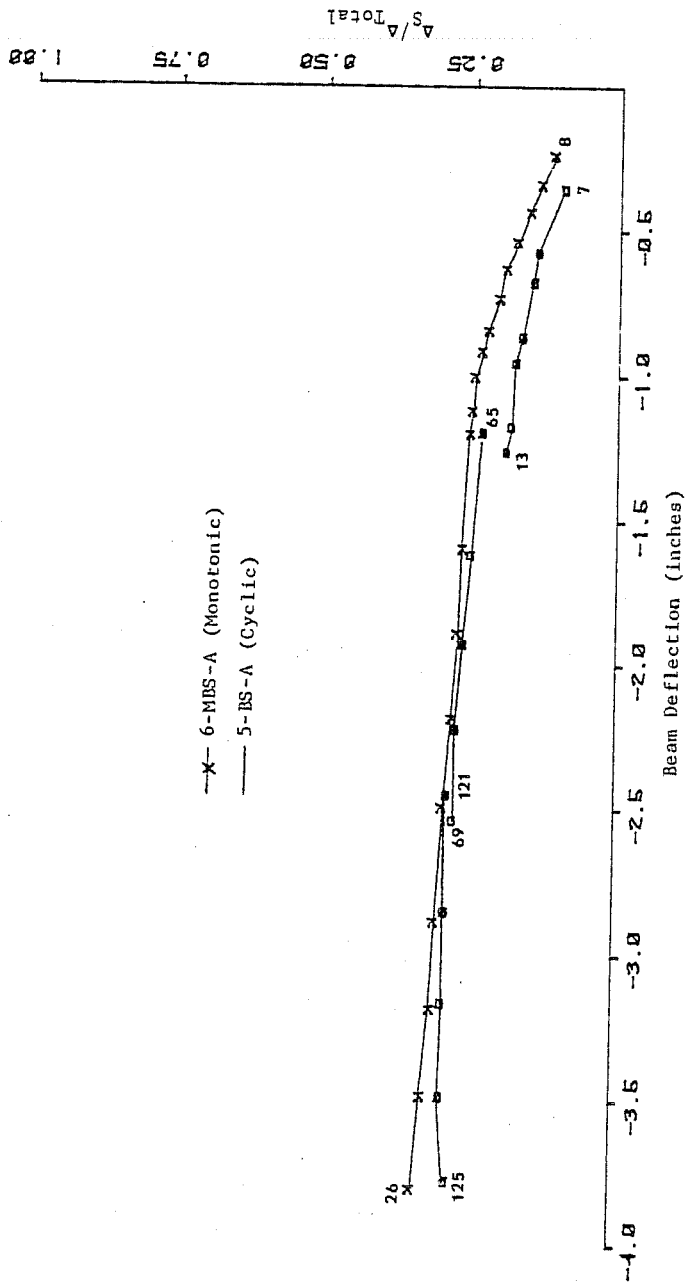
Fig. 4.23 Ratio of joint shear deformation
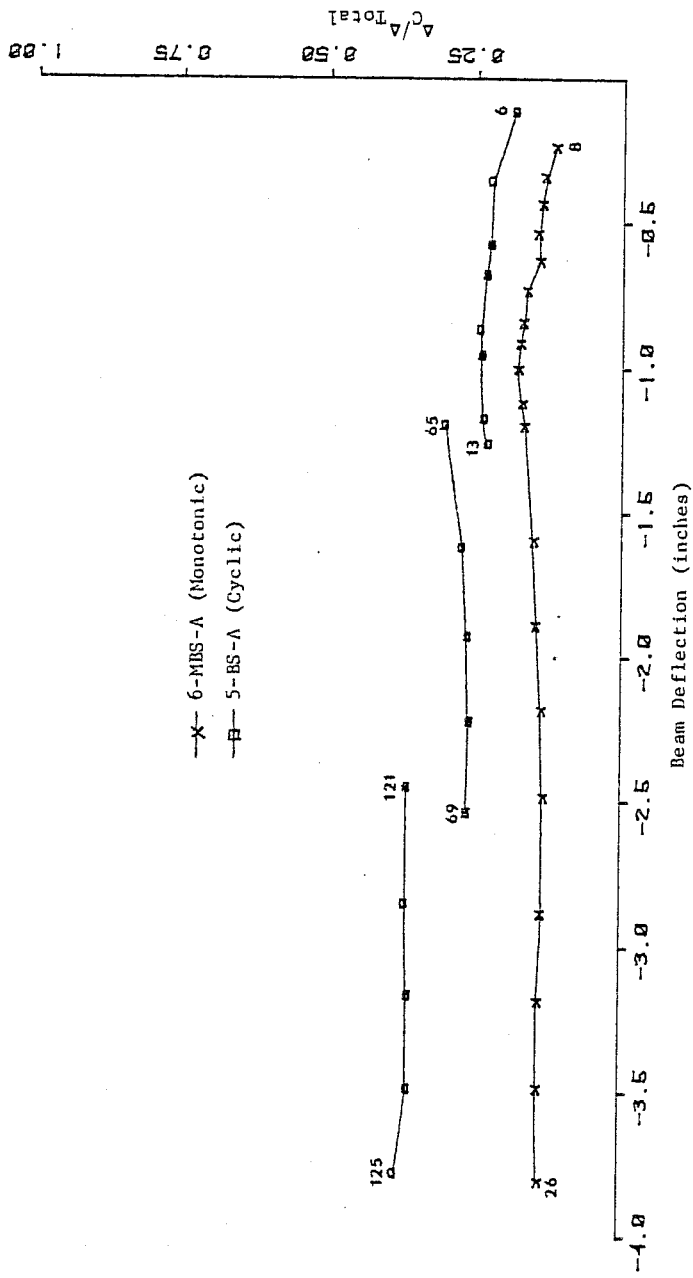
Fig. 4.24   Ratio of inelastic column deformation

Δ_B/Δ_{Total}

1.00   0.75   0.50   0.25

—×— 6-MBS-A (Monotonic)

—□— 5-BS-A (Cyclic)

-0.5   -1.0   -1.5   -2.0   -2.5   -3.0   -3.5   -4.0

Beam Deflection (inches)

8
7
65
13
69
121
125
26
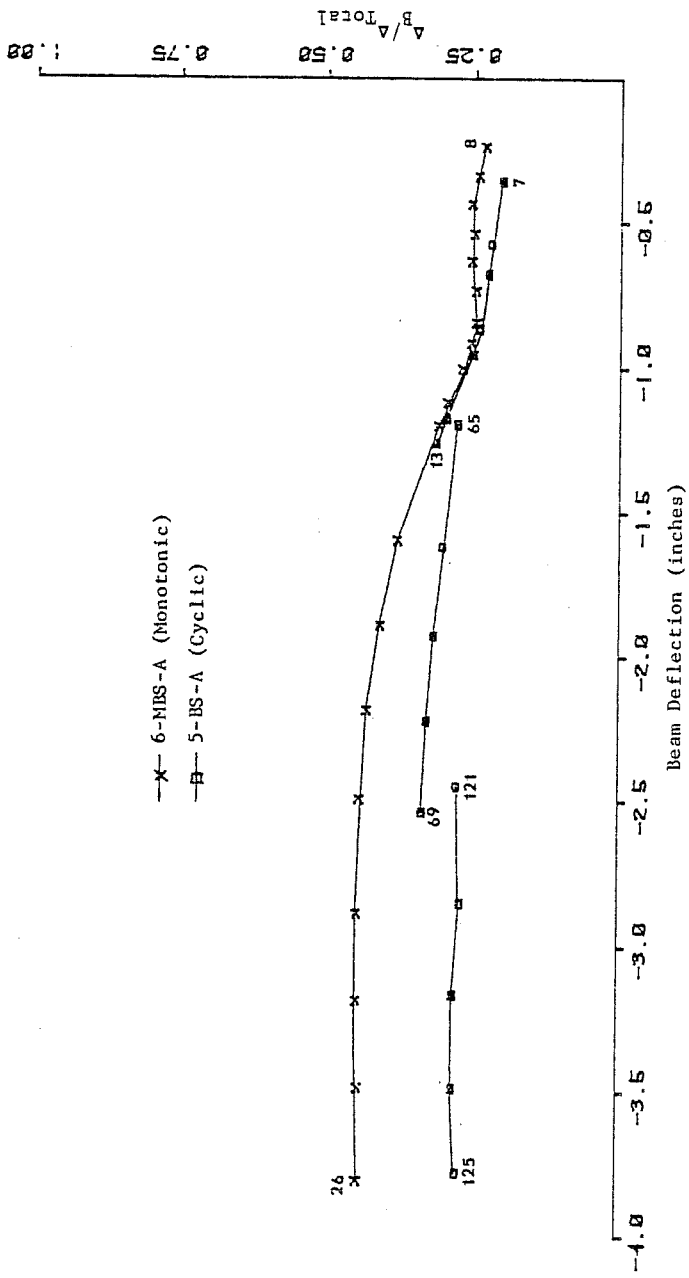
Fig. 4.25   Ratio of inelastic beam deformation

flexural deformation was not significantly different for the two tests. Figure 4.23 is a plot of the ratio of beam deflection due to joint shear strain and shows that joint shear strain contributed a significant portion of the total beam deflection. Thus, joint shear strain had a significant influence on the stiffness of the specimens. However, there was not a significant difference in the amount of joint shear strain between the monotonically and cyclically tested specimens. The ratio of beam deflection due to inelastic column rotation is shown in Fig. 4.24. There was a substantial difference in the amount of inelastic column rotation between the two tests. The cyclically loaded column had much larger inelastic rotations which may have occurred as a result of bond degradation of the reinforcement in the joint region. Beam inelastic rotation, on the other hand, was higher for the monotonically tested specimen as shown in the plot of the ratio of beam deflection due to beam inelastic rotation (see Fig. 4.25). The absence of cycling of deformations resulted in better joint performance for the monotonically tested specimen, and the imposed beam deflections resulted in larger beam rotations.

4.4.3 Bar Slip Measurements. Slip of top and bottom beam bar reinforcement was measured at the critical sections of the beam. A characteristic of all the bar slip measurements was the slip of the bar away from the face of the column as the beams were cycled at larger deformation levels (see Figs. 4.26 and 4.27). Tensile yielding and the subsequent elongation of the bars caused progressive slip of the reinforcing bars away from the column face. The amount of slip toward the joint was not great enough for the bars to return to their original neutral position.

The compression zones of the column may have had an effect on the magnitude of bar slip toward the joint (negative slip). Since the specimens were loaded on a 45° diagonal, the compression zones of the column were located at the northwest and southeast corners
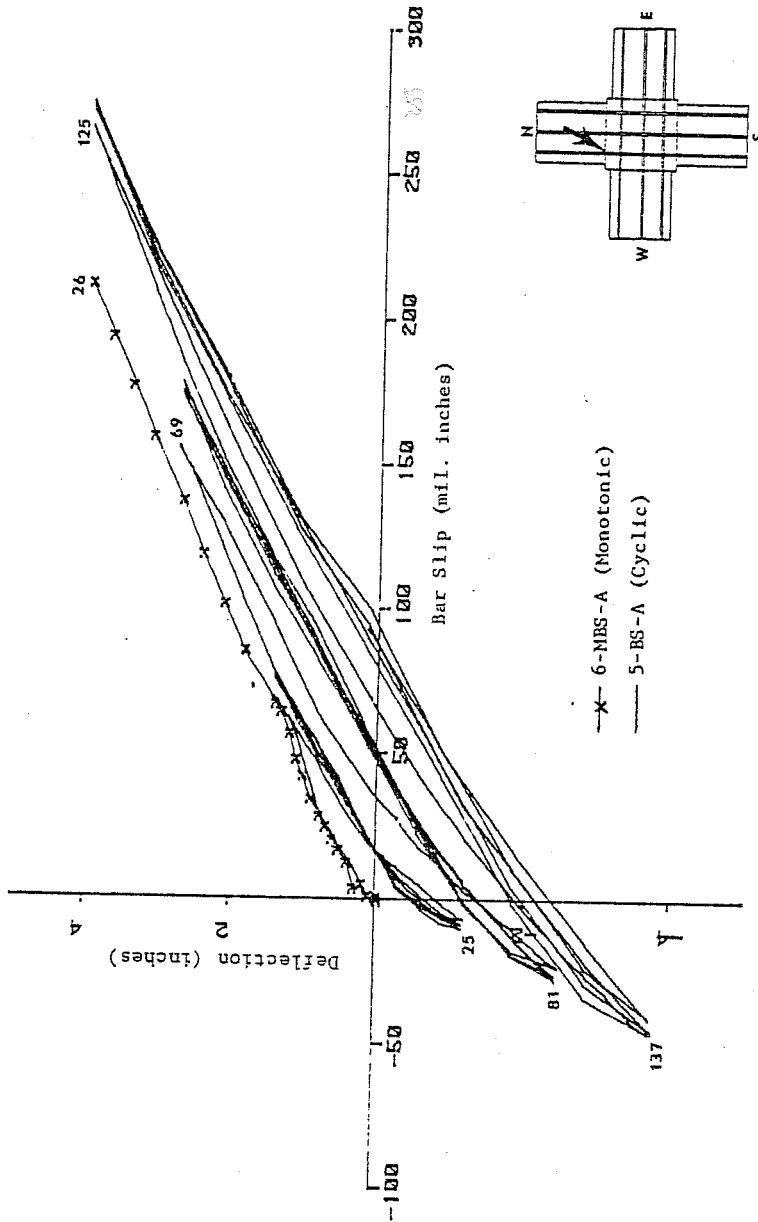
Fig. 4.26 North beam deflection versus #8 top bar slip

84
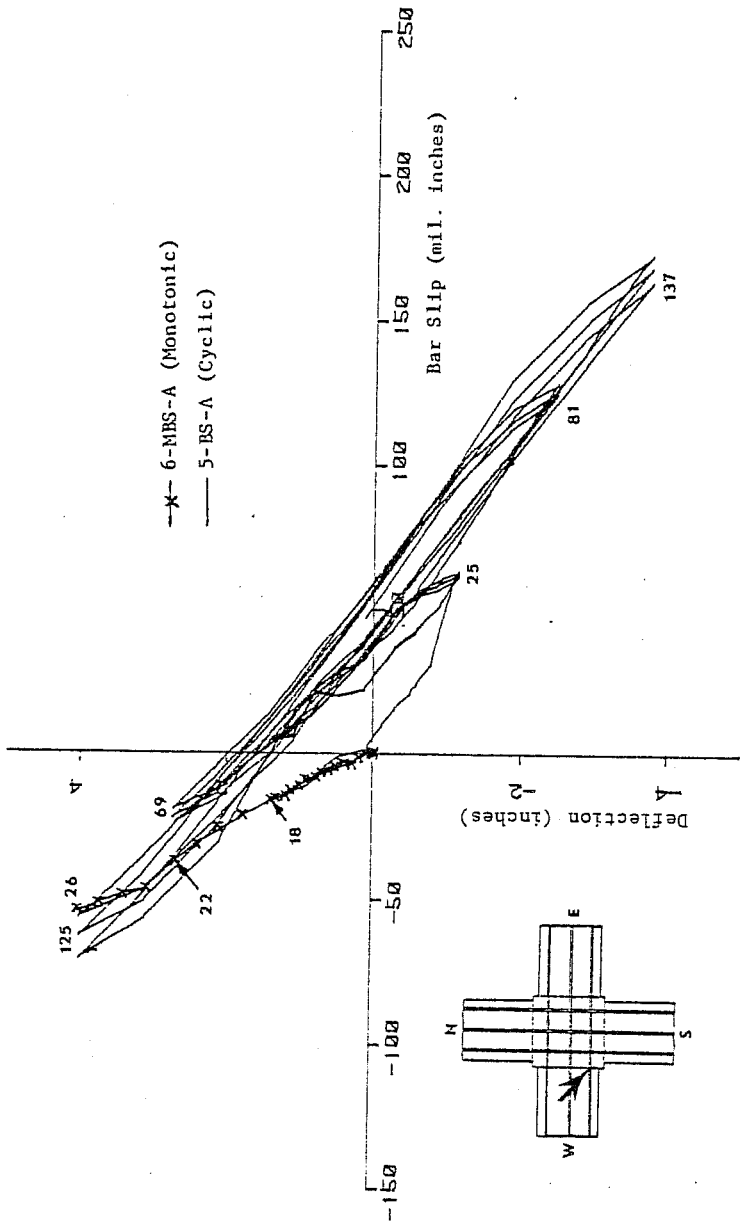
Fig. 4.27 West beam deflection versus #6 bottom bar slip

of the column, and the northeast and southwest corners were near the neutral axis. The bars at the northwest and southeast corners of the column had lower negative slip than measured at the northeast and southwest corners. Figures 4.28 and 4.29 are plots of beam load versus bar slip measured at the southwest and southeast corners, respectively. In Fig. 4.28, one can see that slip is greater in the negative direction, but less in the positive direction than the slip for the bar in the southeast corner (Fig. 4.29). The column compressive zone in the southeast corner may have had an influence in reducing the negative slip of the top bar in that corner.

The magnitude of the bar slips ranged from about 0.05 in. at the small deformation level to about 0.30 in. at the largest deformation level and varied approximately linearly with beam deflection. The effect of cycling was to shift the neutral position of the bar away from the face of the column due to inelastic elongation of the bar with each cycle. Considering this shift, the magnitudes of slip with respect to the neutral position were not significantly different for the monotonic and cyclic tests. Bar slip depended on beam end deflection and the total amount of inelastic bar strain.

Even though cycling had little influence on the magnitude of bar slip, it should be recognized that frictional resistance between the concrete and bar and the bearing force of the bar deformations against the concrete are greatly reduced after the initial excursion to a given deformation. This had a significant effect on the stiffness of the joint for the second and third cycles at the given deformation.

4.4.4 Bar Stresses and Strains. Strains were measured in the beam and column longitudinal bars and in the joint hoops at the location shown in Fig. 3.18. Because of high joint shear

86
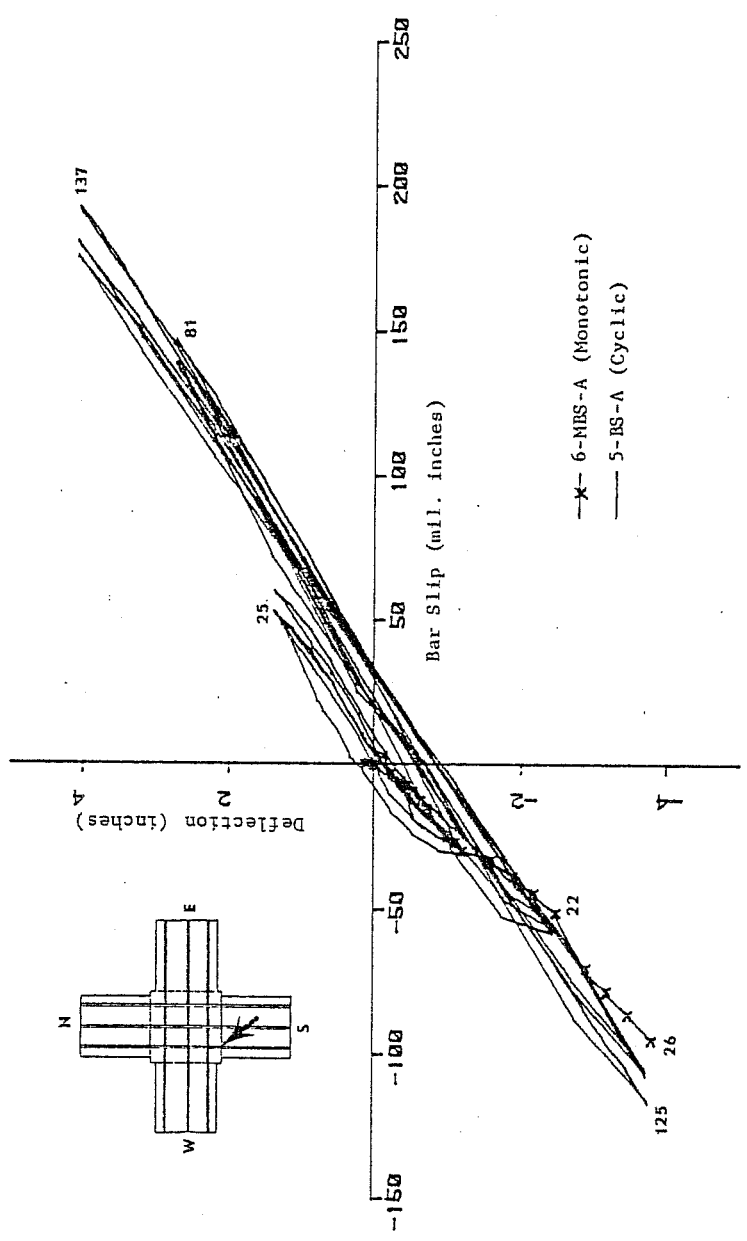
Fig. 4.28   South beam deflection versus #8 top bar slip
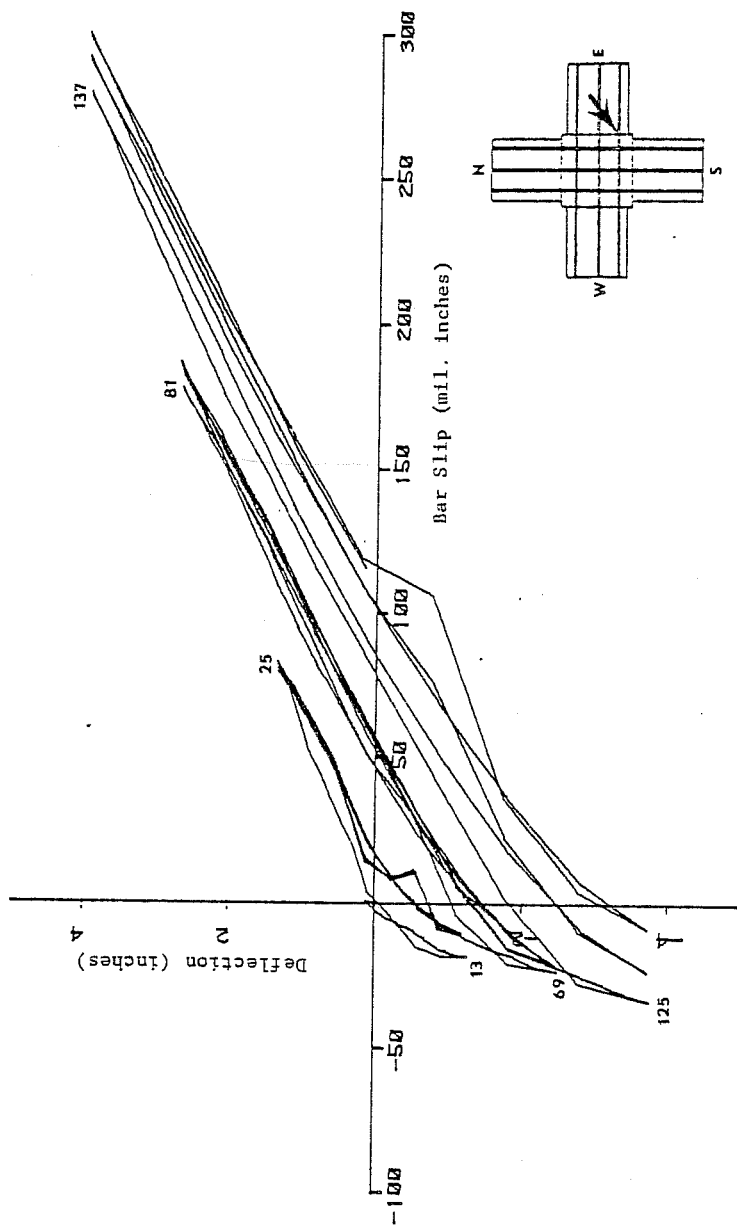
Fig. 4.29 East beam deflection versus #8 top bar slip (5-BS-A)

distortion and beam inelastic rotation, considerable bending of the bars occurred at the beam-column boundaries. As a result, the strains measured at the beam-column boundaries included bending strains as well as axial strains. However, strain measurements taken at 8 in. and 16 in. away from the beam-column boundaries did not appear influenced by bar bending. Therefore, only the strain measurements of the longitudinal beam and column bars away from the beam-column boundaries were considered.

Reinforcing bar stresses were calculated using Program STRESS (see Appendix) which is based on Thompson's method for calculating steel stresses for cyclically loaded bars in the inelastic range.[7] A modification of Thompson's method was necessary so that the stress after strain hardening was not underestimated. The yield stress in the equation for calculating characteristic stress was replaced by the maximum stress reached for that loading direction prior to the half cycle under consideration. In other words, if the stress was greater than yield, then that stress was assumed to be the new yield stress for subsequent calculations. It should also be noted that the equations were used in their original form and were calibrated using data from cyclic tests on reinforcing bars performed at the University of Canterbury. For qualitative purposes, the original calibration was assumed to be adequate.

Beam Bars. The stresses of an instrumented #8 top bar of the east beam are shown in plots of bar stress versus beam deflection (see Figs. 4.30 and 4.31). The east beam was first loaded in the negative direction (up), which would normally cause the top bars to go into compression. The plots, however, show that tensile stresses were produced in the top bars of both the monotonically and cyclically loaded specimens even though the compression zone was at the top. Analysis of the east beam cross section indicated

89
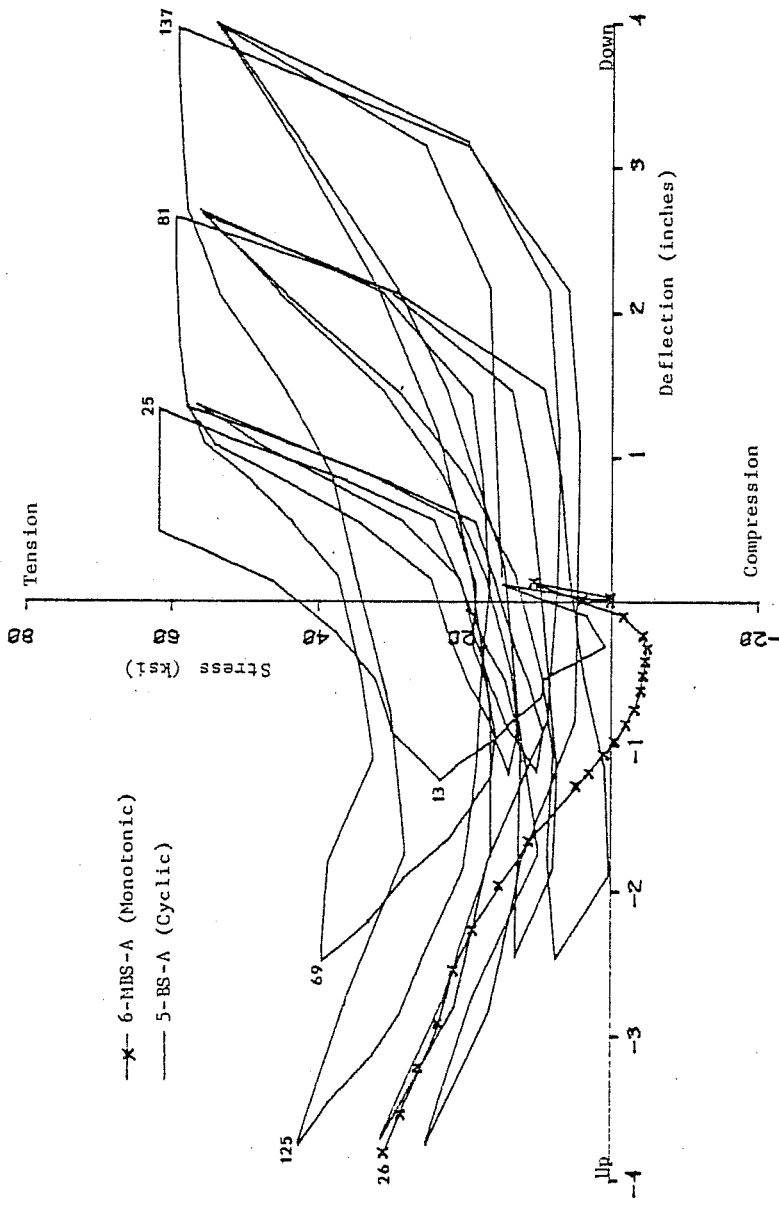
Fig. 4.30 #8 top bar stress versus east beam deflection
(8 in. from joint boundary)
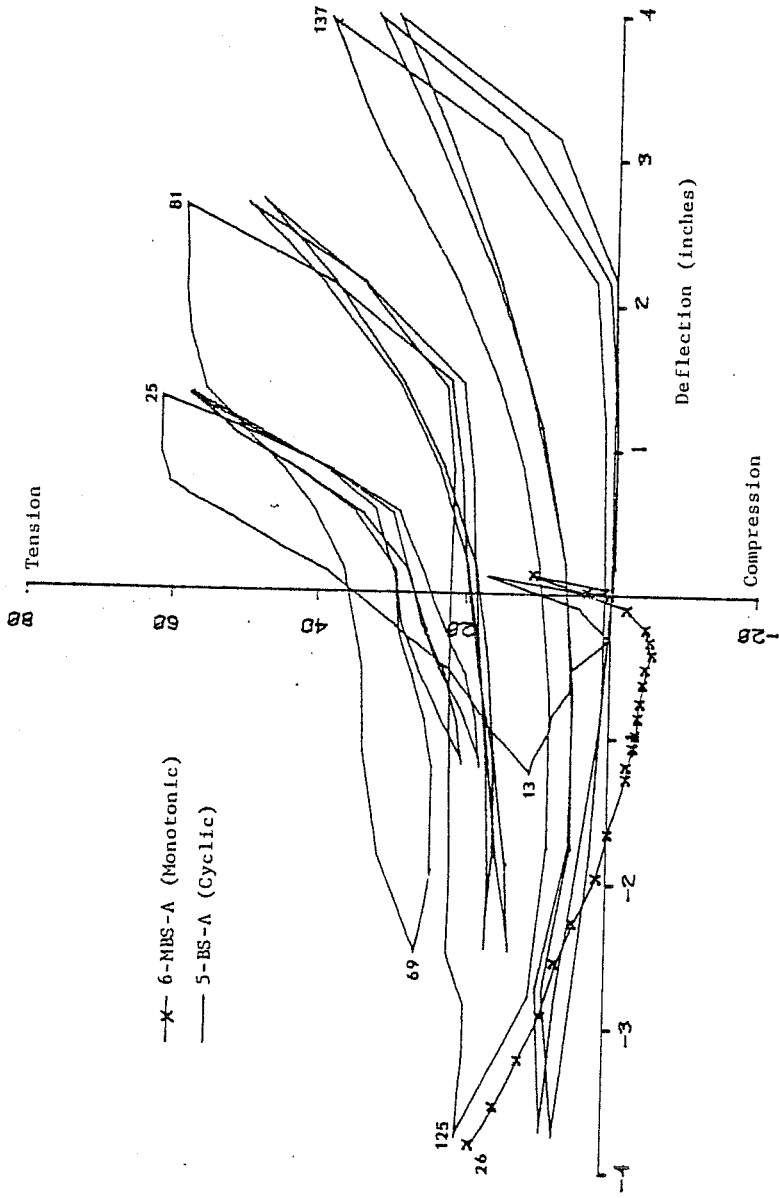
Fig. 4.31 #8 top bar stress versus east beam deflection
(16 in. from joint boundary)

that at the ultimate load, the neutral axis was above the compression reinforcement putting the top bars in about 20 ksi tension. The tensile stress of the top bar of the cyclically loaded specimen, however, was approaching 40 ksi at the extreme deformation. This indicates that a portion of the tensile stress in the bar occurred because of bond degradation through the joint (see Fig. 4.13).

Plots of beam load versus #6 bottom bar strain (Figs. 4.32 and 4.33) show that inelastic strains occurred as far away as 8 in. from the joint, but remained elastic at 16 in. away. The inelastic elongation of the #6 bottom bars was concentrated closer to the critical section than the larger top bars which had inelastic strains at 16 in. into the beams. These observations indicate that the bond condition was more favorable for the #6 bars than the #8 bars. Also, the monotonically loaded specimen had larger bar strains than the cyclically loaded specimen which indicates a less favorable bond condition for the cyclically loaded specimen.

Column Bars. Since the columns were loaded on the northwest-southeast diagonal, the extreme fibers were located at the northwest and southeast corners of the column. Strain measurements of the southeast column bar which had gages at 8 in. and 16 in. above and below the joint remained in the elastic range indicating that the column capacity was governed by a compressive rather than a tensile failure. Plots of the southeast column bar stress versus interstory displacement (Figs. 4.34 and 4.35) show that the compressive bar stress of specimen 5-BS-A was higher at 8 in. below the joint compared to the compressive bar stress of specimen 6-MBS-A. At 16 in. below the joint, however, the compressive stress of specimen 6-MBS-A was higher. Indications are that cycling of deformations caused the deterioration of the concrete near the joint and resulted in higher stresses in the reinforcement. The tensile stresses of the same column bar were about the same at both
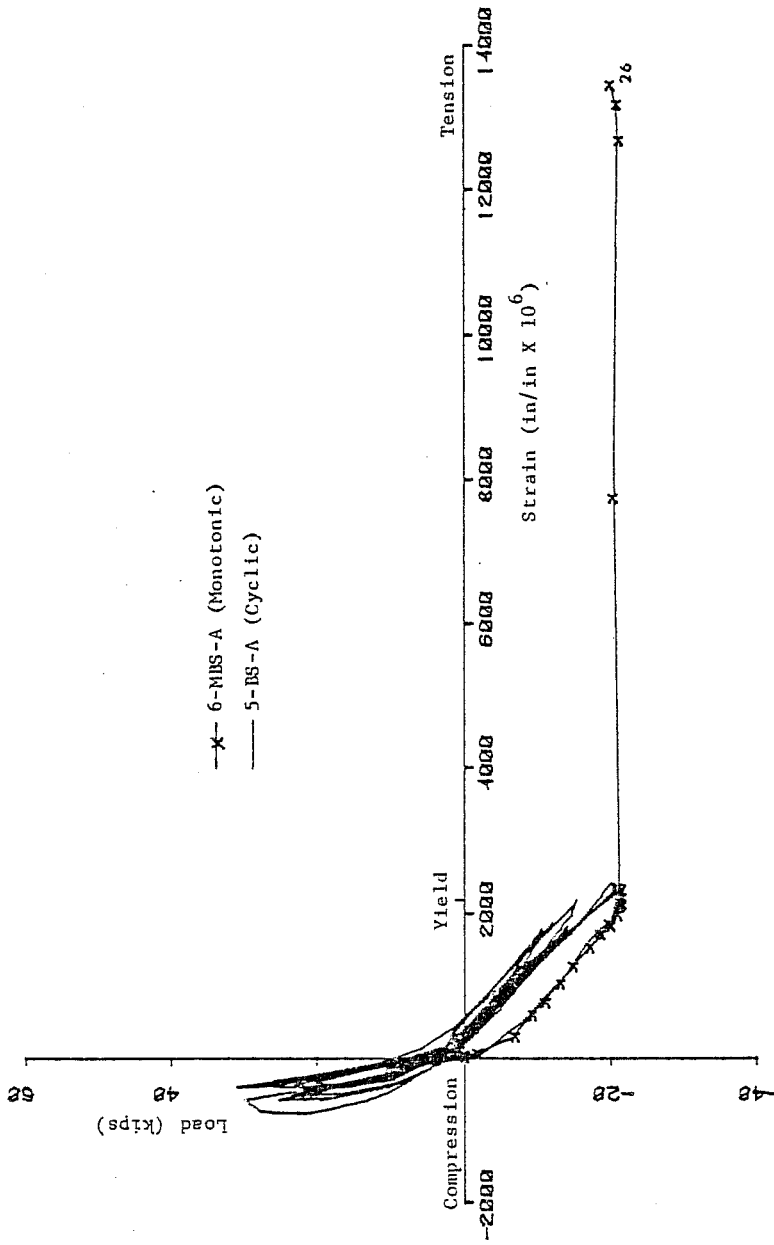
Fig. 4.32 East beam load versus #6 bottom bar strain
(8 in. from joint boundary)

93
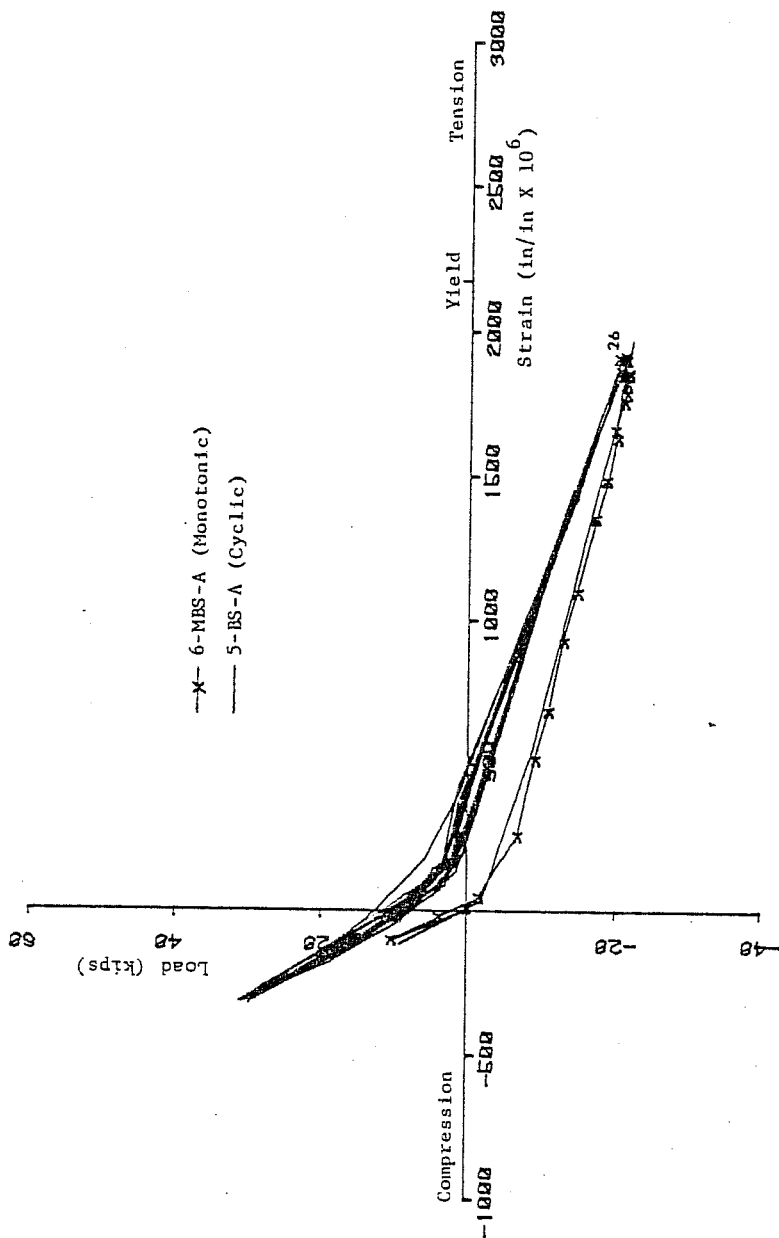
Fig. 4.33 East beam load versus #6 bottom bar strain
(16 in. from joint boundary)
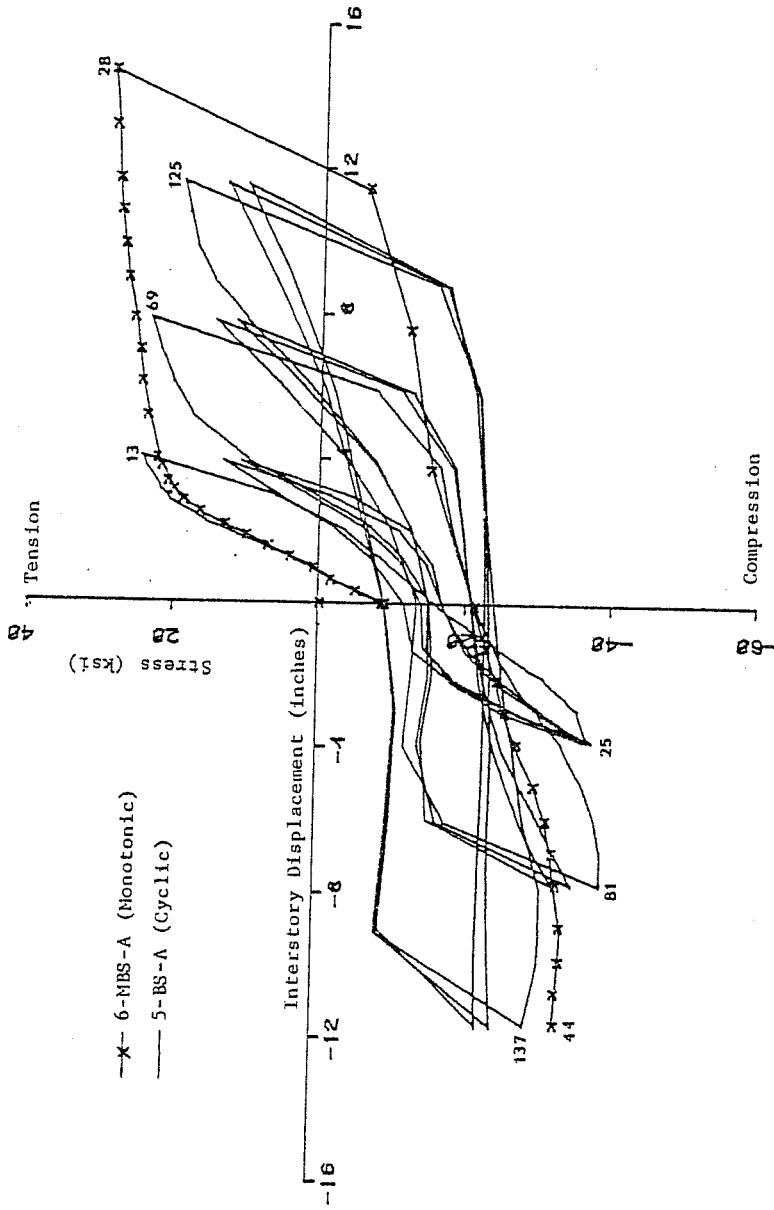
Fig. 4.34 Southeast column bar stress versus interstory displacement (8 in. below joint boundary)

95
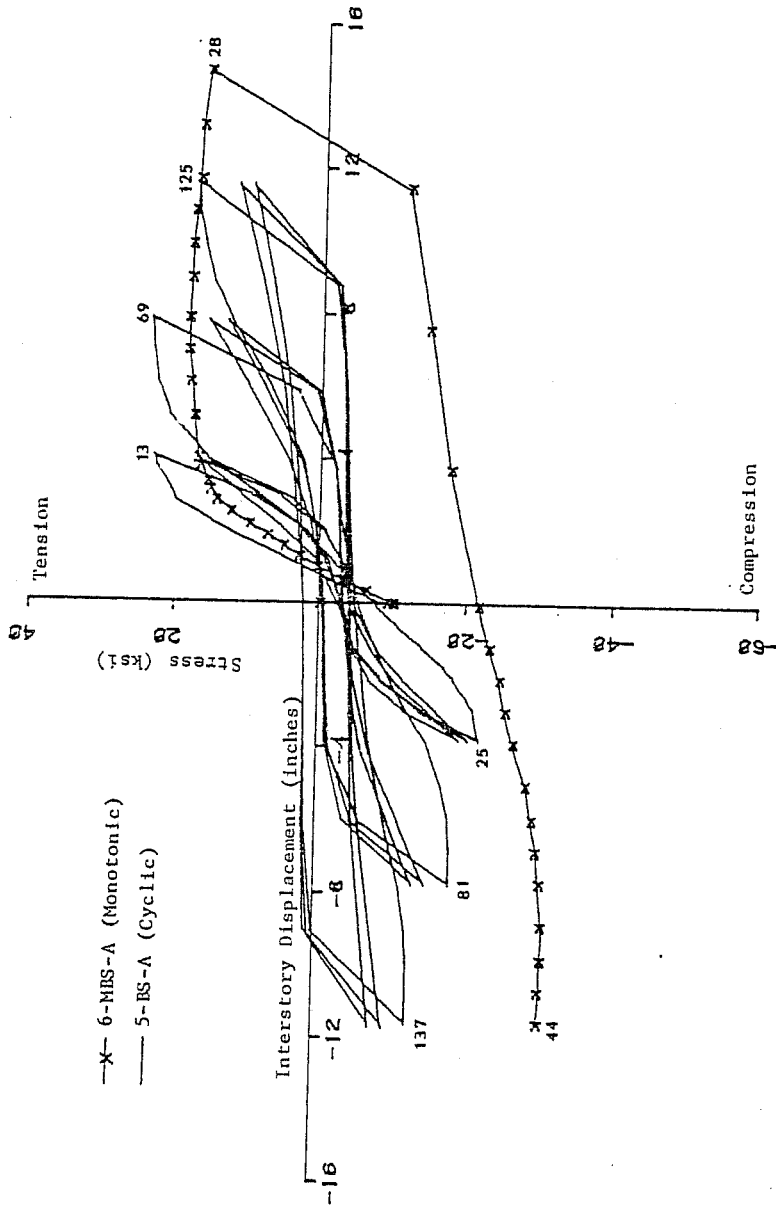
Fig. 4.35 Southeast column bar stress versus interstory displacement
(16 in. below joint boundary)

8 in. and 16 in. below the joint of the cyclically loaded specimen
indicating that the bond deterioration of the column bars occurred
well below the joint boundary. Greater bond deterioration of the
cyclically loaded specimen may be the reason for the high
inelastic column rotations observed for that specimen.

Joint Hoops. Joint hoops of both the monotonically and
cyclically loaded specimens had tensile strains well above yield
as shown in the plots of stress versus strain in Figs. 4.36 and
4.37. Each specimen had two joint hoops as shown in Fig. 3.4.
At the lower deformations, the top joint hoop of the cyclically
loaded specimen consistently had higher strains than the bottom
joint hoop. The different sizes of the top and bottom reinforce-
ment may have been an influencing factor for this behavior. At
the larger deformations, however, the trend broke down as larger
strains were reached. The magnitude of the strains varied
considerably at the larger deformations. The monotonically loaded
specimen had hoop strains that ranged from 0.00213 to 0.0215 at $3\Delta_i$.
(load stage 26). The cyclically loaded specimen also had a wide
range of hoop strains that varied from 0.002571 to 0.0178 at $3\Delta_i$
(load stage 125). Joint shear cracks crossing the hoops at the
position of the strain gage may have resulted in large strains
at those points.

Plots of hoop stress versus interstory displacement of the
cyclically loaded specimen are shown in Figs. 4.38 and 4.39. During
the early cycles, tensile stresses of the joint hoops remained
locked in when the specimen was returned to the original position.
Cracks which opened in the joint region may not have closed
completely because of concrete particles which could have lodged
in the open cracks. However, as cycling progressed, the amount of
locked-in stress decreased, and eventually compressive stresses
were achieved. This may have happened because as cracks grew

97
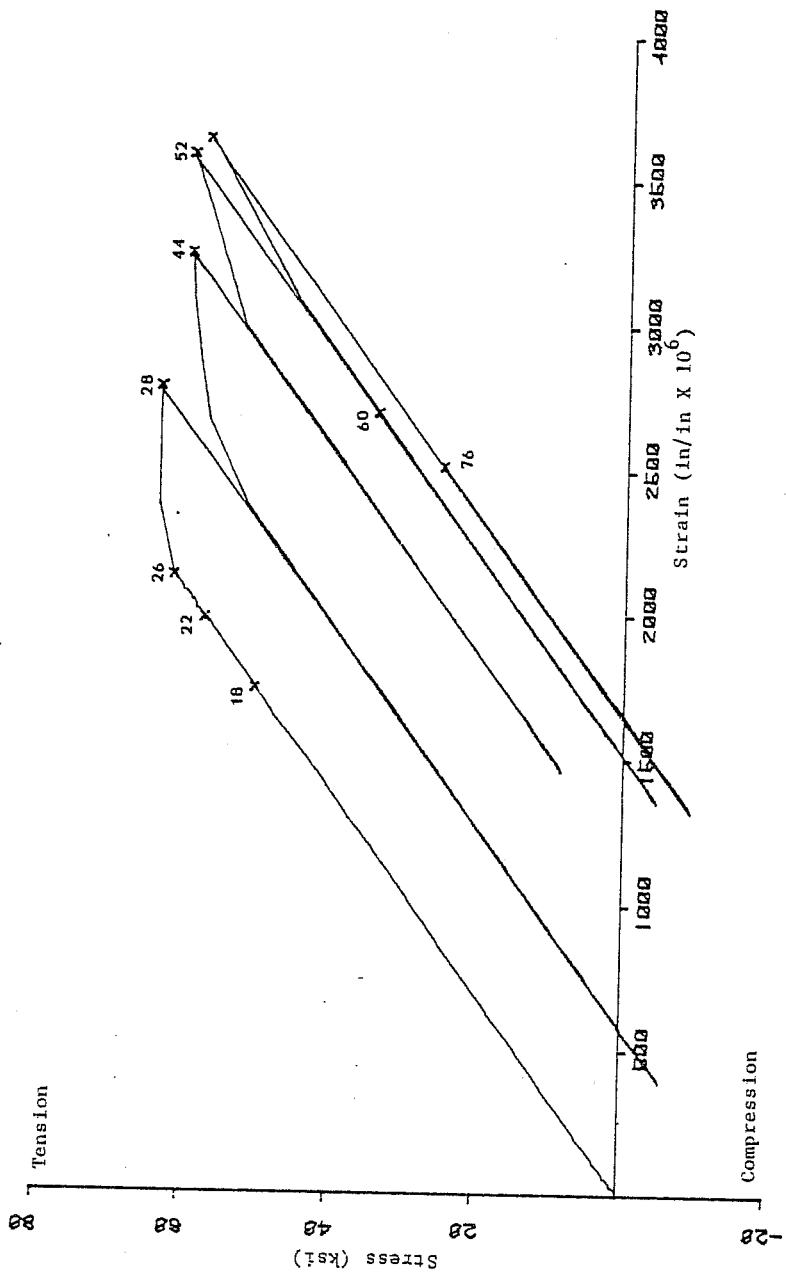
Fig. 4.36 Top joint hoop stress versus strain (6-MBS-A)

98
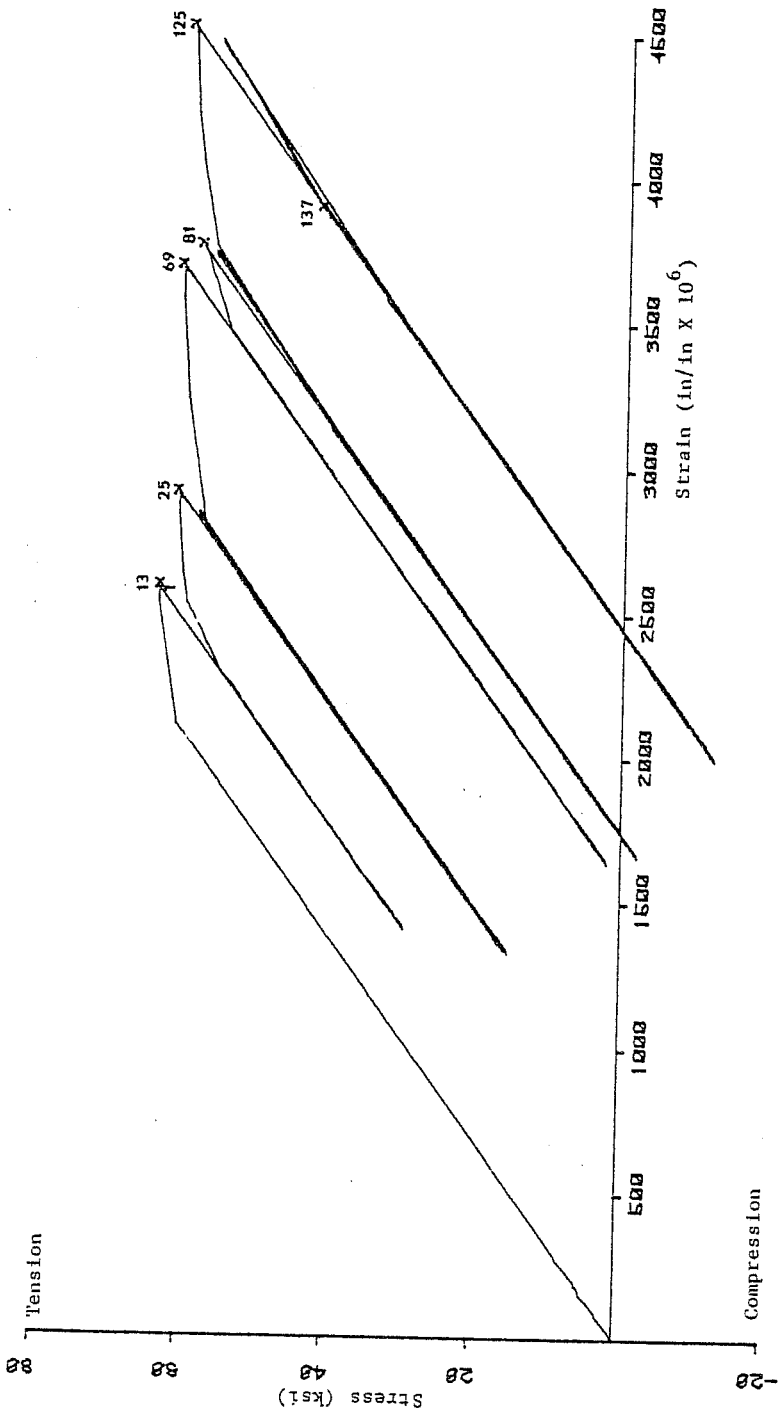
Fig. 4.37 Top joint hoop stress versus strain (5-BS-A)
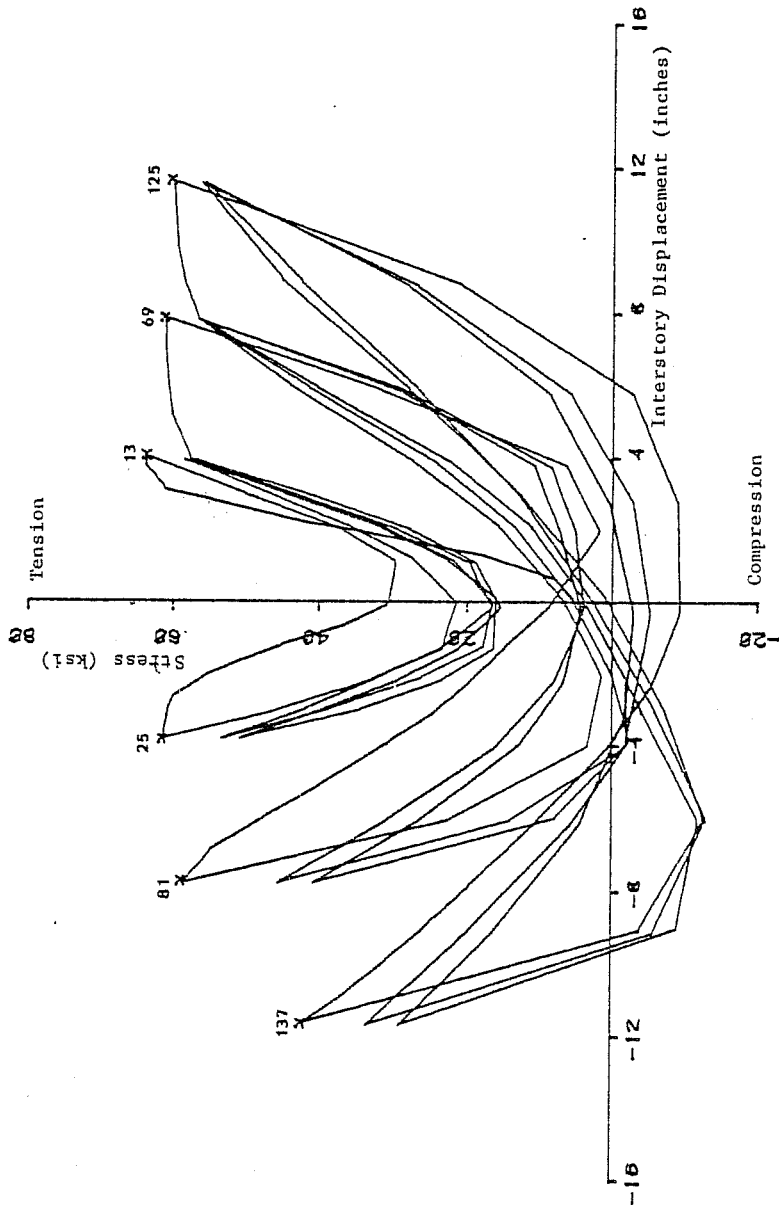
Fig. 4.38 Top joint hoop stress versus interstory displacement (5-BS-A)

100
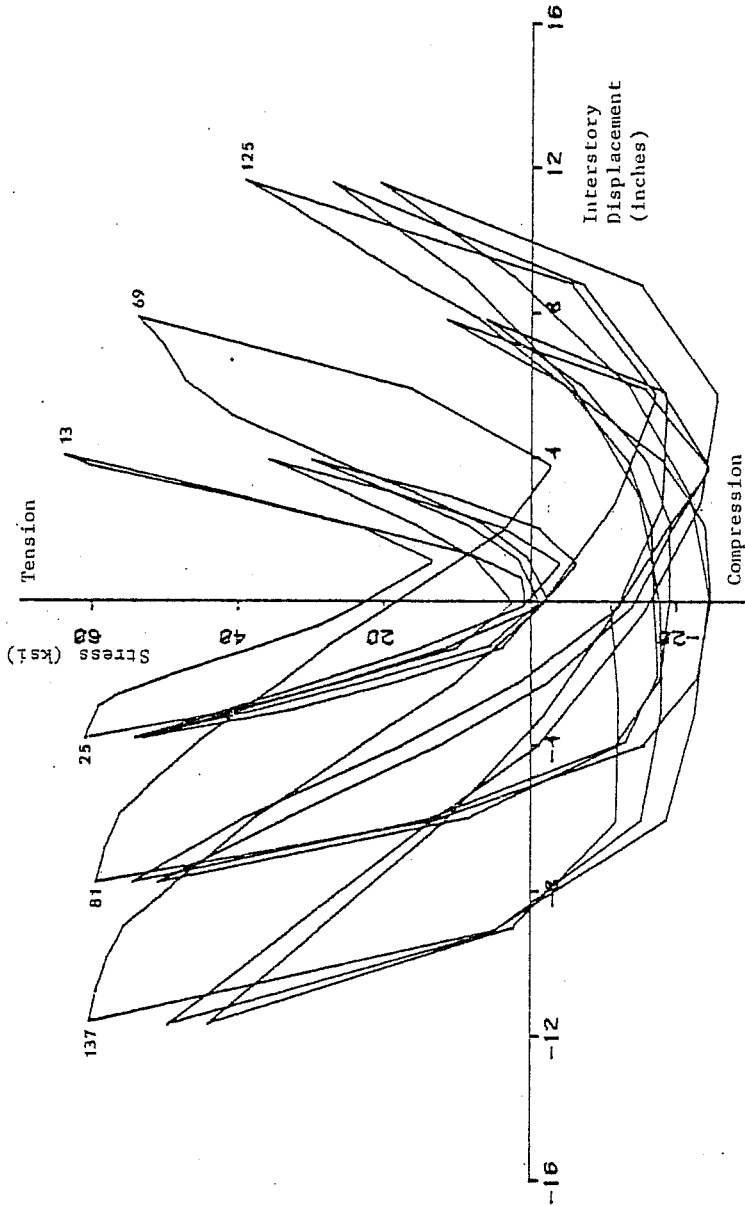
Fig. 4.39   Bottom joint hoop stress versus interstory displacement (5-BS-A)

larger and greater in number, inelastic elongation of the hoops occurred, and when the load was reversed, the cracks closed and compressive stresses were produced. Generally, the joint hoops of both the monotonically and cyclically loaded specimens underwent large inelastic strains indicating that the joints were under considerable distress.

CHAPTER 5

COMPARISON OF EXPERIMENTAL AND CALCULATED
JOINT SHEAR STRENGTH

5.1 General

Joint shear was calculated using internal moment arms, d_1 and d_2 as shown in Fig. 5.1. The values of d were selected based on calculations of the internal moment arms in the elastic range and at ultimate. The average value of d at the two conditions was chosen to be used in the calculations. The values of d varied because of the different levels of the reinforcement in the N-S and E-W beams and because of the different amounts of positive and negative reinforcement. Considerable spalling of the cover concrete occurred at the higher levels of deformation, and it is likely that the actual values of d were less than those indicated in the figure. If so, the joint shear would be greater than that calculated. Joint shear was calculated using constant internal moment arms thoughout the tests, so at the higher deformations where spalling occurred, the values of joint shear are probably conservative. Figures 5.2 and 5.3 are plots of joint shear versus interstory displacement and Table 5.1 lists the values of joint shear at various load stages. The maximum joint shear was approximately 225 kips in each of the principal directions for both tests 5-BS-A and 6-MBS-A. Thus, the component of nominal joint shear stress in each direction is calculated as follows:

$$v_u = \frac{V_u}{bd} = \frac{225,000 \text{ lbs.}}{(15 \text{ in.})(12.4 \text{ in.})}$$

$$= 1210 \text{ psi}$$

$$= 18.3 \sqrt{f'_c}$$
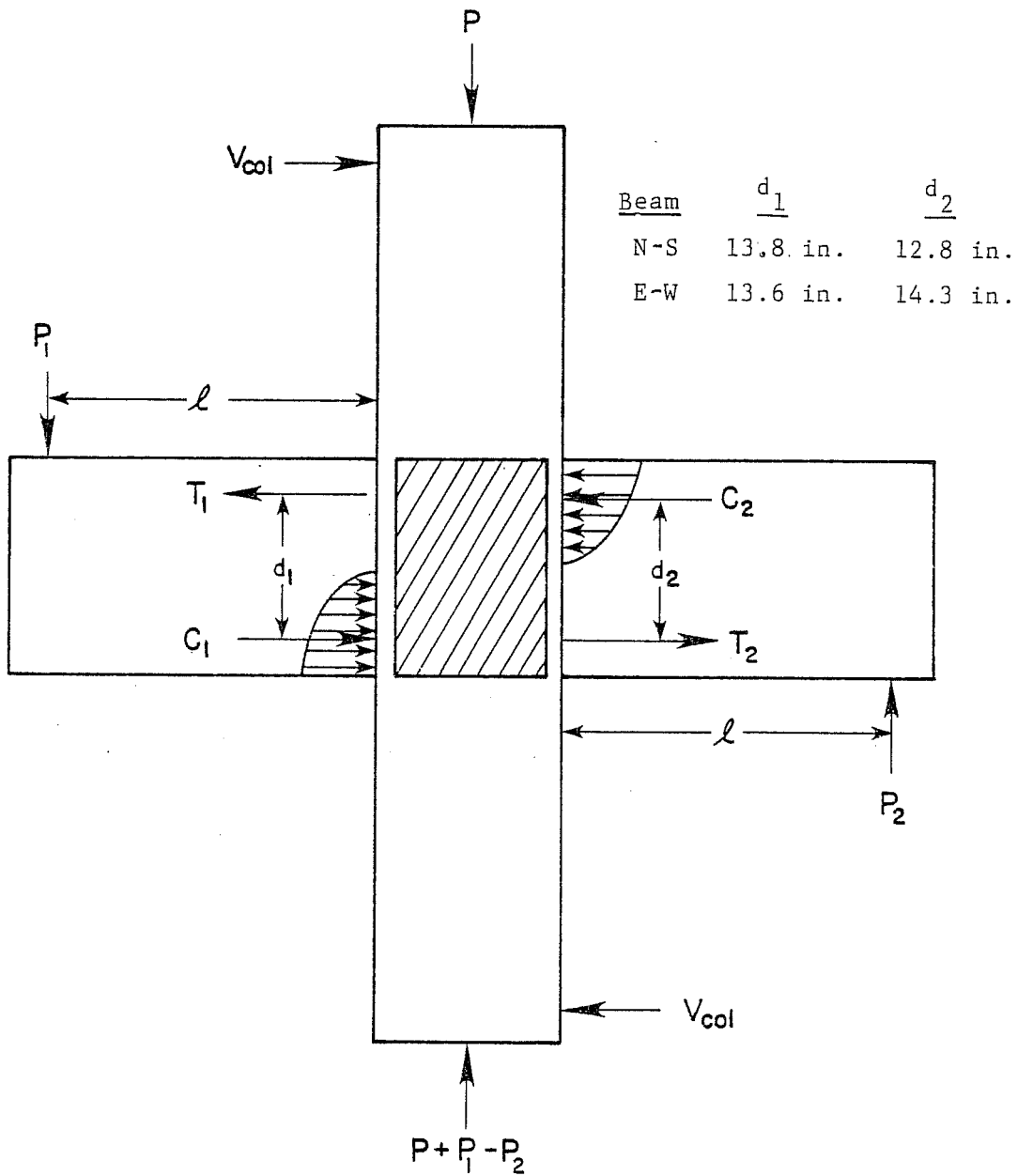
$$\text{Joint Shear} = T_1 + C_2 - V_{col}$$

$$= P_1 \ell/d_1 + P_2 \ell/d_2 - V_{col}$$

Fig. 5.1 Joint shear calculation
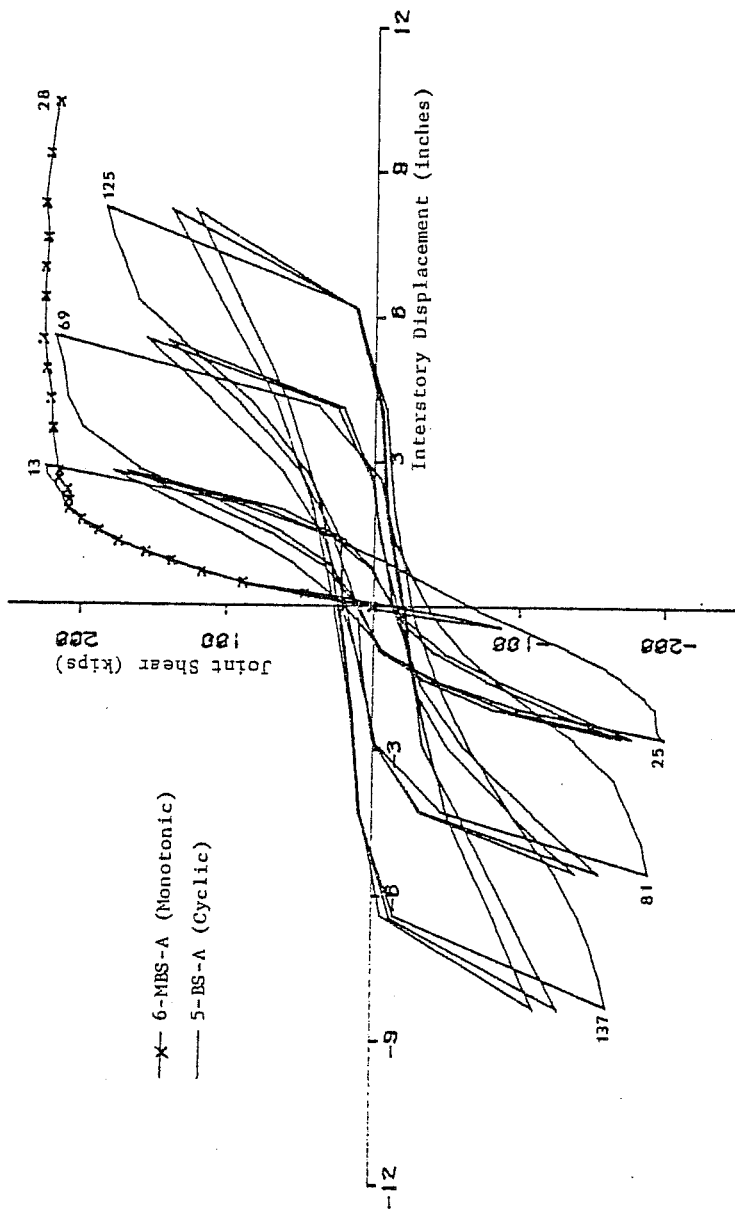
Fig. 5.2   Joint shear versus interstory displacement (N-S direction)
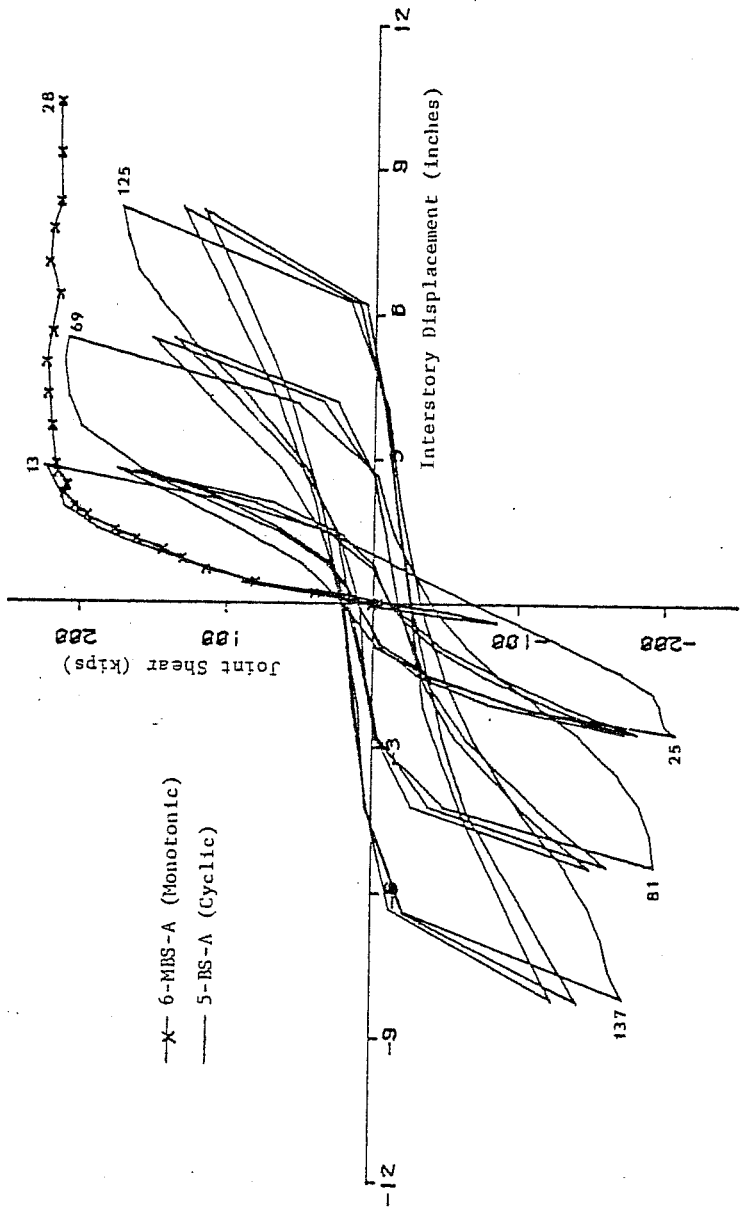
Fig. 5.3   Joint shear versus interstory displacement (E-W direction)

TABLE 5.1 JOINT SHEAR

Specimen 5-BS-A			Specimen 6-MBS-A		
	Joint Shear (kips)			Joint Shear (kips)	
Load Stage	N-S	E-W	Load Stage	N-S	E-W
2	85	90	2	89	94
4	89	86	4	85	81
13	225	225	9	138	131
25	201	208	18	216	218
33	179	176	22	227	220
41	178	183	26	225	215
49	170	163	28	217	216
57	171	174	44	176	186
69	219	209	52	99	101
81	189	194	60	134	149
89	156	153	68	94	94
97	156	161	76	117	129
105	141	137			
113	139	150			
125	185	174			
137	162	173			
145	140	133			
153	129	144			
161	125	118			

In this section, the joint shear strength of the test specimen will be calculated using several design approaches based on previous studies of planar joints. Comparisons of the maximum applied joint shears with the calculated values should give some insight as to the relative magnitude of the joint shear strength of biaxially loaded joints as well as to the validity of the various design approaches. The design approaches which will be considered were developed by ACI-ASCE Committee 352,[5] Park and Paulay at the University of Canterbury,[8] Sugano and Koreishi at the University of Tokyo,[9] and Meinheit and Jirsa at The University of Texas at Austin.[6]

5.2 ACI-ASCE Committee 352[5,6]

The ACI ASCE Committee 352 design procedure divides the joint shear strength into two components; one portion is attributed to the concrete and the other to the joint reinforcement. This method is based on the classical truss analogy which is also the basis for the shear design of reinforced concrete beams. The allowable unit stress carried by the concrete is calculated with the following equation.

$$v_c = 3.5\beta\gamma \left[f'_c(1 + 0.002N_u/A_g)\right]^{-\frac{1}{2}}$$

where β = factor reflecting the amount of energy absorbing capacity or type of loading imposed on the structure

  = 1.4 for joints which must have strength but no expected significant inelastic deformations (Type 1)

  = 1.0 for joints which must have sustained strength under load reversals in the inelastic range (Type 2)

  γ = factor reflecting lateral confinement by members perpendicular to the plane in which the shear stress is calculated

γ = 1.4 if the confining members cover at least three-quarters of the width and three-quarters of the depth of the joint face.

= 1.0 if the confining members do not meet the above requirements

f_c' = concrete compressive strength, psi

N_u = magnitude of column load (compressive positive), lbs.

A_g = gross area of column, in^2.

The unit stress carried by the steel reinforcement is calculated as follows:

$$v_s = A_{sv} f_y / bs$$

where A_{sv} = area of reinforcement crossing a shear crack within a distance s, in^2.

f_y = yield strength of reinforcement, psi

b = width of the column in the joint, in.

s = spacing of reinforcement, in.

The ultimate shear stress is the addition of the two components:

$$v_u = v_c + v_s$$

For the test specimens,

β = 1.4

γ = 1.4

f_c' = 4350 psi

N_u = 300,000 lbs.

A_g = (15)(15) = 225 in^2.

$$v_c = 3.5(1.4)(1.4)\left[4350\left(1 + 0.002\frac{300,000}{225}\right)\right]^{\frac{1}{2}}$$

$$= 866 \text{ psi}$$

$$V_c = v_c bd = 866(15)(12.4) = 162,000 \text{ lbs.}$$

$$A_{sv} = 0.40 \text{ in.}^2$$

$$f_y = 63,800 \text{ psi}$$

$$b = 15 \text{ in.}$$

$$s = 5 \text{ in.}$$

$$v_s = \frac{0.40(63,800)}{(15)(5)} = 340 \text{ psi}$$

$$V_s = v_s bd = 340(15)(12.4) = 63,000 \text{ lbs.}$$

$$V_u = V_c + V_s = 162 + 63$$

$$= 225 \text{ kips}$$

When inelastic load reversals are expected, $\beta = 1.0$ instead of 1.4. Therefore, the sustained shear strength is calculated as follows:

$$v_c = 866/1.4 = 619 \text{ psi}$$

$$v_{sustained} = 619 + 340 = 959 \text{ psi}$$

$$V_{sustained} = 959(15)(12.4) = 178,000 \text{ lbs.}$$

5.3 <u>Park and Paulay</u>[8]

The design approach suggested by Park and Paulay attributes none of the shear strength to the concrete when load reversals in the inelastic range are anticiapted. This approach assumes the concrete will degrade under seismic loading conditions and will have little or no shear strength. Also, cracks that form at the joint boundaries may remain open due to inelastic elongation and the concrete will become ineffective in transferring the shear through the joint. The steel reinforcement must then be capable

of transferring the shear through the joint by means of the "truss" mechanism. If the loadings are skewed with respect to the principal axes of the frame, the joint core must resist the forces from four beams simultaneously. The shear in the joint core is increased by $\sqrt{2}$ above that of the uniaxial case if the beams are similar in each direction. Also, the steel reinforcement will cross the diagonal cracking pattern at a 45 degree angle and will be $1/\sqrt{2}$ times as effective. Hence, if resistance is by the "truss" mechanism alone, twice the amount of steel will be required for biaxial design.[10]

The joint shear strength will be equal to the portion attributed to the steel reinforcement in the ASCE-ACI Committee 352 method.

$$v_u = v_s = 340 \text{ psi}$$

$$V_u = v_u bd = 340\ (15)(12.4) = 63,200 \text{ lbs.}$$

5.4 Sugano and Koreishi[9]

The Sugano and Koreishi design approach is similar to the ACI-ASCE Committee 352 recommendation in that the shear resistance is divided into two components. The shear resistance assigned to the steel reinforcement and to the concrete are calculated separately and then combined to obtain the total joint shear strength. Equations for calculating cracking strength were also included in their recommendations and are given below.

$$v_{cr} = (f_t^2 + f_t(P_u/A_g))^{\frac{1}{2}}$$

where f_t = tensile strength of concrete, kg/cm^2

P_u = column load, kg

A_g = gross area of column, cm^2

and f_t = $0.205f'_c - 0.0004f'^2_c$ $(f'_c \leq 420kg/cm^2)$

where f'_c = concrete compressive strength, kg/cm^2

For the test specimens:

f'_c = 4350 psi = 305 kg/cm^2

P_u/A_g = $\dfrac{300,000 \text{ lb.}}{(15 \text{ in.})(15 \text{ in.})}$ = 1330 psi = 93.7 kg/cm^2

f_t = $0.205(305) - 0.0004(305)^2$

= 25.3 kg/cm^2

v_{cr} = $(25.3^2 + 25.3(93.7))^{\frac{1}{2}}$

= 54.9kg/cm^2

= 781 psi

V_{cr} = $v_{cr}bd$

= 781(15)(12.4)

= 145 kips

The concrete contribution to the ultimate shear strength is given by the following equation:

$$v_c = 0.51f'_c - 0.001f'^2_c \quad (f'_c \leq 420kg/cm^2)$$

And the shear strength provided by the steel reinforcement is calculated as follows:

$$v_s = 2.7(\rho_w f_y)^{\frac{1}{2}}$$

where ρ_w = the steel ratio (A_s/bs)

A_s = total area of hoop reinforcement in the joint

f_y = yield strength of joint hoops, kg/cm^2

b = width of column

s = spacing of hoops

v_c = $0.51(305) - 0.001(305)^2$

= 62.3 kg/cm^2

= 893 psi

V_c = $v_c(b)(d)$ = $893(15)(12.4)$ = 35,000 lbs.

ρ_w = $0.40/(15)(15)$

= 0.00533

f_y = 63,800 psi

= 4485 kg/cm^2

v_s = $2.7[0.00533(4485)]^{-\frac{1}{2}}$

= 13.2 kg/cm^2

= 188 psi

V_s = $188(15)(12.4)$ = 166,000 lbs.

V_u = $V_c + V_s$

= 35 + 166

= 201 kips

5.5 Meinheit and Jirsa[6]

The design approach recommended by Meinheit and Jirsa does not divide the shear resistance due to the concrete and the steel reinforcement into separate components. The shear strength of the joint is assigned primarily to the concrete and any increase in

strength provided by the reinforcement is due to the confinement
of the concrete. Confinement provided by lateral beams is also
considered to improve the joint shear strength. The equations
proposed by Meinheit and Jirsa for the ultimate joint shear
strength were used previously in the design of the test specimens
and are described in Chapter 2. In addition to the ultimate
strength formula, an equation was given for the cracking strength
which is calculated below:

$$v_{cr} = 0.0124(f'_c)^{0.85} \ (P/A_g)^{0.485} \ (1 + W_c/h_c)^{0.57}$$

$$= 0.0124(4350)^{0.85} \left(\frac{300,000}{15^2}\right)^{0.485} \left(1 + \frac{13}{15}\right)^{0.57}$$

$$= 718 \text{ psi}$$

$$V_{cr} = v_{cr}bd$$

$$= 718(15)(12.4)$$

$$= 134,000 \text{ lbs.}$$

Calculations of ultimate joint shear strength follows.

From Chapter 2,

$$\rho_s = 0.0133$$

$$\zeta = 1.08$$

$$\beta = 1.22$$

$$v_u = 5.1\beta \ \zeta \ (f'_c)^{2/3}$$

$$= 5.1(1.22)(1.08)(4350)^{2/3}$$

$$= 1790 \text{ psi}$$

$$V_u = v_u bd$$

$$= 1790(15)(12.4)$$

$$= 333,000 \text{ lbs.}$$

For joints designed for load reversals producing inelastic deformations, Meinheit and Jirsa recommend a reduction factor of 0.6 to obtain the sustained shear strength:

$$V_{sustained} = 0.6(333,000)$$

$$= 200,000 \text{ lbs.}$$

5.6 Cracking Shear Strength

The results of the calculations of cracking shear strength obtained with equations by Sugano and Koreishi and Meinheit and Jirsa were compared with the experimental cracking strengths listed in Table 5.2. In each direction, the component shear on the joint core at cracking was about the same as predicted by the cracking equations which were based on studies of uniaxially loaded planar joints. These results indicate that the joint cracking strength is not adversely affected in one direction by loadings in the orthogonal direction. It appears that the initial cracking of a biaxially loaded joint occurs when the shear in either principal direction reaches the "uniaxial" cracking strength. Although the experimental values of the N-S and the E-W components of joint shear were close to the calculated values, the resultant joint shear on the specimens was about $\sqrt{2}$ times the calculated cracking strengths. The confining effect of the compression zones of the orthogonal beams may have improved the cracking strength of the joint.

115

TABLE 5.2   CRACKING SHEAR STRENGTH, KIPS

	5-BS-A V_5	6-MBS-A V_6	Sugano & Koreishi $V_{s\&k}$	$V_5/V_{s\&k}$	$V_6/V_{s\&k}$	Meinheit & Jirsa $V_{m\&j}$	$V_5/V_{m\&j}$	$V_6/V_{m\&j}$
N-S	142	138	145	0.98	0.95	134	1.06	1.03
E-W	130	131	145	0.90	0.90	134	0.97	0.98
Resultant	193	190	145	1.33	1.31	134	1.44	1.42

TABLE 5.3   ULTIMATE SHEAR STRENGTH

Design Approach	V_s (kips)	V_c (kips)	V_u(calc.) = V_s + V_c	V_u(test)*/V_u(calc.)
ASCE-ACI Committee 352	63	162	225	1.00
Meinheit & Jirsa	0	333	333	0.68
Sugano & Koreishi	35	166	201	1.12
Park & Paulay	63	0	63	3.55

*V_u(test) ≈ 225 kips (N-S or E-W component)

5.7 Ultimate Shear Strength

The calculated ultimate joint shear strength and the
maximum joint shear that was applied to the specimens is compared
in Table 5.3. It should be noted that the maximum applied joint
shear may have been less than the potential ultimate joint shear
strength of the specimens because the applied joint shear was
limited by the flexural capacity of the beams. The maximum joint
shear applied to the specimens was exactly the same as the joint
shear strength predicted by the ASCE-ACI design equations. It is
probably coincidental that when the beams reached their flexural
capacity, the joint shear on the specimen was the same as the
calculated shear strength. While it cannot be concluded that the
ASCE-ACI design approach accurately models joint behavior, it is
reassuring that the ASCE-ACI method gives values of joint shear
strength that are in the correct range for biaxially loaded joints.

It is reasonable to assume that the N-S and E-W components
of joint shear capacity would be less for a biaxially loaded beam-
column joint than the joint shear capacity of the same joint loaded
uniaxially. If the ultimate shear capacity of a joint is the
same regardless of the direction of the resultant shear, then the
N-S and E-W components of the ultimate joint shear strength of a
joint loaded equally in each direction will be $1/\sqrt{2}$ or 0.71 times
the "uniaxial" strength. Two of the design approaches, however,
predicted that the "uniaxial" joint shear strength would be less
than each component of the joint shear that was actually applied
to the specimens. Park and Paulay's design approach underestimated
the joint shear strength by 72 percent. It should be obvious from
this comparison that the joint shear strength contributed by the
concrete should not be totally neglected. Sugano and Koreishi's
design approach attributed 83 percent of the joint shear strength
to the concrete, but also underestimated the capacity by 11 per-
cent. However, both the N-S and E-W components of applied joint

shear were 0.68 times the "uniaxial" joint shear strength predicted
by Meinheit and Jirsa's method. This is very close to 0.71 which
is the ratio that would be expected if the joint shear capacity
is independent of the orientation of the applied shear.

Depending on the design approach which is considered,
different conclusions about the relative strength of biaxially
loaded joints may be drawn from the comparisons of calculated
ultimate and applied joint shear. Park and Paulay's design
approach, which considers only the joint shear strength contribu-
tion by the steel, did not accurately predict the joint shear
strength of the specimens, so no meaningful conclusions could be
made. Sugano and Koreishi's equations gave values of joint
shear strength which were fairly close to the N-S and E-W components
of the maximum joint shear applied to the specimens. This indicates
that biaxial shear on the specimens did not decrease the joint
shear capacity in either the N-S or E-W directions, so the
resultant joint shear strength was improved by the biaxial loads.
The joint shear strength predicted by Meinheit and Jirsa's
equations, however, was higher than the maximum applied joint
shear. Contrary to the conclusions drawn from the results of
Sugano's and Koreishi's method, this indicates that the joint
shear strength in the principle directions may be less for biaxial
loadings than for uniaxial loadings. If so, the resultant shear
strength of the joint may be the same as predicted by the "uniaxial"
equations.

These results indicate that all of the design approaches
considered, except for Meinheit and Jirsa's are conservative and
can be used in their present form to design joints for biaxial
loads. The "uniaxial" joint shear strength calculated with
Meinheit and Jirsa's method may be unconservative if bidirectional
loads are present. Therefore, the calculated joint shear strength

should be multiplied by approximately $1/\sqrt{2}$ to obtain the strength
in each direction when biaxial loads are expected. These
conclusions are valid for the two specimens being considered and
may not be true for joints with different geometry or reinforcing
details.

After six cycles into the inelastic range, Specimen 5-BS-A
continued to carry high joint shear. At the first peak of the $3\Delta_i$
deformation (load stage 137), the N-S and E-W components of joint
shear were 185 and 174 kips, respectively. This is a 20 percent
reduction from the maximum applied joint shear. The decay in
strength probably resulted from a combination of factors including
loss of cover concrete in the beams and column, loss of strain
compatibility between the compression reinforcement and the concrete,
and decay of the concrete strength in the joint region. Considering
the severe load history that was applied, the strength decay was
small.

5.8 Concluding Remarks

The different design approaches yielded conflicting
conclusions about the strength of biaxially loaded joints relative
to the strength of uniaxially loaded joints. The difficulty is
made even greater because so little test data are available. But
to further explore the implications of the comparisons, it is
necessary to select the design method which is believed to best
represent the actual joint behavior of the specimens. The speci-
mens being considered in this paper were similar in geometry and
reinforcement details to the specimens which Meinheit and Jirsa
used in their test program; therefore, it is logical that their
method should give a more meaningful comparison. Comparison of the
test results with the calculated results of Meinheit and Jirsa's
method indicated that resultant joint shear strength may be
independent of the orientation of the applied shear and may be the

the same as the "uniaxial" joint shear strength predicted by the design equations. For practical design, it may be necessary to proportion a joint to carry a resultant shear of approximately $\sqrt{2}$ or 1.4 times the shear capacity necessary in each principal direction. For joints with unequal size beams framing into the column from orthogonal directions, a smaller factor may be adequate. This approach to the design for biaxial loads is a consideration which should be explored in greater detail as additional test results become available.

CHAPTER   6

SUMMARY AND CONCLUSIONS

6.1 Summary

The objectives of this study were to compare the behavior
of monotonically and cyclically loaded beam-column joints under
biaxial loadings and to compare their behavior with design
approaches based on uniaxial tests.

Two reinforced concrete beam-column joints with the same
geometry and reinforcing details were tested under bidirectional
loads. The specimens were designed to exhibit joint distress
while avoiding large inelastic rotations'of the column and were
tested with deformation controlled load histories. The applied
joint shear on both of the specimens was limited by the flexural
capacity of the beams. Specimen 6-MBS-A showed no sign of a joint
shear failure during the monotonic loading. Specimen 5-BS-A,
which was cyclically tested, also showed no clear sign of a joint
shear failure, although at the $3\Delta_i$ deformation, the capacity of the
specimen did decrease by 20 percent. The stiffness of the speci-
mens decreased considerably after the first excursion to a new
deformation level and severe pinching of the hysteresis loops was
evidence that the stiffness was influenced largely by joint shear
strain and reinforcing bar slip through the joint.

The major difference between the two tests was the amount
of inelastic rotation of the beam and columns. As the beam
deformations were increased, the percentage of the total deforma-
tion due to inelastic column rotation increased for the cycled
specimen, but remained constant during the monotonic loading. The
opposite trend was true for the beam rotations. Loss of

120

compatibility of the column reinforcement caused by cycling was probably the key factor for this behavior. Surprisingly, the amount of joint shear distortion was not affected by cycling of deformations.

In Chapter 5, the applied joint shear on the specimens was compared with the calculated strengths using several design approaches which were based on studies of uniaxially loaded joints. The cracking shear strengths of the joints were about the same in each of the principal directions as predicted by the cracking equations by Sugano and Koreishi and Meinheit and Jirsa. The ultimate joint shear strength of the specimens was calculated with several design equations, and large variations were obtained. Based on a comparison of the observed joint shear strength with the calculated joint shear strength using Meinheit and Jirsa's method, it appears that the ultimate joint shear strength is independent of the orientation of the applied joint shear, and that biaxial loadings may reduce the strength in the principal directions. Considering this behavior, it may be necessary to proportion joints to resist greater shears in each direction if the "uniaxial" design approaches are adopted.

6.2 Conclusions

The following conclusions regarding the behavior of biaxially loaded beam-column joints are based on the test results of two specimens and may not be valid for joints with different geometry or reinforcing details.

(a) Conclusions Regarding Joint Behavior

(1) Joint shear strength was high enough to develop the flexural strength of the beams and deteriorated little with cycling.

(2) Joint stiffness depended on the level of deformation imposed and was influenced substantially by bar slip and joint shear strain.

(3) Cycling of deformations had a large influence on the deterioration of the column.

(b) Conclusions Regarding Design Approaches

(1) Based on a comparison of the joint shear cracking strength of the specimens with the "uniaxial" cracking strengths calculated with equations by Sugano and Koreishi and Meinheit and Jirsa, it appears that initial cracking of the joint does not occur until the "uniaxial" cracking strength in either direction is reached.

(2) The joint shear strength calculated with the design equations by the ACI-ASCE Committee 352 and by Sugano and Koreishi were close to the N-S and E-W components of the maximum applied joint shear.

(3) The design method by Park and Paulay, which neglects the strength of the concrete, grossly underestimated the ultimate joint shear strength of the specimens.

(4) Based on a comparison of the maximum applied joint shear and the ultimate joint shear strength calculated with Meinheit and Jirsa's method, it appears that the joint shear strength in one direction may be reduced by loading in the orthogonal direction. If this design approach is used, it may be necessary to proportion joints to carry a higher joint shear in each direction to account for the effects of bidirectional loads.

6.3 Concluding Remarks

It is difficult to make general conclusions regarding the effects of biaxial loadings on beam-column joints from the test results of two specimens. This study, however, marks the beginning of an ongoing endeavor to understand and quantify the behavior of joints subjected to bidirectional loads.

APPENDIX A

PROGRAM STRESS

STRESS is a Fortran program which calculates the stress history of mild steel reinforcing bars which have strain histories in the inelastic range. The basis for the program is the method developed by K. J. Thompson at the University of Canterbury.[7] Included in this appendix are the equations which were used, an input guide, a listing of the program, and sample output.

The monotonic loading envelope is calculated according to the following rules:

If $\quad \epsilon_s \leq \epsilon_{sy}$, $\qquad f_s = E_s \epsilon_s$

if $\quad \epsilon_{sy} \leq \epsilon_s \leq \epsilon_{sh}$, $\qquad f_s = f_{sy}$

if $\quad \epsilon_{sh} < \epsilon_s \leq \epsilon_{su}$, $\qquad f_s = f_{sy}\left(\dfrac{Q(\epsilon_s - \epsilon_{sh}) + 2}{60(\epsilon_s - \epsilon_{sh}) + 2} + \dfrac{(\epsilon_s - \epsilon_{sh})(60 - Q)}{2(30q + 1)^2}\right)$

where $\quad f_s$ = stress value on analytical curve

$\qquad f_{sy}$ = yield stress

$\qquad f_{su}$ = ultimate stress

$\qquad E_s$ = Young's modulus

$\qquad \epsilon_s$ = strain value on analytical curve

$\qquad \epsilon_{sy}$ = yield strain

$\qquad \epsilon_{sh}$ = strain at strain hardening

$\qquad \epsilon_{su}$ = ultimate strain

$\qquad Q = \dfrac{\dfrac{f_{su}}{f_{sy}}(30q + 1)^2 - 60q - 1}{15q^2}$

and $\quad q = \epsilon_{su} - \epsilon_{sh}$

The equations for cyclic loading are given below:

$$E_s(\epsilon_s - \epsilon_o) = (f_s - f_o)\left[1 + \left|\frac{f_s - f_o}{f_{ch} - f_o}\right|^{r-1}\right]$$

where ϵ_o = strain value at beginning of analytical curve

f_o = stress value at beginning of analytical curve

f_{ch} = characteristic stress

= $f_{max}(0.973 - 9.806\epsilon_{pl})$

f_{max} = maximum prior stress for that direction $\geq f_{sy}$

ϵ_{pl} = plastic strain imposed during previous cycle

r = $12.231 + \dfrac{45.071}{e^{1000\epsilon_{pl}}} - \dfrac{9.771}{\log_e(1000\epsilon_{pl} + 2)}$

Interested persons should see Ref. 7 for more detail about the equations and the rules for their use.

Input Guide--Program STRESS

Card	Columns	Variable	Format
1st	1-80	Title	8A10
2nd	1-10	NP, no. of points	I10.0
	11-20	E, Young's modulus	F10.0
	21-30	FY, yield stress	F10.0
	31-40	FU, ultimate stress	F10.0
	41-50	ESU, ultimate strain	F10.0
	51-60	ESH, strain at strain hardening	F10.0
3rd --> $(2+NP)^{+h}$	1-10	EP, strain history (1 value per line)	F10.0

```
      PROGRAM STRESS(INPUT,OUTPUT,TAPE5=INPUT,TAPE6=OUTPUT)
      COMMON EP(400)
      REAL F(400)
      INTEGER TITLE(8)
      READ(5,100) (TITLE(I),I=1,8)
100   FORMAT(8A10)
      READ(5,200) NP,E,FY,FU,ESU,ESH
200   FORMAT(I10,5F10.0)
      READ(5,600) (EP(I),I=1,NP)
600   FORMAT(F10.0)
      WRITE(6,700) (TITLE(I),I=1,8)
700   FORMAT(*1*,8A10)
      WRITE(6,300) NP,E,FY,FU,ESU,ESH
300   FORMAT(///,5X,35HNO. OF POINTS *******************,I10,/5X,
     C35HYOUNG#S MODULUS (KSI) *************,F10.1,/5X,
     C35HYIELD STRESS (KSI) ***************,F10.1,/5X,
     C35HULTIMATE STRESS (KSI) ************,F10.1,/5X,
     C35HULTIMATE STRAIN *****************,F10.4,/5X,
     C35HSTRAIN AT STRAIN HARDENING *******,F10.4)
      WRITE(6,400)
400   FORMAT(//,9X,3HNO.,5X,13HSTRAIN(IN/IN),2X,11HSTRESS(KSI),/)
      EP(1)=0.
      F(1)=0.
      I=1
      J=49
      WRITE(6,500) I,EP(1),F(1)
500   FORMAT(7X,I5,3X,F12.8,F15.3)
      FMAX=FY
      FMIN=-FY
      EZMX=0.
      EZMN=0.
      ES0=0.
      ES0L=0.
      F0=0.
      F0L=0.
      FCH=0.
      FCHL=0.
      R=-1.
      EPL=0.
      RL=-1.
      L=1
      LL=1
      I=2
      ESY=FY/E
      Q=ESU-ESH
      Q2=((30.*Q+1.)**2*FU/FY-60.*Q-1.)/Q/Q/15.
      F(1)=0.
10    CONTINUE
      IF (ABS(EP(I)).LT.ABS(EP(I-1)).AND.ABS(EP(I-1)).GT.ESY) GO TO 20
      CALL STSENV(I,L,E,EZMN,EZMX,ESH,ESY,Q,Q2,FY,FS)
      F(I)=ABS(FS)
      IF (EP(I).LT.0.) F(I)=-ABS(FS)
      IF (F(I).GT.FMAX) FMAX=F(I)
      IF (F(I).LT.FMIN) FMIN=F(I)
      WRITE(6,500) I,EP(I),F(I)
      I=I+1
      IF (I.GT.NP) STOP
      IF (I.EQ.J) WRITE(6,400)
      IF (I.EQ.J) J=J+58
      GO TO 10
20    CONTINUE
```

```
      SN1=EP(I-1)-EP(I-2)
      SN2=EP(I)-EP(I-1)
      SN3=SN1*SN2
      IF (SN3.GE.0.) GO TO 30
      ES0LL=ES0L
      ES0L=ES0
      ES0=EP(I-1)
      F0LL=F0L
      F0L=F0
      F0=F(I-1)
      LLL=LL
      LL=L
      FCHLL=FCHL
      FCHL=FCH
      RLL=RL
      RL=R
      EPL=ABS(ES0-ES0L-(F0-F0L)/E)
      A=45.071/EXP(1000.*EPL)
      B=9.771/ALOG(1000.*EPL+2.)
      R=12.231+A-B
      EZ=ES0-F(I-1)/E
      IF (EZ.GT.EZMX) EZMX=EZ
      IF (EZ.LT.EZMN) EZMN=EZ
      X=EP(I)-EP(I-1)
      IF (X.GT.0.) L=1
      IF (X.LT.0.) L=-1
      FX=FMIN
      IF (L.EQ.1) FX=FMAX
      FCH=FX*(.973-9.806*EPL)
30    CONTINUE
      CALL STSENV(I,L,E,EZMN,EZMX,ESH,ESY,Q,Q2,FY,FS1)
      CALL BISECT(I,L,R,FCH,F0,ES0,FU,E,FS2)
      F(I)=FS2
      IF (L.EQ.1.AND.FS2.GT.FS1) F(I)=FS1
      IF (L.EQ.-1.AND.FS2.LT.FS1) F(I)=FS1
      IF (EPL.GT..0005) GO TO 40
      IF (L.EQ.-1.AND.ES0.GE.ES0LL) GO TO 40
      IF (L.EQ.1.AND.ES0.LE.ES0LL) GO TO 40
      IF (RLL.LT.0.) GO TO 40
      CALL BISECT(I,LLL,RLL,FCHLL,F0LL,ES0LL,FU,E,FS)
      IF (L.EQ.1.AND.F(I).LT.FS) GO TO 40
      IF (L.EQ.-1.AND.F(I).GT.FS) GO TO 40
      F(I)=FS
      IF (F(I).GT.FMAX) FMAX=F(I)
      IF (F(I).LT.FMIN) FMIN=F(I)
      F0=F0LL
      ES0=ES0LL
      R=RLL
      FCH=FCHLL
      L=LLL
40    CONTINUE
      WRITE(6,500) I,EP(I),F(I)
      I=I+1
      IF (I.GT.NP) STOP
      IF (I.EQ.J) WRITE(6,400)
      IF (I.EQ.J) J=J+58
      IF (R.LT.0.) GO TO 10
      GO TO 20
      END
      SUBROUTINE BISECT(I,L,R,FCH,F0,ES0,FU,E,FS)
      COMMON EP(400)
      B=FCH-F0
```

```
       IF (L.EQ.-1) GO TO 10
       FUP=FU
       FLO=F0
       FS=(FUP+FLO)/2.
       GO TO 20
10     CONTINUE
       FUP=F0
       FLO=-FU
       FS=(FUP+FLO)/2.
20     CONTINUE
       A=FS-F0
       ES=A*(1.+(A/B)**(R-1.))/E+ES0
       IF (ES.GT.EP(I)) FUP=FS
       IF (ES.LE.EP(I)) FLO=FS
       FSS=FS
       FS=(FUP+FLO)/2.
       IF (ABS(FSS-FS).GT..01) GO TO 20
       RETURN
       END
       SUBROUTINE STSENV(I,L,E,EZMN,EZMX,ESH,ESY,Q,Q2,FY,FS)
       COMMON EP(400)
       IF (L.EQ.1) ES=EP(I)-EZMN
       IF (L.EQ.-1) ES=EP(I)-EZMX
       IF (ABS(ES).LT.ESY) FS=E*ES
       IF (ABS(ES).GE.ESY) FS=FLOAT(L)*FY
       IF (ABS(ES).LE.ESH) RETURN
       ES=ABS(ES)
       A=ES-ESH
       B=Q2*A+2.
       C=60.*A+2.
       D=(60.-Q2)*A
       G=2.*(30.*Q+1.)**2
       FS=FY*(B/C+D/G)
       FS=FLOAT(L)*FS
       RETURN
       END
```

SAMPLE PROBLEM - PROGRAM STRESS

```
NO. OF POINTS ***********************        40
YOUNG*S MODULUS (KSI) *************   29000.0
YIELD STRESS (KSI) ****************      60.0
ULTIMATE STRESS (KSI) *************     100.0
ULTIMATE STRAIN ******************      .0500
STRAIN AT STRAIN HARDENING ********     .0100
```

NO.	STRAIN(IN/IN)	STRESS(KSI)
1	0.00000000	0.000
2	-.00040000	-11.600
3	-.00080000	-23.200
4	-.00120000	-34.800
5	-.00080000	-23.200
6	-.00040000	-11.600
7	-0.00000000	0.000
8	.00040000	11.600
9	.00080000	23.200
10	.00120000	34.800
11	.00160000	46.400
12	.00200000	58.000
13	.00360000	60.000
14	.00520000	60.000
15	.00680000	60.000
16	.00840000	60.000
17	.01000000	60.000
18	.01160000	64.824
19	.01320000	69.109
20	.01160000	22.750
21	.01320000	64.892
22	.01160000	18.492
23	.01000000	-27.995
24	.00840000	-52.814
25	.00680000	-56.236
26	.00520000	-57.906
27	.00360000	-59.823
28	.00200000	-59.859
29	.00040000	-60.533
30	-.00120000	-61.097
31	-.00280000	-61.570
32	-.00440000	-61.992
33	-.00600000	-62.375
34	-.00760000	-62.707
35	-.00920000	-63.019
36	-.01080000	-63.301
37	-.00920000	-16.920
38	-.00760000	22.546
39	-.00600000	39.689
40	-.00440000	48.181

BIBLIOGRAPHY

1. Aleman, M. A., Meinheit, D. F., and Jirsa, J. O., "Influence of Lateral Beams on the Behavior of Beam-Column Joints," Sixth World Conference on Earthquake Engineering, New Delhi, January 1977.

2. Park, R., "Accomplishments and Research and Development Needs in New Zealand," Proceedings of a Workshop on Earthquake-Resistant Reinforced Concrete Building Construction, The University of California, July 1977.

3. Jirsa, J. O., "Behavior of Elements and Subassembleges--R. C. Frames," Proceedings of a Workshop on Earthquake-Resistant Reinforced Concrete Building Construction, the University of California, July 1977.

4. Bertero, V. V., "Seismic Behavior of Structural Concrete Linear Elements (Beams, Columns), and Their Connections," Symposium on Structural Concrete under Seismic Actions, Vol. 1, Rome, May 1979.

5. ACI-ASCE Joint Committee 352, "Recommendations for Design of Beam-Column Joints in Monolithic Reinforced Concrete Structures," Journal of the American Concrete Institute, Proc. V. 73, No. 7, July 1976.

6. Meinheit, D. F., and Jirsa, J. O., "The Shear Strength of Reinforced Concrete Beam-Column Joints," CESRL Report No. 77-1, The University of Texas at Austin, January 1977.

7. Thompson, K. J., "Ductility of Concrete Frames under Seismic Loading," Department of Civil Engineering, The University of Canterbury, October 1975.

8. Park, R., and Paulay, T., Reinforced Concrete Structures, John Wiley and Sons, New York, 1975.

9. Sugano, S., and Koreishi, I., "An Empirical Evaluation of Inelastic Behavior of Structural Elements in Reinforced Concrete Frames Subjected to Lateral Forces," Fifth World Conference on Earthquake Engineering, Paper 99, Session 2D: Dynamic Behavior of Structural Elements, Rome, 1973.

10. Paulay, T., "Capacity Design of Reinforced Concrete Ductile Frames," notes for Seminar on Earthquake Resistant Reinforced Concrete Bridge Design, University of Toronto, July 5, 1977.

V I T A

Joe Eldon Longwell was born in Raymondville, Texas, on November 30, 1952, the son of Garnet Jeanette Longwell and Percy Eldin Longwell. After completing his work at Raymondville High School in 1971, he entered Sam Houston State University at Huntsville, Texas. After one year of college, he was drafted into the United States Army, and his term of service lasted from May 1972 to May 1974 and included a tour in West Germany. In January 1975, he entered the College of Engineering at The University of Texas at Austin and received a Bachelor of Science in Civil Engineering in May 1978. In June 1978 he entered The Graduate School of The University of Texas at Austin.

Permanent address: Box 208
                     Hargill, Texas

This thesis was typed by Tina Robinson